STUDY OF TRIMMING BEHAVIOR OF AUTOMOTIVE MAGNESIUM SHEET MATERIALS

STUDY OF TRIMMING BEHAVIOR OF AUTOMOTIVE MAGNESIUM SHEET MATERIALS

By PENG ZHANG, B.Eng.

A Thesis Submitted to the School of Graduate Studies in Partial Fulfillment

of the Requirements for the Degree Master of Applied Science

MASTER OF APPLIED SCIENCE (2014) McMaster University

(Mechanical Engineering) Hamilton, Ontario

TITLE:	STUDY OF TRIMMING BEHAVIOR OF AUTOMOTIVE MAGNESIUM SHEET MATERIALS
AUTHOR:	PENG ZHANG, B.Eng (China University of Petroleum, Beijing)
SUPERVISOR:	Professor Mukesh K. Jain Department of Mechanical Engineering McMaster University
NUMBER OF PAGES:	xx, 162

Abstract

Sheet trimming is an important forming operation in stamping industry. However, trimming of automotive magnesium sheet materials is not well understood. The objective of present study was to investigate the trimming behavior of AZ31 and ZEK100 automotive magnesium sheet materials using a laboratory-based experimental set-up and complementary finite element (FE) simulations of the lab-based experiments. The effects of the trimming process parameters that included tool setup configuration, punch speed, clearance, sheet thickness and sheet orientation (rolling and transverse directions) on the quality of trimmed edge were analyzed. Experimental results indicated that the trimmed edge quality depended strongly on the trimming conditions. The optimal trimming parameters for AZ31 and ZEK100 sheets were experimentally obtained. Interrupted trimming experiments were conducted to examine crack initiation and development, the mechanism of fracture, and the generation of the fracture profile of the trimmed edges. The R-value as a measure of material anisotropy and fracture strain of both materials were measured using uniaxial tension and plane strain tests and incorporated in the FE model.

General purpose Finite Element software ABAQUS/Explicit was employed to simulate the trimming process where five different fracture criteria and element deletion method were used to predict profile of trimmed edge and the fracture initiation and development during the trimming process. Good general agreement was observed between experiments

and FE simulations. However, some discrepancies were also observed. These are presented and discussed in the thesis.

Acknowledgements

First, I would like to express my heartfelt gratitude to my supervisor, Dr. Mukesh K. Jain for giving me a very precious opportunity to study and participate in various research work, and his encouragement, support and guidance throughout my master study.

I would also like to specially appreciate Dr. Junchao Li and Dr. Guowei Zhou for their valuable and insightful suggestions and assistance with Finite Element analysis.

I would also like to thank Dr. Michael Bruhis and Mrs. Connie Barry for giving me valuable advice and assistance in conducting various experiment tests.

I would also like to thank several research technicians in machine shop; Mr. Michael Lee, Mr. Ron Lodewyks and Mr. Mark MacKenzie for giving the assistance with specimens preparation.

I would also like thank Dr. Xiaogang Li for giving the assistance and guidance in microstructure observation, etc.

I would also like to thank my colleagues in my lab and friends for their help.

Lastly, I would like to express my gratitude to my parents, parents-in-law, my wife, as well as my brothers and sisters for their love, support and encouragement.

Table of Contents

List of Figures

List of Tables

Nomenclature

A, B	Parameters in stress triaxiality equation
a, b, c, d, e	Constants in material constitutive equation of flow stress-strain
C	Clearance between punch and die (Figure 2-3)
C	Critical value for judging material failure
C_1, C_2, C_3, C_4, C_5, C_6	The material constants in different fracture criterias
$\mathrm{C_d}$	Dilatational wave speed of the material
E	Elastic modulus
F, G, H, L, M , N	Hill's anisotropic parameters
f^*	Total effective void volume fraction
$\mathrm{f_c}$	Critical void volume fraction at the onset of void coalescence,
$\mathrm{f_f}$	Void volume fraction at final fracture,
$\mathrm{f_u}$	Material constants of void coalescence in GTN model
I	Integral value of fracture criteria
I_F	Parameters for establishing the occurrence of fracture
L	Ratio between the maximum and minimum plastic strain increments
$\mathrm{L^e}$	Smallest characteristic element length
MS	Mesh size
MSFs	Mass scaling factors
$\mathrm{R_{RD}}$, $\mathrm{R_{45°}}$, $\mathrm{R_{TD}}$	Anisotropy values for RD, 45°and TD sheet orientations
R	Definition of anisotropy value

R_{Av}	Average coefficient of normal anisotropy
p	Hydrostatic stress
q_1, q_2 , q_3	Calibration coefficients for GTN model
T	Temperature (Unit: Kelvin)
Δt	Stability limit in ABAQUS/Explicit
σ	Material flow stress
σ_{11}, σ_{22}, σ_{33}	Normal stress components
σ_{12}, σ_{13}, σ_{23}	Shear stress components
σ_n	Normal interaction stress
σ_f	Friction stress
$\bar{\sigma}$	Effective stress,
σ_1 , σ_2	In-plane principal stress components,
σ_H	Hydrostatic stress
$\bar{\varepsilon}$	Equivalent strain,
$\bar{\varepsilon}_f$	Equivalent or effective strain at failure,
ε, ε_1, ε_2	Plastic strain , major and minor principal strains
ε_w^{pl} , ε_t^{pl}, ε_l^{pl}	Plastic strains in the width, thickness and length directions
μ	Friction coefficient
ρ	Material density
δ	Stress triaxiality
β	Ratio of major to minor principal strains
α	Ratio of Principal stress

Chapter 1. Introduction

1.1. Background

Magnesium alloys are the lightest of the structural metallic materials used in the automotive stamping industry. They are a quarter of the weight of steel and a third lighter than aluminum (Magnesium Elektron). The combination of low density, good high temperature mechanical properties, high specific strength and stiffness makes magnesium alloy an attractive choice for automotive, aerospace, computer parts, communication and other consumer electronics applications.

With the highest strength-to-weight ratio of any of the commonly used materials, magnesium alloys are becoming the most promising engineering materials for manufacturing of light weight structural components. In automotive industry, an effective way to increase the fuel efficiency and reduce gas emission is to lower the weight of vehicle with the use of lightweight materials. Therefore, nowadays, magnesium alloy is very popular with the automotive manufacturers around the world. For example, automotive magnesium components are predominantly used in interior applications such as in transfer case, front end structures, transmission case, instrument panel set frames, steering column bracket etc., as shown in Figure 1-1 (Gwynne and Lyon 2007). Currently, the applications of wrought magnesium alloy AZ31 and the newer alloy ZEK100 for automotive and aerospace industries for automotive stamping applications are becoming increasingly attractive.

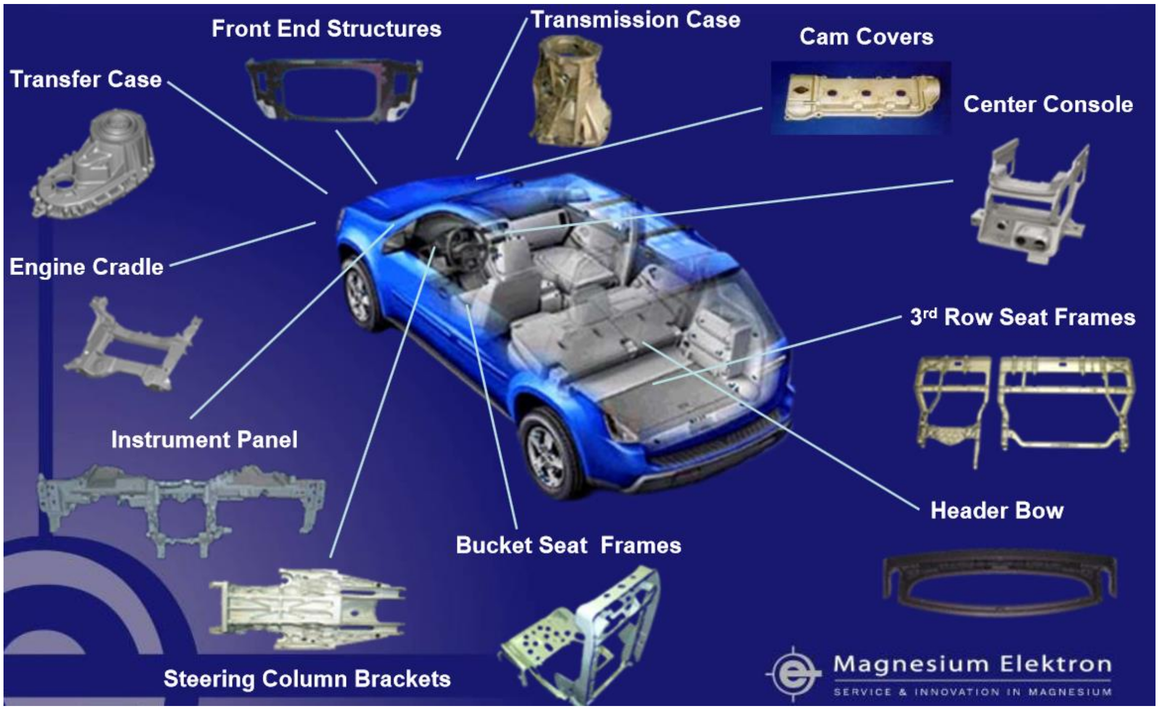

Figure 1-1. Major Magnesium based auto products (Gwynne and Lyon 2007).

Of all metal forming processes employed in automotive production, trimming is one of the most widely techniques for material separation. Trimming is a process in which the outer perimeter of a formed or a flat region such as binder region of the blank, referred to as offal, is cut away to yield a final part. The typical tool setup configuration for trimming process consists of punch, die, blank-holder and sometimes an option cushion as shown in Figure 1-2. The sheet is clamped between the blank-holder and die and held stationary while the punch and cushion (if applicable) are moved perpendicular to the sheet plane to trim the sheet. A clearance or the gap between the punch and die exists in trimming to allow the punch to pass through the clamped sheet to cut. Clearance is usually expressed as some fraction of sheet thickness.

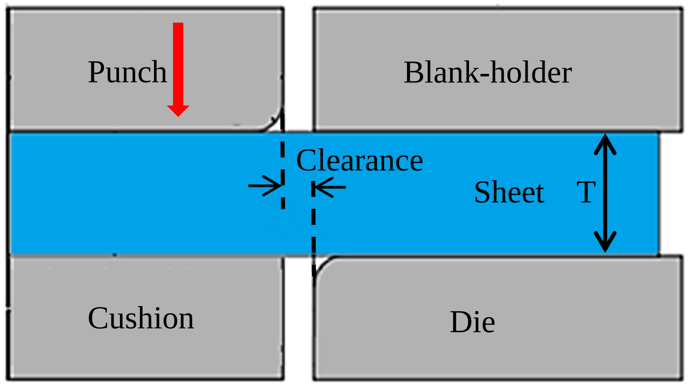

Figure 1-2. Tool setup configuration and parts for trimming test.

The trimmed edge of parts is characterized in terms of four different quantities: rollover, burnish zone, fracture zone and burr (Figure 1-3). The different zones determine the profile and the quality of the trimmed edge.

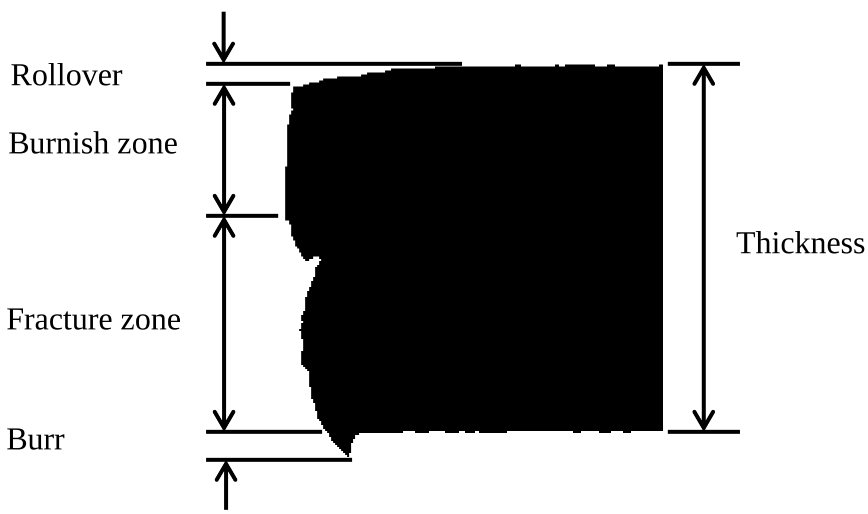

Figure 1-3. Typical profile of trimmed edge.

1.2. Project Objectives

The project objectives of this work were to study the trimming characteristics of AZ31 and ZEK100 magnesium alloys sheet materials by laboratory-based experiments and corresponding finite element (FE) simulations of experiments to gain a better understanding of trimming of magnesium sheet materials.

The major objectives of this thesis were to achieve the following:

1. Systematically study the trimming behavior of AZ31 and ZEK100 magnesium alloy materials via experiments and numerical models.
2. Investigate the effect of various trimming factors on shape and quality of the trimmed edge for AZ31 and ZEK100 magnesium alloy sheets.
3. Develop a FE model of the lab based experiments and implement different fracture criteria to predict the trimming process for AZ31 and ZEK100 magnesium alloy sheets.

1.3. Thesis Structure

This thesis is divided into eight chapters. This first chapter provides introduction to trimming, motivation and objectives of the project. A literature review of previous work related to trimming process is presented in Chapter 2. The experimental procedure and the details of FE modelling are described in Chapter 3 and 4 respectively. The corresponding experimental and simulation results are analyzed, compared and discussed in Chapter 5. Some further overarching discussion about the experimental and Finite Element modelling results is provided in Chapter 6. The conclusion of this study and suggestions for future work are presented in Chapters 7 and 8 respectively.

Chapter 2. Literature Review

The behavior of sheet material during trimming process can be divided into four stages. At the beginning of the process, the sheet is pushed into the die by punch and the sheet is deformed elastically. When the yield strength of the sheet material is reached, plastic deformation starts with the progress of trimming process. Subsequently, cracks initiate and propagate from both surfaces of the sheet in the through-thickness direction. Finally, the two propagating cracks join to create a final rupture or separation of part and offal (Quazi and Shaikh 2012).

Sheet trimming is very similar to blanking process. Extensive experiment and simulation work about trimming or blanking process has been conducted by many researchers, which provide considerable valuable background information about the characteristics of various metallic materials. The previous research work shows the trimmed edge quality and shape are determined by various factors such as material properties (mechanical and thermal properties, microstructure, geometry), operation parameters (trimming speed, clearance), friction, tooling conditions (tool setup configuration, tool wear, lubrication, fixturing) etc.

FE simulations of trimming offer a further means of understanding the trimming characteristics of sheet materials. The FE method allows for incorporation of actual tool geometry, clamping of sheet between the die and clamp plate, contact and friction between the tool and sheet materials. The material itself can be treated as elastic-plastic and fracture process can also be included.

In this chapter, previous experimental research work about the trimming or blanking behavior of various metal sheets is presented first. This is followed by a review of available FE models of trimming in the literature.

2.1. Trimming Process Parameters

The effect of various factors affecting the trimmed edge quality has been studied by many researchers through experiments. Some representative trimming process parameters are listed in Table 2-1.

Table 2-1. Representative tests of process parameters.

Researcher(s)	**Topic**	**Materials**	**Experimental parameters**
Chang and Swift,1950	Blanking	Aluminum	Clearance, Tool sharpness
Johson,1973	Blanking	Al alloys, Steel, Copper	Clearance, Blanking speed
Grünbaum, 1996	Blanking	Steel, Copper, Al alloys	Blanking speed
Goijaerts,1999	Blanking	Steel	Blanking speed, Grain size
Li,2000	Trimming	Steel, Al alloys	Clearance; cutting angle, Blade sharpness
Situ,2003	Trimming	Al alloys	Trimming speed, Clearance, Tool setup configuration
Golovashchenko,2006	Trimming	Al alloys	Punch radii, Clearance Tool setup configuration
Golovashchenko,2008	Trimming	Al alloys	Tooling wear, Trimming angle Tool setup configuration, Die radii
Krrabaj,2011	Blanking	Steel, Copper, Al alloys	Clearance, Blanking speed

2.1.1. Trimming speed

Goijaerts (1999) investigated the effect of punch speed and grain size on ductile fracture initiation and maximum blanking force for steel, and found punch speed (or strain rate) has no influence on the ductile fracture initiation (shear zone) up to punch speed of 10 mm/sec, but the maximum blanking force increases with an increase in blanking speed. For higher speeds, the effect of thermal softening reduces the yield stress and promotes fracture, so that both the maximum blanking force and the size of shear zone decrease. The blanking force decreases with larger grains that are typically softer. Situ et al. (2005) found that trimming speeds up to 10 mm/sec have no influence on the maximum trimming force for automotive aluminum AA6111-T4 sheet material, a result different from Goijaerts (1999) for steel, but the same trend was reported in both studies with regard to crack initiation. Higher speeds led to earlier crack initiation. Krrabaj et al. (2011) conducted a range of experiments using different materials, punch die clearances and blanking speeds, and found higher blanking speeds can improve the part edge quality, resulting in smaller burr height and rollover, and a larger shear zone. Tehy also found that steel sheet exhibits larger improvement in trimmed edge quality with high blanking speed than copper and aluminum sheets.

2.1.2. Clearance

Clearance between punch and die is generally reported as the most important trimming process parameter. Chang and Swift (1950) first studied the effect of clearance on tool wear, and found that, for the ductile materials like aluminum alloy, an optimal clearance of about 5% to 10% of thickness exists. Johnson and Mellor (1973) further studied the significance of clearance, and found clearance was a critical factor that governs the trimmed edge quality (burnish, burr size and fracture shape) in most cases. As shown in Figure 2-1, proper clearance can make the cracks initiate from the tips of punch and die, and the cracks will propagate and meet each other near the center of sheet thickness, so that a good trimming surface with large burnish, small fracture zone and burr height and without sliver is obtained. Sliver is a general term for debris and small metal pieces produced in the trimming process (Li 2003). For small clearance, the cracks from the two ends may propagate in different directions and may not meet up with each other resulting in sliver. For large clearance, the cracks propagate different directions, because the shear band is quite large so that the trimmed edge has poor quality, and sometimes jagged trimmed fracture surfaces are created.

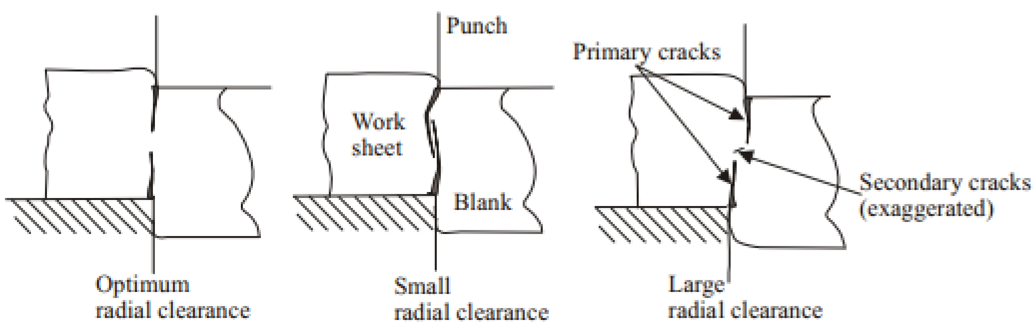

Figure 2-1. Effect of clearance on trimmed edge (Johnson & Mellor, 1973).

Other researchers have confirmed that clearance has the most significant influence on the quality and profile of the trimmed edge, regardless of which material is blanked or what cutting speed is used (Grünbaum et al. 1996; Li 2000; Situ et al. 2005; Golovashchenko 2006; Krrabaj et al. 2011).

2.1.3. Tool setup configuration

Li (2000, 2003) modified the conventional orthogonal trimming where the punch is perpendicular to the sheet surface and first developed a new trimming process for aluminum alloys: trimming with an angle for aluminum sheet materials as shown in Figure 2-2. He systematically studied the effects of process parameters (tool sharpness, clearance, and cutting angle) on cut surface quality, burr heights and production of silvers. His experiments have shown that trimming with a proper angle ($15-20^{\circ}$) could greatly improve the cut surface quality with almost no burrs and silvers even when a larger clearance and extremely dull tools are used. He also found that burnish depth was more sensitive to blade sharpness and influenced moderately by clearance, whereas the burr height and silver were sensitive to clearance.

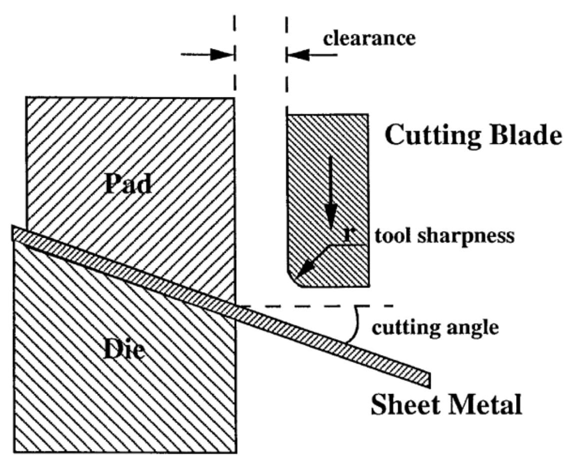

Figure 2-2. Tool setup configuration with angle and trimming parameters evaluate in experiment (Li 2000,2003).

Golovashchenko (2006) studied trimmed surface formation in aluminum autobody sheets with different clearances and modified the conventional trimming setup by designing a support pad underneath the offal (see Figure 2-3). The mechanical support of the offal prevents its bending and excessive rotation, so that it eliminates burrs and prevents the generation of slivers from the trimmed surface. Situ et al.(2005) also compared the conventional and the improved trimming tool configurations by adding steel and elastic supports and found the latter tool setup configuration produced the best cut edge quality for aluminum alloy AA6111-T4. Golovashchenko (2008) further proposed a new trimming tool setup configuration combining an elastic cushion and trimming with an angle (see Figure 2-4). His experimental results show that, compared the conventional trimming process, the new improved trimming process provides stable results for a range of clearances between the shearing edges.

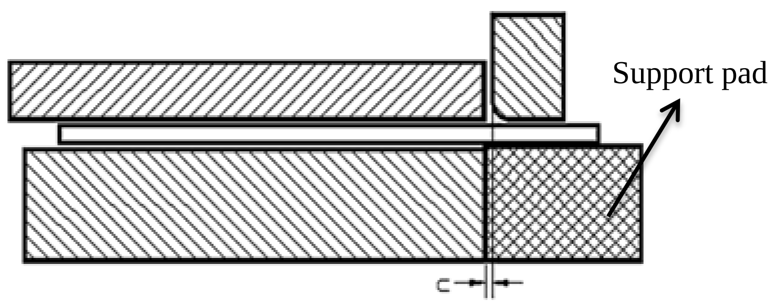

Figure 2-3. Trimming scheme with cushion of the offal (Golovashchenko, 2008).

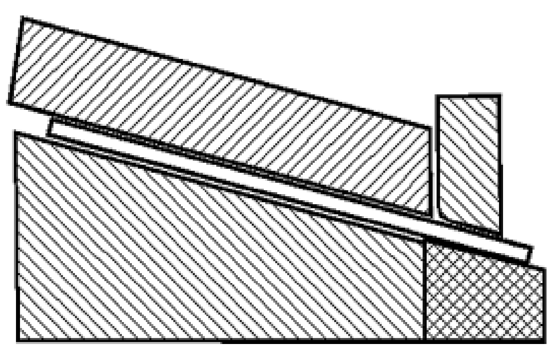

Figure 2-4. Trimming scheme with cushion and an angle (Golovashchenko, 2008).

2.2. Finite Element Model of Trimming Process

Finite Element Analysis (FEA) method is being increasingly used in the automotive industry as a powerful numerical tool for design analysis and manufacturing process feasibility to reduce the cycle time for introduction of new models that often employ more aggressive styling of body components. There is also increased emphasis towards introduction of new materials, and FEA allows virtual experimentation via computer simulations that can analyze the interaction of part geometry, material, and forming process parameters in order to make a successful part. Additionally, FEA provides researchers with an effective approach to analyze the deformation process that might be difficult to observe in experiments. However, success of the FEA critically depends upon choice of constitutive material model, suitable determination of input material parameters for the chosen constitutive model, and careful selection of many numerical parameters such as element type, element density, solver used for FEA etc. Since trimming process involves fracture, and therefore, one of the most important tasks in FE simulation of trimming process is to implement suitable fracture criterion to simulate the crack initiation and propagation.

In this section, previous research work related to constitutive material model (yield criteria and strain hardening law), various fracture criteria, and other numerical details of the available FE models of trimming are described.

2.2.1. Constitutive material model

Constitutive material model usually relates stress to other variables such as strain, strain rate and temperature etc., to describe yielding and work hardening behavior of a material. In literature, the most widely used constitutive model are the classical Von Mises yield criterion and Prandtl–Reuss flow rule with isotropic strain hardening for isotropy materials (Samuel 1998; Goijaerts et al. 2001; Lin and Chen 2007; Lemiale et al. 2009; Komori 2013) and Hill’48 yield criterion for anisotropic materials to characterize the anisotropy. The most important and widely used work hardening laws are power law (also referred to as Hollomon law or its variant called Swift law) (Samuel 1998; Hatanaka et al. 2003; Lin and Chen 2007; Lemiale et al. 2009; Komori 2013) and Voce law (Goijaerts et al. 2001). For power law, the main characteristics is that the applied stress continuously increases with increase of strain and never saturates. Voce law, on the other hand, show saturation in stress at large strains.

2.2.2. Friction models

The most widely used friction model in trimming or blanking process is the standard Coulomb’s friction law as shown below:

$$\sigma_f = \mu\sigma_n \tag{2.1}$$

where σ_f and σ_n the are the friction and normal interaction stresses, and μ is the friction coefficient (Faura et al. 1998; Samuel 1998; Brokken et al. 2000; Fang et al. 2002; Thipprakmas et al. 2008; Husson et al. 2008).

Maiti et al.(2000) investigated the effect of friction on the maximum blanking load for mild steel via FE model, and found that blanking load increases with increase in the coefficient of friction at the tool sheet interface. Husson et al.(2008) focused on the effect of friction coefficient on the blanked edge (sheared edge) quality for copper via FE model, and his study demonstrated the friction coefficient varying in the range 0.02-0.15 have no influence on the rollover depth and burr height,. However, the burnish depth increases and the fracture depth decreases as friction increases.

2.2.3. Ductile Fracture criteria

Fracture and failure in metal forming process almost always occurs in the form of ductile fracture. The ductile fracture theories for metallic materials typically consider that fracture ensues from initiation or nucleation, growth, and coalescence of voids after the material has been deformed to large strains as shown in Figure 2-5 (Broek 1971; Goijaerts 1999). The nucleation of voids is caused by the internal cracking of second phase particles or inclusions or by de-cohesion of particle-matrix interface (Jain et al. 1999). Under the continuous external plastic deformation, the nucleated voids will grow and subsequently coalesce to from a final crack or fracture.

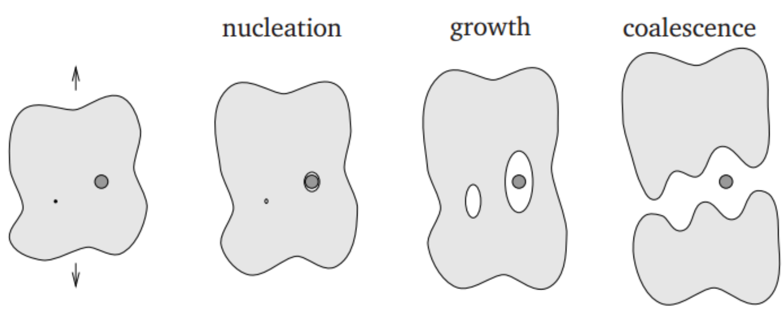

Figure 2-5. Scheme of the nucleation, growth and coalescence of voids (Goijaerts, 1999).

Many ductile fracture criteria have been proposed during the past 3 decades, and these fracture criteria are classified into two types: empirical criteria or uncoupled damage models and microstructure-based criteria or coupled damage models.

2.2.3.1. Empirical fracture criteria

Currently, the most effective way to predict the ductile fracture in the metal forming process is to study stress or strain of the material, and apply a reasonable and practical local fracture criteria. The empirical criteria are based on the stress and strain deformation history. They can be written as an integral of stress-based functions over effective strain field as shown below:

$$I = \int_0^{\bar{\varepsilon}_f} f(\bar{\sigma}, \sigma_H, \sigma_1, \sigma_2 \ldots.)d\bar{\varepsilon} = \mathrm{C} \quad (2\text{-}2)$$

where $\bar{\varepsilon}$ is the equivalent strain, $\bar{\varepsilon}_f$ is the equivalent or effective strain at failure, I is the integral value, $f(\bar{\sigma}, \sigma_H \ldots\ldots)$ is a certain function of stress state. If the integral of left side of the above equation reaches a critical value C, the ductile fracture is assumed to occur.

(Freudenthal 1950) first postulated that initiation and propagation of a crack can be determined by a critical value of the absorbed plastic energy. During the following decades, many researchers proposed their own fracture criteria motivated by Freudenthal original fracture criteria. Some well-known empirical fracture criteria in their mathematical form are listed in Table 2-2 where $\bar{\sigma}$ is the effective stress, σ_1 and σ_2 are the in-plane principal stress components, σ_H is the hydrostatic stress, and L is the ratio between the maximum and minimum plastic strain increments.

Table 2-2. Common empirical fracture criteria from the literature.

Ductile Fracture Criteria	**Formula**
Freudenthal,1950	$I = \int_0^{\bar{\varepsilon}_f} \bar{\sigma} d\bar{\varepsilon}$
Cockcroft-Latham,1968	$I = \int_0^{\bar{\varepsilon}_f} \frac{\sigma_1}{\bar{\sigma}} d\bar{\varepsilon}$
Brozzo,1972	$I = \int_0^{\bar{\varepsilon}\mathrm{f}} \frac{2\sigma_1}{3(\sigma_1 - \sigma_H)} \mathrm{d}\bar{\varepsilon}$
Norris et al.,1978	$I = \int_0^{\bar{\varepsilon}\mathrm{f}} \left(\frac{1}{1 - c_N \sigma_H}\right) \mathrm{d}\bar{\varepsilon}$
Atkins,1981	$I = \int_0^{\bar{\varepsilon}\mathrm{f}} \left(\frac{1 + 1/2L}{1 - c_N \sigma_H}\right) \mathrm{d}\bar{\varepsilon}$
Ayada,1984	$I = \int_0^{\bar{\varepsilon}_f} \frac{\sigma_H}{\bar{\sigma}} d\bar{\varepsilon}$
Clift,1999	$I = \int_0^{\bar{\varepsilon}\mathrm{f}} \bar{\sigma} \mathrm{d}\bar{\varepsilon}$

Cockroft and Latham (1968) proposed that the maximum principal tensile stress is most relevant in the initiation of fracture. Thus, for a given material, temperature and strain rate, the Cockroft-Latham criteria suggests the fracture initiates when the integral of the ratio of maximum principal tensile stress to effective stress reaches a critical value. Brozzo (1972) modified the Cockcroft-Latham criteria and took into account the hydrostatic pressure. Norris et al. (1978) proposed an empirical criteria based only on the hydrostatic stress. Atkins (1996) modified the Norris' fracture criteria and introduced strain ratio (or strain path) as a parameter. Ayada et al. (1987) suggested the hydrostatic stress and equivalent strain are the main driving force behind the growth of voids. Clift et al. (1990) proposed that a critical value of generalized plastic work per unit volume at fracture is capable of predicting the site of fracture initiation.

It is to be noted that there is no single criteria that can predict fracture of all ductile materials. Specific empirical fracture criteria is often advanced for a given material and forming process. Simpler ones are employed more often in the FE analysis because they require fewer experimental tests to determine the model parameters.

2.2.3.2. Microstructure-based criteria

The microstructure-based criteria incorporate damage accumulation into constitutive equation, and the effects of the local damage development on the stress-strain field, especially after the onset of void coalescence. Some commonly used microstructure-based criteria are listed in Table 2-3 below. McClintock (1968) divided the material into quadrilateral elements containing elliptical cylindrical voids and analyzed its growth for different loading conditions. Rice and Tracey (1969) proposed a fracture criteria based on the analysis of the growth of spherical voids under triaxial stress state. McClintock(1968) and Rice and Tracey (1969) fracture criteria are both based on analysis of growth of an isolated void and neglect void interaction (Jain et al. 1999). Oyane (1972) developed a ductile fracture criteria from the equations of plasticity theory for porous and dense metallic materials. The model postulates that the ductile fracture occurs when the volume fraction of voids reaches a critical value.

Table 2-3. Representative Microstructure-based criteria.

Ductile Fracture Criteria	**Formula**
McClintock,1968	$I=\int_0^{\bar{\varepsilon}_f}\left\{\frac{\sqrt{3}}{2(1-\mathrm{n})}sinh\left[\frac{\sqrt{3}}{2}(1-n)\frac{\sigma_1+\sigma_2}{\bar{\sigma}}\right]+\frac{3}{4}\left(\frac{\sigma_1-\sigma_2}{\bar{\sigma}}\right)\right\}d\bar{\varepsilon}$
Rice and Tracy,1969	$I=\int_0^{\bar{\varepsilon}f} exp\left(\frac{3}{2}\frac{\sigma_m}{\bar{\sigma}}\right)d\bar{\varepsilon}$
Oyane,1972	$I=\int_0^{\bar{\varepsilon}\mathrm{f}}\left(\frac{\sigma_H}{\bar{\sigma}}+\mathrm{C}_1\right)\mathrm{d}\bar{\varepsilon}$
Gurson-Tvergaard-Needleman (GTN)	$\Phi=\left(\frac{q}{\bar{\sigma}}\right)+2q_1f^*\cosh\left(-\frac{3}{2}\frac{q_2p}{\bar{\sigma}}\right)-(1+q_3f^{*2})=0$ where $f^*=\begin{cases} f & f\le f_c \\ f_c+\frac{f_u-f_c}{f_f-f_c}(f-f_c) & f>f_c \end{cases}$,

Gurson (1977) proposed an approximate yield function for the material containing voids considering the effect of hydrostatic stress. Gurson's model takes into consideration the interaction between the internal damage and flow behavior of material, and this model can describe the softening effect caused by the voids on material behavior. The original Gurson model was modified by Tvergaard (1981, 1982) and Needleman & Tvergaard (1984) by introducing three additional fitting parameters. This model is often referred to as Gurson-Tvergaard- Needleman (or GTN) model in the literature and is included in Table 2-3. In the expression for GTN model, q is the macroscopic von Mises equivalent stress, p is the hydrostatic stress, $\bar{\sigma}$ is the equivalent stress, q_1, q_2 and q_3 are the calibration coefficients, and f^* is the total effective void volume fraction introduced by Tvergaard (1984) and Needleman (1984) to account for the gradual loss of stress carrying capability of the material due to void coalescence. If the material is undamaged, f^* is equal to zero, and the above yield function reduces to the standard von Mises form. Additionally, f_c is the critical void volume fraction at the onset of void coalescence, f_f is void volume fraction at final fracture, and $f_u = 1/q_1$.

2.2.4. Simulation of fracture

For the simulation of crack initiation and propagation, Taupin et al. (1996) proposed an element deletion method in the FE model, when a predefined fracture criterion reaches its critical value in an element, this element is deleted and removed from the mesh. Element deletion method can be easily implemented in FEA and is widely used as a standard method to simulate the crack propagation. However, element deletion method is somewhat unrealistic because it brings a mass loss in the material thus results in additional numerical inaccuracies. One of methods to minimize the effect of mass loss is to apply a fine mesh in the critical region in the model where fracture is likely to occur.

In order to overcome the shortcomings of mass loss, Komori (2001) suggested the node separation method shown in Figure 2-6. When a specific fracture criteria is satisfied at a node adjacent to the crack tip, the node becomes the new crack tip and the old one is split in two. The crack extends along the element boundary by nodal release.

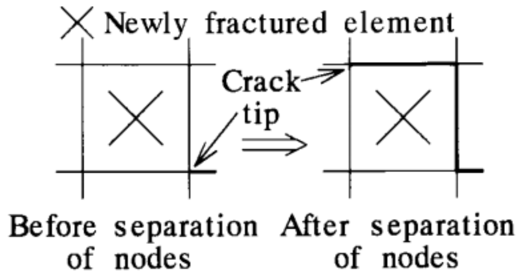

Figure 2-6. A schematic illustration of nodal separation method during crack growth (Komori, 2001).

As the above two methods are strongly mesh dependent, Brokken (1998) developed a so-called discrete cracking method in which the crack does not propagate along the edge of an element, but may be inside of the element, and the crack propagation path is specified by the maximum value of a certain predefined fracture criteria. Representative crack implementation methods in FE models of trimming for various ductile fracture criteria and methods are listed in Table 2-4.

Table 2-4. Representative crack implementation methods in FEA for simulation of trimming of sheet materials.

Researchers	**FEM code**	**Crack method**	**Element type**	**Adaptive re-meshing**	**Fracture criteria**
Goijaerts, 1999	MARC/ Implicit	No	2D- Axisymmetric	Arbitrary Lagrangian-Eulerian (ALE)	Freduenthal; Cockroft-Latham; Rice&Tracy; Oyane et al.
Brokken, 2000	MARC/ Implicit	Discrete crack	2D- Plane strain	ALE	Rice-Tracy
Rachik, 2002	ABAQUS/ Explicit -VUMAT	No	2D- Axisymmetric	ALE	GTN
Ghosh, 2005	ABAQUS/ Explicit -VUMAT	Element deletion	2D- Plane strain 3D- Brick elements	ALE	Shear Failure Cockroft-Latham; GTN
Komori, 2005	------	Node separation	2D- Axisymmetric	YES	Gurson; Fredudenthal; Cockcroft-Latham; Brozzo et al.; Oyane
Thipprakmas, 2008	DEFORM/ Implicit	------	2D- Axisymmetric	YES	Ayada; McClintock; Rice and Tracy
Lemiale, 2009	BlankForm/ Implicit	Element deletion	2D- Axisymmetric	YES	GTN; Fredudenthal
Komori, 2013	------	Node separation	2D- Axisymmetric	YES	Fredudenthal; Cockcroft-Latham; Brozzo et al.; Oyane

Goijaerts (1999) compared and evaluated four different fracture criteria for ductile fracture prediction in metal forming, and found that Oyane and Rice-Tracy criteria produced very good results by considering the influence of stress tri-axiality. Brokken et al. (2000) successfully used Rice-Tracy criteria to predict geometrical properties like burr size, length of sheared and fractured zone, and the roll over shape and found good agreement with the experimental results. Rachik et al. (2002) successfully applied the GTN model to the numerical modelling of the blanking process for mild and stainless steels. They found that GTN model provides satisfactory predictions of not only the maximum punch force but also the punch penetration at fracture and the burr height. Ghosh et al. (2005) found Cockroft–Latham and GTN model do not predict the cut-surface profile as observed in the experimental studies, whereas shear failure model is reasonably successful in predicting the cut-surface profile and burr heights for the shear-slitting process. Komori (2005) compared and evaluated four different fracture criteria, and found that punch load-displacement curves and the lengths of sheared and fractured surfaces of chips and holes for various clearances were accurately predicted by the Gurson fracture criteria. Brozzo et al., Oyane and Gurson criteria could all predict the shape of the sheared and fracture surfaces observed in experiment rather well. Thipprakmas (2008) applied Rice and Tracy, Ayada and McClintock criteria in conventional and fine blanking and found that the fracture, tearing and secondary shear surfaces predicted by Rice and Tracy criteria agreed closely with the experimental results. Lemiale et al.(2009) analyzed the blanking process using uncoupled and coupled GTN model to study the ductile damage and fracture. They found that GTN model provided a better prediction of the loading curve shape and the maximum blanking force. Komori (2013) analyzed the shapes of the scraps and the punch force-displacement curves calculated using Cockcroft and Latham fracture criteria, Brozzo et al. fracture criteria, and Oyane fracture criteria. All of the above fracture criterion agreed fairly closely with data obtained in the experiment.

2.3. Summary

After reviewing the previous research work about the trimming process, it can be said that the shape and quality of trimmed edge is a function of various factors (material properties, trimming and tooling conditions etc.). By controlling these trimming process parameters, the desirable cutting quality with designated parameters can be achieved from the trimming process. Much of the review of reasearch work also demenstrated that there are no universal optimal trimming process parameters and there is no universal uniform fracture criteria for all metallic materials. Much of the work has focused on trimming or blanking for the steel, copper and aluminum sheet materials. The study of trimming behavior of AZ31 and ZEK100 magnesium alloy sheet is a relatively new field, so, a study of the characteristics of AZ31 and ZEK100 in trimming process and the effect of various trimming process parameters through lab-based experiments and FE simulations is an interesting topic for research. In pursuing this topic, judicious choices based on the above literature review can be made in the selection of experimental trimming parameters as well as in the development of practical and efficient FE models.

Chapter 3. Experimental Procedure

3.1. Introduction

Experimental work consisted of standard trimming test, interrupted trimming test for examining crack initiation and propagation, and uniaxial tensile test for characterizing the stress-strain behavior and anisotropy parameter (or R-value) of AZ31 and ZEK100 sheet materials for use in the Finite Element (FE) modeling work. The uniaxial tension test and plane strain tests were also utilized to obtain fracture strain in order to calculate the material parameters of the different fracture criteria employed in the FE work. Further, metallographic work was carried out to measure parameters of the trimmed edge. In this chapter, the details of experimental procedure of trimming, uniaxial tensile and plain strain test are described.

3.2. Trimming test

The main objective of the trimming test was to experimentally investigate the trimming behavior of AZ31 and ZEK100 magnesium alloy sheet materials. In this chapter, experimental details related to trimming process parameters including tool setup configuration, trimming speed, clearance between the punch and die, sheet thickness and sheet orientation (along rolling and transverse directions) as well as trimmed edge parameters are described.

3.2.1. Materials and Specimen Preparation

The materials studied in this thesis are commercial grade rolled AZ31 and ZEK100 magnesium sheets with the initial thickness of 1.58 mm and 1.53 mm respectively. The chemical composition of AZ31 and ZEK100 Mg alloy sheets in weight percent are shown in Table 3-1.

Table 3-1. Chemical composition of AZ31 and ZEK100 magnesium sheet (wt %).

AZ31	Mg	Al	Zn	Mn	Fe	Ce	Cu	Zr	Ni
	Bal	3.03	0.97	0.31	0.01	0.006	0.006	0.002	0.001
ZEK100	Mg	Zn	Zr	Nd	Ce	La			
	Bal	1.34	0.23	0.182	0.008	0.001			

The specimens for trimming test, tensile and plane strain test were all annealed at a temperature of 300° C for 15 minutes, and then furnace cooled to room temperature of 20°C. The dimension of specimen for trimming test was chosen as 75 mm in length and 15.8 mm width while keeping the original sheet thickness of 1.58 mm for AZ31 and 1.53 mm for ZEK100. Since the ratio of width to thickness was over 10:1, the deformation in the width direction was assumed to be negligible, and the trimming process was treated as a plane strain process. As shown in Figure 3-1, the specimens for trimming tests were cut with the length dimensions along rolling direction (RD) and transverse direction (TD) to investigate the effect of specimen orientation on trimming behavior. Once a test specimen was trimmed, two pieces were obtained, the smaller trimmed-off piece of length 10 mm represented offal and was discarded. The other longer part was retained for examination (See Figure 3-1 below).

In order to obtain good experimental accuracy, the sides of the specimens were milled and deburred prior to testing to make sure the samples were quite uniform, i.e., flat, orthogonal and straight.

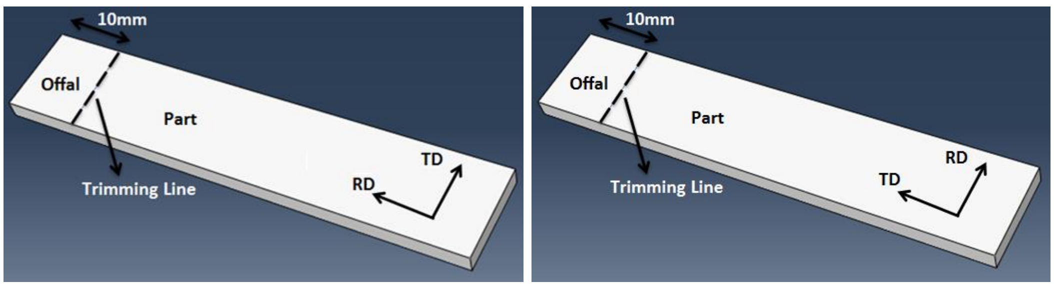

(a). RD) (b). TD

Figure 3-1. Specimens for trimming test, sheet orientation: (a) RD, (b) TD.

3.2.2. Mechanical test system

All trimming tests were conducted on a computer-controlled screw-driven INSTRON mechanical test system of 10 kN load capacity (Model:5566). The test system had a base plate at the bottom of the load frame and a crosshead with a load cell above it as shown in Figure 3-2. The trimming tool setup was mounted on the base plate while a compression platen was attached to the load cell and positioned directly above the punch of trimming tool setup. The punch was kept unattached but guided in a housing at the top of the die. When the cross-head moved downward, and the compression platen with it, the latter came in contact with the punch. The punch then delivered a quick downward blow to the sheet metal clamped between the die and the blank-holder to perform the trimming process. During the trimming process, the punch load and displacement were continuously recorded.

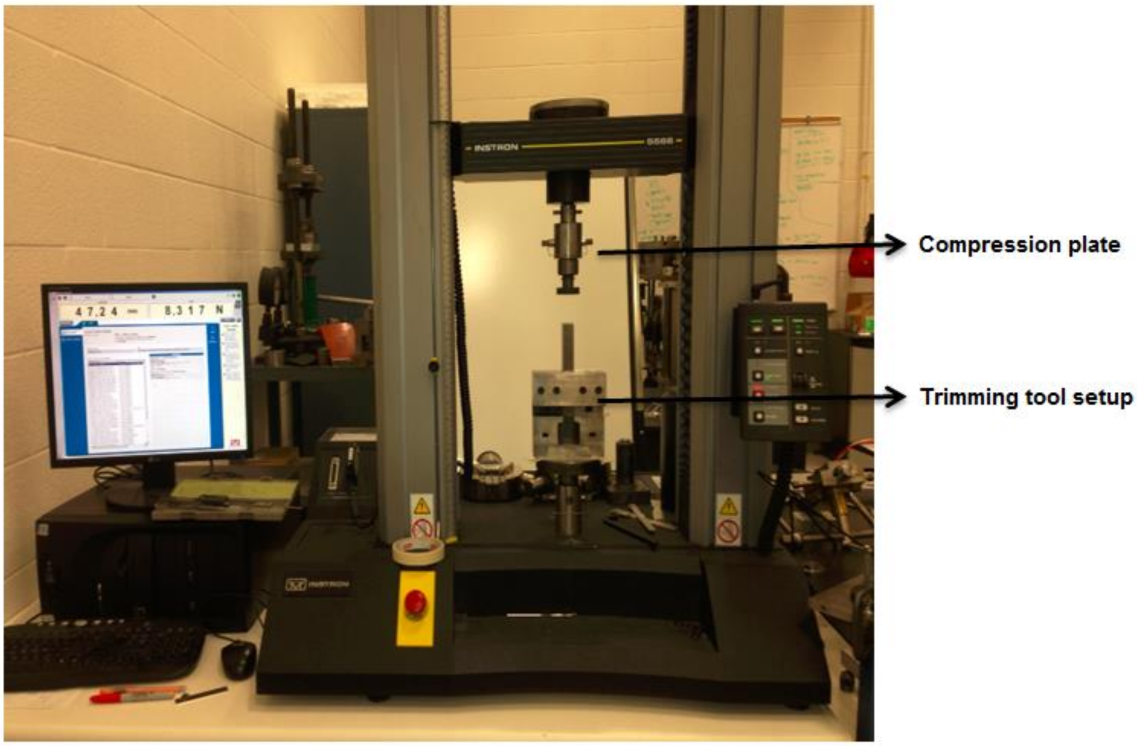

Figure 3-2. INSTRON 10 KN mechanical test system for trimming test.

3.2.3. Tool setup configuration

The tool setup used for trimming test is shown in Figure 3-3. An existing trimming test rig available in the Metal Forming Laboratory was modified and improved. Two tool setup configurations, were utilized; (i) a conventional tool setup that consisted of punch, blank-holder and die (see Figure 3-3(a)), and (ii). an alternative tool setup configuration that consisted of punch, blank-holder, die, and a steel and an elastic (foam) cushion both located below the clamped test specimen (see Figure 3-3(b)). In the second tool setup configuration, the top of the steel cushion first contacted the bottom surface of the test specimen and the punch moved down together with the steel and EVA-Foam cushion (both elastic) during the trimming process. The main function of the steel and foam cushion was to support the sheet and minimize the effect of excessive rotation of the sheet in the trimming process.

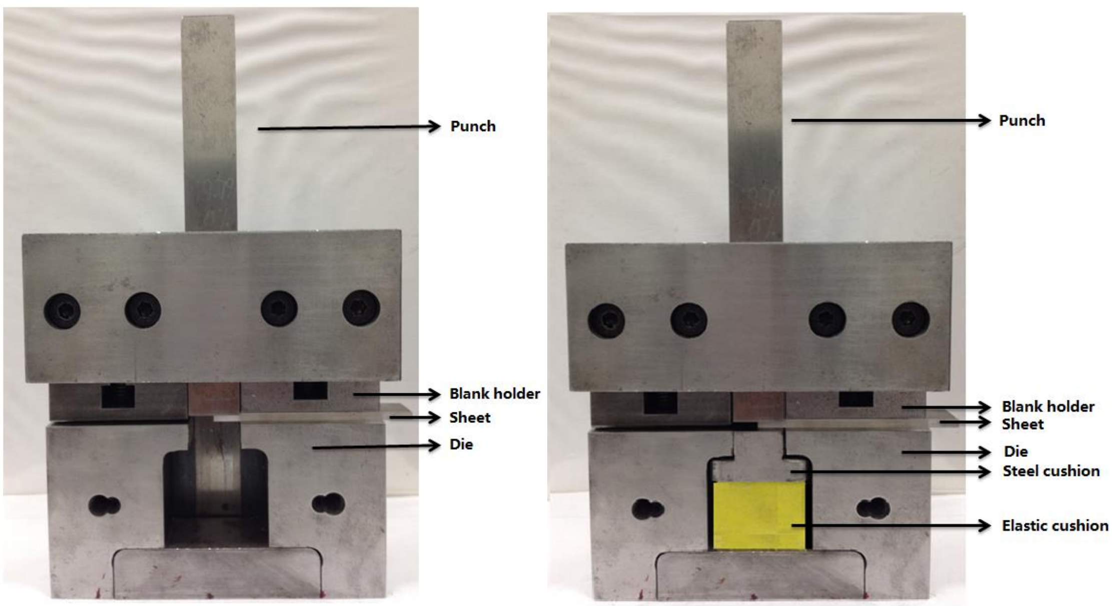

(a). without cushion (b). with cushion

Figure 3-3. Tool setup configuration for trimming test.

3.2.4. Experimental test matrix

Factors reported in the literature that can have significant influence on the quality of trimmed edge of metal sheet include its material properties (mechanical and thermal properties, microstructure, geometry, sheet thickness, sheet orientation (rolling and transverse directions), trimming process parameters (trimming speed, clearance), tool setup configuration and tooling condition (tool wear, lubrication, fixture). In this study, the effects of the factors such as the trimming process parameters: punch speed and clearance, tool setup configuration as described above, sheet thickness and sheet orientation were considered for assessing the trimming behaviour of AZ31 and ZEK100 sheets. The trimming test matrix is presented in Table 3-2, and the test conditions for investigating the effect of each factor are given in Tables 3-3 to 3-6. To obtain more representative experimental results, the trimming test for each test condition was repeated 5 times. All of the tests were conducted at room temperature (20°C).

Table 3-2. Experiment matrix for trimming test.

Experiment Matrix	
Materials	Magnesium sheet material: AZ31 and ZEK100
Tool setup configuration	1. Die, punch, blank-holder
	2. Die, punch, blank-holder, cushion
Clearance /thickness	4%, 11% , 20% , 26%
Trimming speed	0. 1 mm/sec, 1 mm/sec, 3 mm/sec, 5 mm/sec
Sheet Orientation	TD, RD
Thickness	1.58 mm, 3 mm
Number of repeat tests/test condition	4 or 5 times

Table 3-3. Test conditions for effect of trimming speed.

AZ31&ZEK100	Trimming speed (Punch speed)			
Tool setup configuration without cushion, Clearance: 11%	0.1mm/sec	1mm/sec	3mm/sec	5mm/sec

Table 3-4. Test conditions for effect of clearance and tool setup configuration.

AZ31&ZEK100	Clearance (/thickness)			
Tool setup configuration without cushion, Trimming speed: 5 mm/sec	4%	11%	20%	26%
Tool setup configuration with cushion, Trimming speed: 5 mm/sec	----	11%	----	----

Table 3-5. Test conditions for effect of sheet orientation.

AZ31&ZEK100	Trimming Direction	
Tool setup configuration without cushion, Clearance:11%, Trimming speed:5mm/sec	RD	TD

Table 3-6. Test conditions for effect of sheet thickness.

AZ31	Sheet Thickness	
Tool setup configuration without cushion, Clearance: 4%, Trimming speed: 5 mm/sec	1.58 mm	3.20 mm

3.2.5. Observations of trimmed edge

Figure 3-4 (a,b) shows the typical profile of through-thickness trimmed edge and the corresponding fracture surface of cross section of sheet respectively. Based on published literature on sheet trimming, rollover depth, burnish depth, fracture depth, burr height were considered to be the most important parameters to assess the quality of trimmed edge. Therefore, the microscope image of the trimmed surface was divided into four parts: rollover zone, burnish zone, fracture zone and burr (see Figure 3-4(a)).

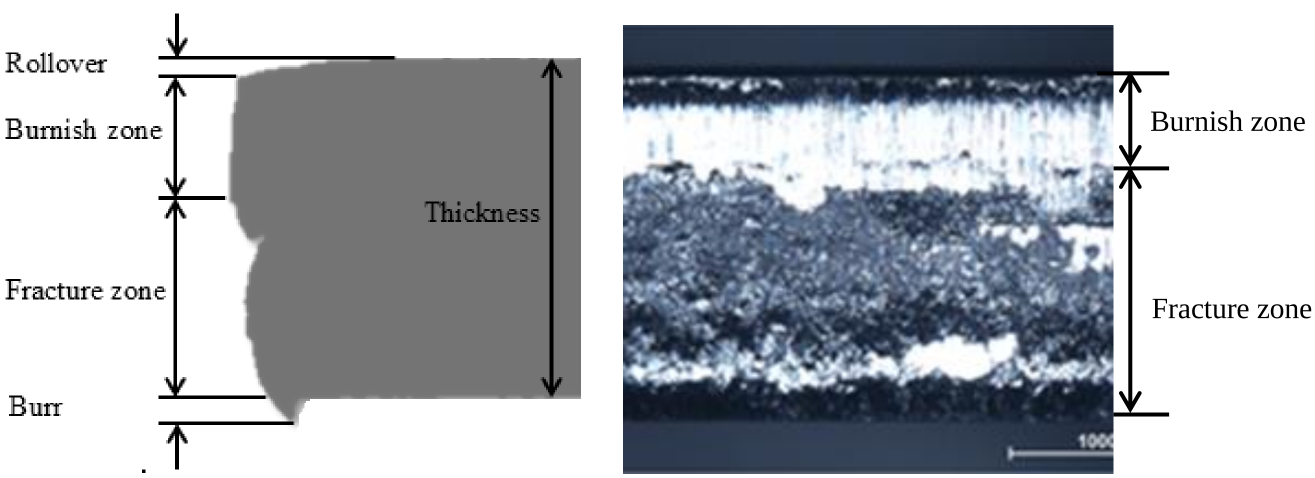

(a) (b)

Figure 3-4. The typical profile of trimmed edge (a) profile through thickness, (b) fracture surface of cross section.

For these measurements, the following procedure was adopted. The trimmed surface was first observed using Nikon Stereoscope (Model: AZ-STDM), and the burnish depth was measured (Figure 3-4 (b)).

Then the trimmed specimens were cold mounted in a cylindrical container and filled with epoxy resin and epoxy hardener in proper proportion. After that, the mounted specimens were ground and polished to obtain a smooth surface. Finally, the epoxy mounted specimen was observed using a microscope equipped with a camera to record the trimmed edge profile and measure the burr height, rollover and fracture depths. The photographs of the trimmed edge were also used for comparing with the others produced from different trimming process conditions. Because each trimming test was typically conducted 4 or 5 times, all the values of trimmed edge parameters in this thesis are the average values.

3.3. Uniaxial tensile test

The tensile test is the most widely used test to characterize the mechanical properties of materials, such as Young's modulus, yield strength, anisotropy coefficient and work hardening behavior. In order to obtain *R*-value and fracture strain, tensile test samples of AZ31 and ZEK100 Mg sheets were prepared according to standards established by the American Society for Testing and Materials (ASTM) as shown in Figure 3-5. The specimens had a gauge length of 31.75 mm and width of 6.35 mm, thickness of 1.58 mm (for AZ31) and 1.53 mm (for ZEK100). The specimens were cut with the length dimension oriented along RD (rolling direction), 45° to the rolling direction and TD (transverse direction) as shown in Figure 3-6.

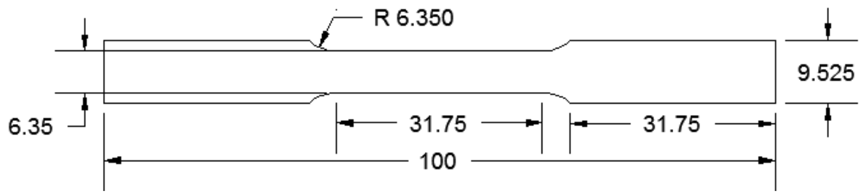

Figure 3-5. Geometry of the uniaxial tensile test specimen (dimension in mm).

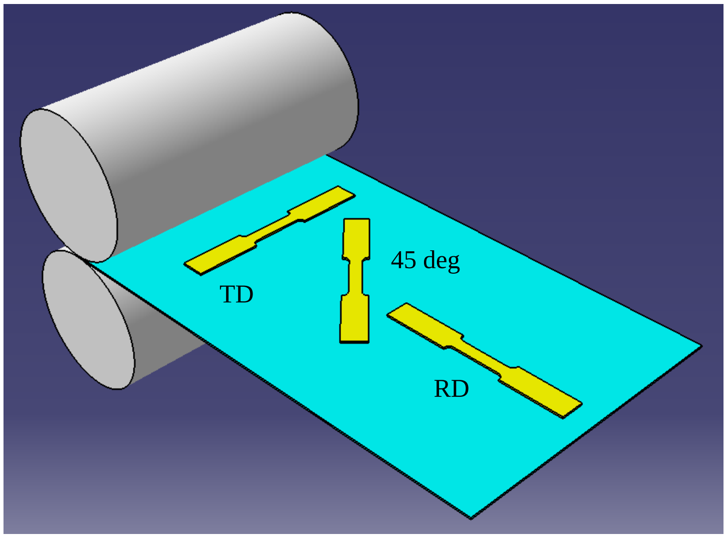

Figure 3-6. Uniaxial tensile test specimens oriented different directions.

The uniaxial tensile tests were conducted using INSTRON 10 KN mechanical test system as shown in Figure 3-7. The samples were loaded until the fracture occurred. The gage length of the test specimen was continuously recorded by Aramis camera. Aramis is a computer-based optical strain analysis system equipped with a camera, data acquisition board, and analysis software that can provide incremental and total strains by comparing the images of selected deformed region and its undeformed image based on a well established method called Digital Image Correlation (or DIC). A fine stochastic (or random) speckle pattern needs to be pre-applied to the region of test specimen undergoing deformation for DIC method to enable strain mapping. Therefore, gage length of the tensile test specimens was pre-applied with a random speckle pattern using a spray can filled with white ink and fitted with an air brush. To obtain representative experiment results, two or three specimens along each orientation were tested with an initial strain rate of 0.001/s at room temperature (20° C).

ARAMIS camera

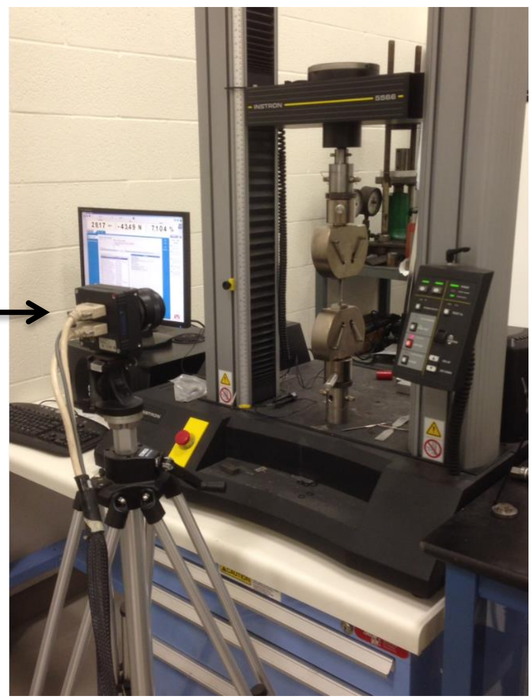

Figure 3-7. Tensile test load frame with tripod mounted ARAMIS camera for strain mapping of the gauge region of the test specimen.

By combining the continuously recorded load data from the load cell with Aramis-based strain data from the gauge region, the flow stress-strain curves were obtained for the two experimental sheet materials in RD, 45°and TD orientations. These are plotted in Figure 3-8(a-b).

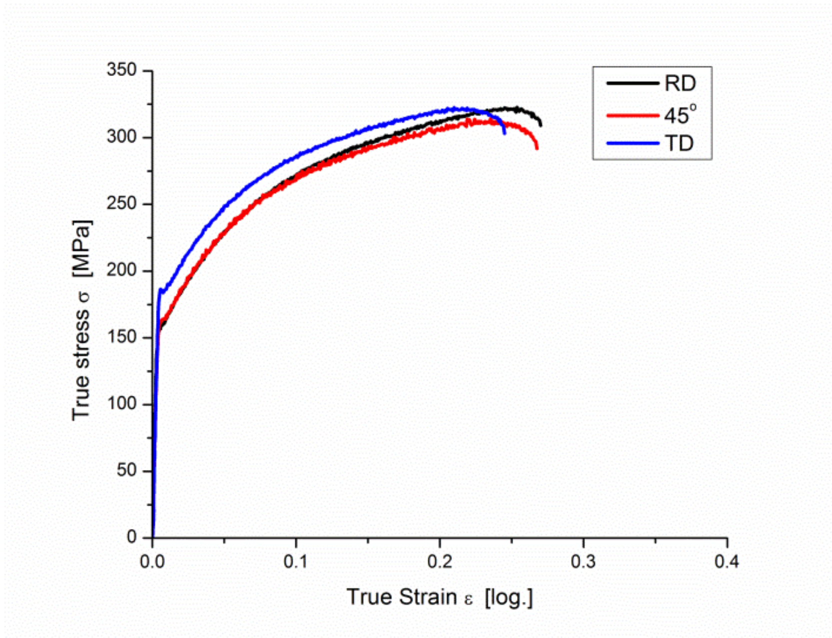

(a). AZ31

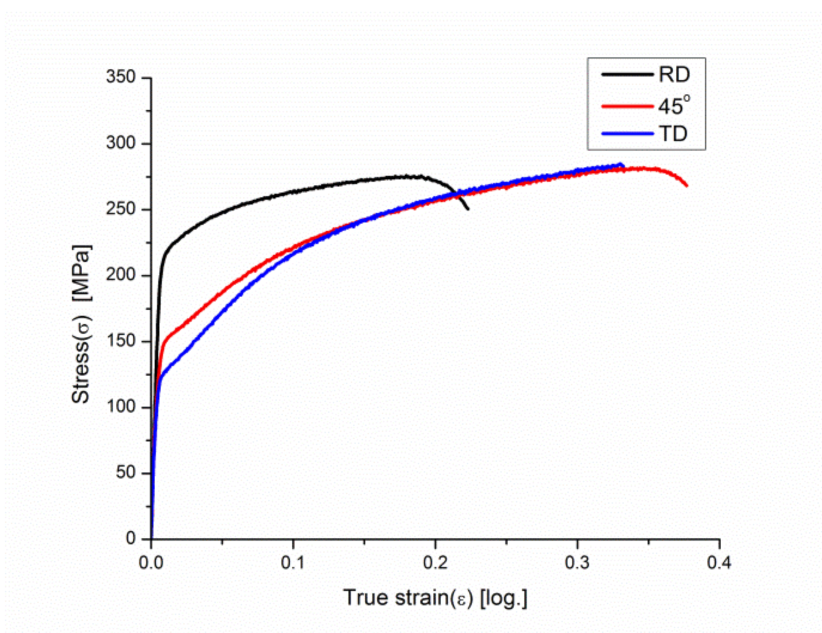

(b). ZEK100

Figure 3-8. Flow strain-stress curves measured for AZ31and ZEK100 at room temperature.

The flow curves for AZ31 show higher yield and flow stress but a slightly lower fracture strain value along TD direction compared to 45° and RD directions, see Figure 3-8 (a). The flow curves and yield stress in 45° and TD are nearly the same. On the contrary, the yield stress for ZEK100 in RD is much higher than 45° and TD, see Figure 3-8 (b).The difference in the flow curves and yield stress is much less pronounced between 45° and TD. From the comparison between AZ31 and ZEK100, it can been seen that yield stress in RD for AZ31 is much less than that for ZEK100, and the yield stress in 45° and TD are higher than that for ZEK100, the ultimate tensile stress for AZ31 is much higher but the total strain to fracture is less than that for ZEK100. The difference in yield stress, ultimate tensile stress and fracture strain along different orientations are expected to result in different response of punch load-displacement characteristics for AZ31 and ZEK100 as presented in Section 5.1.1.6. The differences in R-values for the two materials may also influence their relative punch-displacement curves. ZEK100 is reported to be more ductile than AZ31 sheet because of the rare earth elements in ZEK100 that make its texture distribution more randomly distributed than that AZ31 (Boba et al. 2012). The selection of flow stress-strain curve for Finite Element model is presented in Section 4.4

The local fracture strain along length direction of the specimen was also obtained from ARAMIS as shown in Table 3-7. The fracture strain was used to calculate the constants associated with the various fracture criteria for finite element simulation of trimming. Details related to fracture criteria will be presented in Chapter 4.

Table 3-7. Local fracture strain along sheet orientation for AZ31 and ZEK100.

Mg alloy	RD	TD
AZ31	0.408	0.426
ZEK100	0.509	0.468

The *R*-value used to characterize the anisotropy of a sheet metal is defined as $R = \varepsilon_w^{pl}/\varepsilon_t^{pl}$, where ε_w^{pl} and ε_t^{pl} are the plastic strains in the width and thickness directions respectively. By assuming the material incompressibility, the plastic strain ε_t^{pl} through the thickness can be calculated using the following equations:

$$\varepsilon_t^{pl} = -(\varepsilon_w^{pl} + \varepsilon_l^{pl}), \tag{3.1}$$

$$\text{or } R = -\varepsilon_w^{pl}/(\varepsilon_w^{pl} + \varepsilon_l^{pl}) \tag{3.2}$$

The strains ε_w^{pl} and ε_l^{pl} at all levels of the deformation were obtained from Aramis data. For sheet metals, the *R*-values are usually determined for three different directions (RD, 45° and TD), and the normal *R*-value is taken to be an average given by:

$$R_{Av} = \frac{1}{4}(R_{RD} + 2R_{45^\circ} + R_{TD}) \tag{3.3}$$

The variation of *R*-values with plastic strain for AZ31 and ZEK100 are plotted in Figure 3-9 (a,b) respectively. It can be seen that the different orientations show rather large differences in R-values for AZ31 when compared to ZEK100, which demonstrates that AZ31 exhibits stronger anisotropy than ZEK100 sheet.

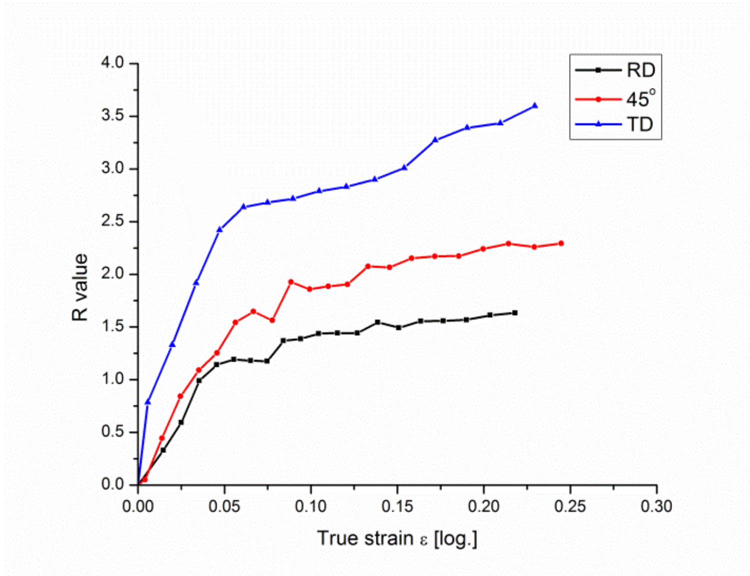

(a). AZ31

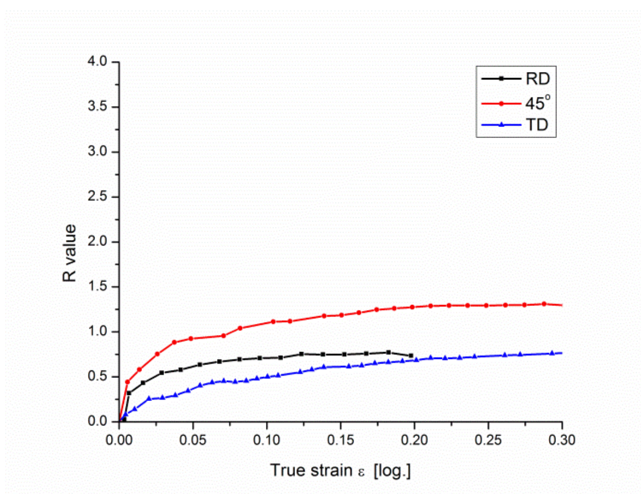

(b). ZEK100

Figure 3-9. R-values versus longitudinal strain for AZ31and ZEK100 sheets tested at room temperature.

In practice, the R value is usually measured within a strain range of 5%~20% in tensile test. In this thesis, the R-values corresponding to the strain of 15% were utilized in quadratic Hill yield criteria and various fracture criteria for FE simulations of trimming. The R-values are presented in Table 3-8 below.

Table 3-8. Normal R-values for AZ31 and ZEK100 at room temperature.

AZ31	**RD**	**45°**	**TD**
R-value	1.5	2.1	2.9
R-Average	2.15		
ZEK100	**RD**	**45°**	**TD**
R-value	0.75	1.26	0.65
R-Average	0.98		

3.4. Plane strain test

Plane strain tensile test was utilized to determine the plane strain fracture limit to obtain fracture criteria parameters in the trimming models. The in-plane plane strain loading state in sheet materials is typically achieved by selecting short gauge length and wide width specimens. Typically, the specimen gauge width is taken to be at least 8 times the gauge length of the specimen. The specimen geometry for plane strain test chosen for the present study is shown in Figure 3-10 where the specimens had overall dimensions of 208.5 mm in length and 100 mm in width with a gauge length of 4.5 mm and width of 80 mm. The specimens were oriented in RD (rolling direction) and TD (transverse direction). The plane strain tests were conducted with an initial strain rate of 0.001/s using a 250kN mechanical test system at room temperature. The specimen grips mounted on the test system for the plane strain test are shown in Figure 3-10(b).

ARAMIS optical system was used to measure the strain evolution in the gauge area of specimen during the plane strain test. The local fracture strain along length direction of specimens oriented RD and TD under plane strain condition listed in Table 3-9.

Table 3-9. Fracture strain for AZ31 and ZEK100 Magnesium alloy in plane strain test.

Mg alloy	RD	TD
AZ31	0.085	0.0875
ZEK199	0.176	0.142

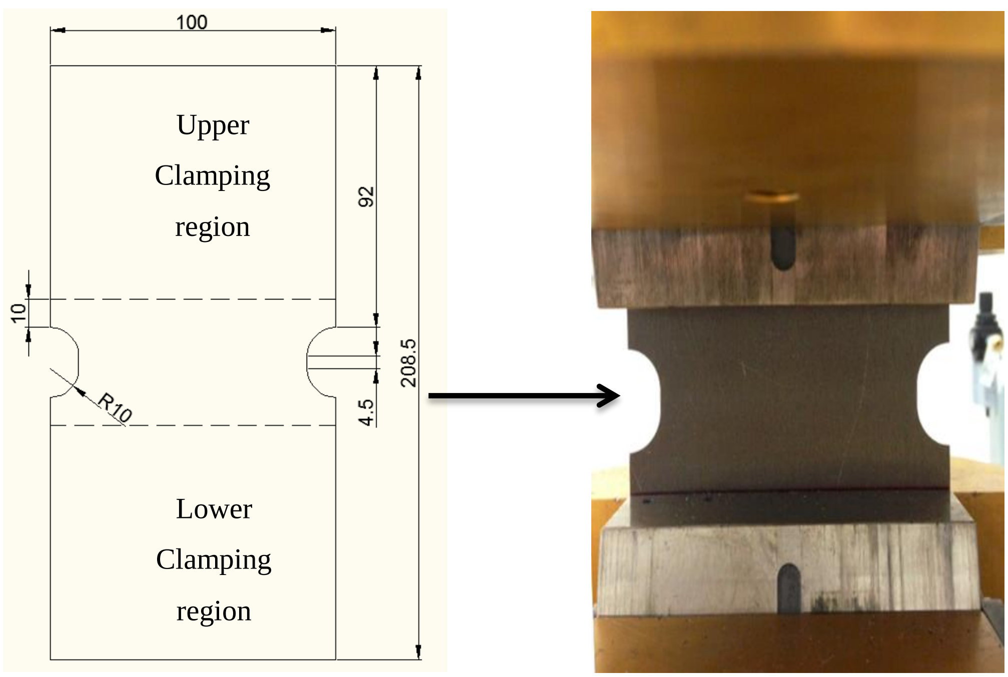

(a) (b)

Figure 3-10. Plane strain test details, (a) geometry of the specimen (dimensions in mm), and (b) clamping grips for plane strain test.

3.5. Summary

This chapter presented the procedural details about various experiment tests related to trimming process. From a large matrix of trimming tests and repeat tests for each of the trimming conditions, reliable and representative experiment data about the punch load-displacement curves and quantitative trimmed edge parameters for AZ31 and ZEK100 sheets were obtained. This data is presented in Chapter 5. From the uniaxial tensile test, the material constitutive models of flow stress-strain curves were obtained and implemented in FE simulation of trimming. In addition, R-values as a measure of anisotropy and uniaxial fracture limit were determined from uniaxial tension test data. Plane strain fracture limit was obtained from separate plane strain tension tests. Uniaxial and plane strain limits were used to determine the parameters for various ductile fracture criteria in the FE models of trimming as shown in Chapters 4 and 5.

Chapter 4. Finite Element Modelling of Trimming Process

4.1. Introduction

Finite Element (FE) method is an important technique to analyze and predict the status of stress, strain, plastic instability and damage development in metal forming processes. In this chapter, procedural details, assumptions and methods involved in FE modeling of the trimming process of AZ31 and ZEK100 magnesium alloy sheets are presented. Various aspects of the FE modelling that include analysis type, geometry and materials modeling, boundary conditions, contact definition, meshing, mass scaling, ductile fracture criteria and user-defined mechanical material behavior subroutine VUMAT are presented.

4.2. Analysis type

General purpose commercially available FE code, ABAQUS/Explicit has been extensively utilized in analyzing problems in the automotive, aerospace, and other material and manufacturing sectors. The code is quite popular due to its wide material modeling capability and high efficiency for solving various linear and nonlinear problems in solid mechanics. ABAQUS “Explicit, Dynamics” analysis is particularly well-suited to simulating large, nonlinear, quasi-static analyses problems in sheet metal forming. Since trimming is a high-speed metal forming process with large deformation and complex contact between the sheet and the tools, Abaqus/Explicit, version 6.12, was selected for simulating the current laboratory based trimming experiments.

4.3. Geometry of FE Model

The two primary FE model geometries for the trimming process are presented schematically in Figure 4-1 (a-b).

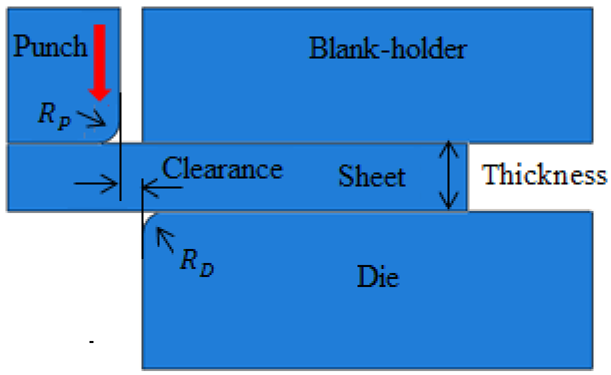

(a). Tool setup configuration without cushion.

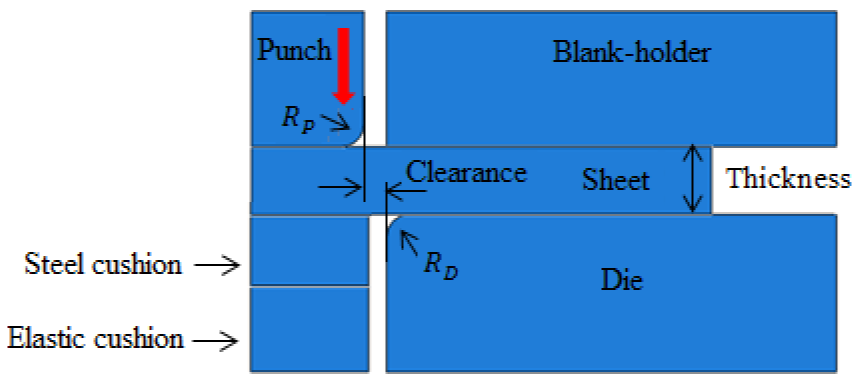

(b). Tool setup configuration with cushion.

Figure 4-1. Geometry of finite element model of trimming process (a) tool setup configuration without cushion, (b) tool setup configuration with cushion.

As in the experiments, the sheet is clamped between the blank-holder and die with a pressure. The punch is moved vertically downward at a certain speed to trim the sheet. The punch and die have a small profile radius of 0.05 mm. The clearance between the punch and die was set to 4%, 11%, 20%, and 26% of sheet thickness as in the experiment. The thickness of the AZ31 and ZEK100 sheets in FE model were 1.58 mm and 1.53 mm respectively.

In FE model, the trimming process was simplified to two-dimensional problem under plane strain condition to reduce the computational effort without sacrificing accuracy of the model. This is because the ratio of the width to thickness of sheet in experiment was over 10:1 and the deformation in the width direction could be ignored. Also, as in simulations of many other metal forming processes by the FE method, the tool set-up (punch, die, blank-holder, steel cushion) were treated as un-deformable (or rigid). An important advantage of treating tool set-up as rigid bodies is to reduce the calculation of the data of nodes and elements associated with the tools, so that, the computational time could be effectively reduced. The emphasis was therefore placed on obtaining the stress, strain and fracture characteristics of deformable test specimen. The sheet material was, therefore, defined as an elastic-plastic body.

4.4. Material modelling

AZ31 and ZEK100 magnesium sheets, were considered as elastic, non-linear plastic materials, and anisotropic whereas the cushion component (foam) was considered as an elastic material. The Young’s Modulus and the flow curves of AZ31 and ZEK100 Mg alloy sheet used in FE model were obtained by conducting the tensile test mentioned in Chapter 3. The elastic properties of the above materials for use in the FE model are presented in Table 4-1.

Table 4-1. The material properties implemented in FE model.

Parts	**Metal Sheet**		**Elastic cushion**
Materials	AZ31	ZEK100	EVA-Foam
Part type	Deformable	Deformable	Deformable
Density	1780 kg/m^3	1780 kg/m^3	105 kg/m^3
Young's Modulus	45 GPa	37 GPa	0.6861 MPa
Poisson's ratio	0.33	0.3	0.45

Modified Fields-Backofen constitutive equation was found to accurately fit the experimental strain-stress curves of AZ31 and ZEK100 sheet materials. This equation is expresses as:

$$\sigma = a\varepsilon^b \exp(-cT - d\varepsilon) + e \quad (4.1)$$

where σ, ε and T are material flow stress, plastic strain and temperature (in Kelvin) respectively and the parameters *a*, *b*, *c*, *d*, and *e* are non-linear fit parameters. Since magnesium sheets were anisotropic materials, there were some differences between the flow stress-strain curves along rolling and transverse directions. However, this difference was relatively small, and for simplicity, the FE models of trimming utilized stress-strain curves along the sheet rolling direction (RD) as input. The yield behavior for AZ31 and ZEK100 was assumed to obey Hill quadratic anisotropic yield criteria. This yield function can be written as:

$$\overline{\sigma}^2 = F(\sigma_{22} - \sigma_{33})^2 + G(\sigma_{33} - \sigma_{11})^2 + H(\sigma_{11} - \sigma_{22})^2 + 2L{\sigma_{23}}^2 + 2M{\sigma_{31}}^2 + 2N{\sigma_{12}}^2 \quad (4.2)$$

where *F, G, H, L, M* and *N* are Hill's anisotropic parameters, which can be expressed by the following Lankford's coefficients:

$$F = \frac{R_0}{R_{90}(R_0+1)} \tag{4.3}$$

$$G = \frac{1}{R_0+1} \tag{4.4}$$

$$H = \frac{R_0}{R_0+1} \tag{4.5}$$

$$N = \frac{(R_0+R_{90})(1+2R_{45})}{2R_{90}(R_0+1)} \tag{4.6}$$

The Lankford's coefficients $R_0,\ R_{45},\ R_{90}$ represent the anisotropy values measured along $0^{\mathrm{o}}, 45^{\mathrm{o}}$ and 90^{o} orientations in uniaxial tensile test. The values of parameters *L*, *M* and *N* were assumed equal to each other.

4.5. Contact definition

Contact control algorithmic plays an important role when simulating the contact interactions between different parts in non-linear large deformation plasticity problems involving contact between rigid and deformable bodies. In the contact algorithms, rigid or elastic surfaces of higher Young's modulus than the workpiece are usually defined as the so-called 'master' surface, and the deformable sheet is treated as 'slave' surface. Two common contact discretization options in ABAQUS are "surface-to-surface" and "node-to-surface" contacts. The latter involves contact between the nodes on the slave surface and a segment of the master surface.

In the FE model of trimming process, the contact interactions need to be established between punch and sheet, sheet and blank-holder, sheet and die, and sheet and cushion. Especially, the contacts between sheet and punch, and sheet and die tend to be complex because there is large deformation of sheet occurring around the sharp corners of the punch and die. Also, new fracture surface is generated in the trimming process, and, correspondingly, new contact between the punch and the fracture surface of the sheet arises. Typically, the contact interactions between different parts are specified in advance for each known contact surface before the program is run. Since the exact location where fracture surface will be generated during the trimming process is unknown, *a priori*, it is difficult to define the contact between the punch and the new fracture surface. Further, in order to avoid the excessive penetration of the punch (as the master surface) into the sheet punch, all nodes in the sheet in the trimming zone are defined as node surface, and "node to surface" contact discretization method was implemented to handle the contact between the punch and sheet as well as the die and the sheet. Furthermore, the mesh size in the trimming zone was kept quite small so that the effect of punch penetration of punch could be minimized. The friction between sheet and tool set-up (punch, blank-holder, die, steel cushion) was assumed to follow the standard Coulomb's friction law as shown below:

$$\sigma_f = \mu \sigma_n \tag{4.7}$$

where σ_f and σ_n the are the friction and normal interaction stresses, and μ is the friction coefficient. A μ-value of 0.1 was assumed in the FE simulations based on data in the literature and separate simulation trials with different μ-values.

4.6. Boundary conditions

Accurate boundary conditions in the model were critical in capturing the experimental trimming characteristics. It is to be noted that the trimming model of tool setup configuration with cushion had two more boundary conditions compared to the model without the cushion. The trimming process was simulated in two steps. For example, for trimming with cushion, the sheet was first clamped between the blank holder and die. The blank- holder, die and elastic cushion were then constrained in all three degrees of freedom but the punch and steel cushion were constrained only along X and Y directions. Second, the punch was moved axially (or in Z direction) downward to trim the sheet.

4.7. Meshing

Meshing is the one of the most important steps in FE modelling of the trimming process because the selection of mesh directly affects the accuracy of results and the computation time. Especially for the fracture problem, such as in the trimming process, the mesh quality has a bearing on the profile of the trimmed edge in the simulations. The models were set-up with 4-node bi-linear plane strain quadrilateral elements (CPE4R) with reduced integration and hourglass control. Because the material was subjected to high level of stress and larger deformation in the trimming zone between die and punch, a very dense mesh was used in this region whereas a coarse mesh was utilized away from the trimming zone to reduce the computation time as shown in Figure 4-2.

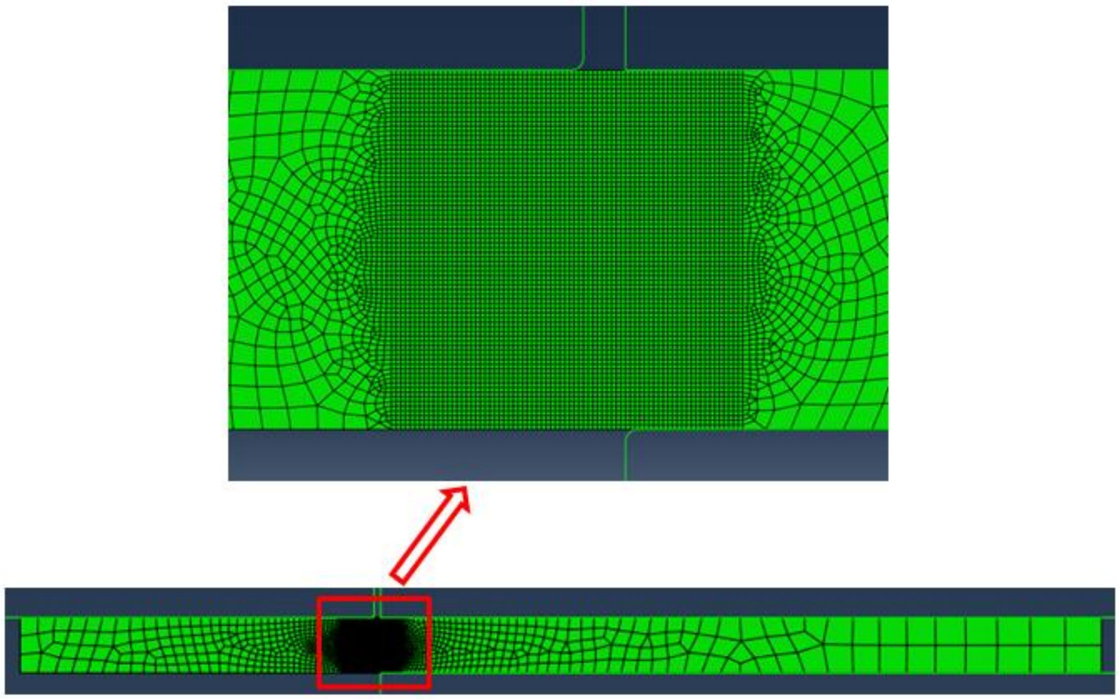

Figure 4-2. Mesh characteristics of the deformable sheet in the trimming models at 2 magnification levels to illustrate the very dense mesh in the trimming zone and less dense mesh away from the trimming zone.

Different mesh density in different regions can accurately reflect the distribution characteristics of stress and strain. Coarse and fine mesh strategy in different regions of the sheet not only improved the accuracy of simulation results, but also decreased the overall computation time. Also, the element deletion method was used to simulate the crack propagation and fracture in the trimming zone. However, one big disadvantage of the element deletion method was the consequent mass loss. In order to minimize the effect of mass loss, separate simulation trials were conducted with 3 different mesh lengths; 0.01 mm, 0.02 mm and 0.03 mm and compared with each other. These results are reported in Chapter 5.

Large deformation may excessively distort the mesh to the point that it is unable to provide accurate results or the analysis may terminates due to non-convergence. To avoid such problems, adaptive meshing with Arbitrary Lagrangian-Eulerian(ALE) method was also implemented to minimize effect of mesh distortion.

4.8. Mass scaling method

Mass scaling is an important technique applied to reduce the computational time and improve computational efficiency by adding mass to certain elements in the FE model. In ABAQUS/Explicit, the computational efficiency depends on the stability limit that dictates the maximum time increment. An estimate of stability limit in the explicit dynamics procedure is expressed as:

$$\Delta t = \left(\frac{L^e}{C_d}\right) \tag{4. 8}$$

where L^e is the smallest characteristic element length and C_d is the dilatational wave speed of the material. The dilatational wave speed in a linear elastic material is expressed as,

$$C_d = \sqrt{\frac{E}{\rho}} \tag{4.9}$$

where E is elastic modulus, and the ρ is the material density

It is clear from equation (4.8) that the stability limit is determined by the element size. By combining equations (4.8) and (4.9), one can observe that the material density is inversely proportional to the stability limit. Therefore, for example, if the material density is increased by a factor of f^2, the wave speed will decrease by a factor of f, and the corresponding stable time increment will increase by a factor of f. In order to obtain accurate results, very small mesh size (e.g. 0.02 mm x 0.02 mm) was used in the trimmed zone. Therefore, the stability limit was quite small and the estimated computational time for completing the simulation of whole trimming process was prohibitive. However, the mass scaling was a good choice to improve the computational efficiency. It is obvious that a larger factor f of the material density will result in higher computational efficiency. However, too large mass scaling factors can not guarantee the accuracy of the simulation results. This is because, when using mass scaling, the materials do not reflect their own true inertia. When too large a mass scaling factor is used, the dynamic effects will increase and may cause incorrect simulation results. How to choose a reasonable mass scaling factor that can reduce the computational time and still maintain accuracy of results is a challenge. Several authors (Prior 1994; Huo and Nakamachi 1995) proposed that dynamic effects can be negligible and the overall deformation and strain distribution could be predicted with acceptable accuracy if the mass scaling factor used yields a low ratio of total kinetic energy to total internal energy, such as less than 10%.

In the present work, mass scaling factors such as f =100, 900, 1600, 2500 and 10000 were employed in a separate trimming trial runs, and compared by analyzing the ratio of total kinetic energy to total internal energy and the trimmed edge. The details related to the selection of mass scaling factors are given in Chapter 5.

4.9. Ductile fracture criteria

In order to simulate the crack initiation, propagation and fracture in the trimming zone during the trimming process, five commonly used ductile fracture criteria from the literature, as presented in Table 4-2, were employed, in a separate FE study, to assess their efficacy in predict the trimming process and fracture of AZ31 and ZEK100 magnesium alloy sheet.

Table 4-2. Ductile fracture criteria from published literature.

Ductile Fracture Criteria	**Formula**
Oyane	$\int_0^{\bar{\varepsilon}_f} \left(\frac{\sigma_H}{\bar{\sigma}} + C_1\right) d\bar{\varepsilon} = C_2$
Cockcroft-Latham (C-L)	$\int_0^{\bar{\varepsilon}_f} \left(\frac{\sigma_1}{\bar{\sigma}}\right) d\bar{\varepsilon} = C_3$
Brozzo	$\int_0^{\bar{\varepsilon}_f} \frac{2\sigma_1}{3(\sigma_1 - \sigma_H)} d\bar{\varepsilon} = C_4$
Clift	$\int_0^{\bar{\varepsilon}_f} \bar{\sigma} d\bar{\varepsilon} = C_5$
Rice-Tracy(R-T)	$\int_0^{\bar{\varepsilon}_f} exp\left(\frac{3}{2}\frac{\sigma_H}{\bar{\sigma}}\right) d\bar{\varepsilon} = C_6$

The various symbols utilized for the fracture criteria in Table 4-2 represent the following quantities: $\bar{\varepsilon}$ is the equivalent strain, $\bar{\varepsilon}_f$ is the equivalent fracture strain, σ_1 is the maximum principal stress, $\bar{\sigma}$ is the equivalent stress, σ_H is the hydrostatic stress. The parameters $C_1 \sim C_6$ are material constants that are obtained from uniaxial tensile and plane strain test as mentioned earlier in Chapter 3.

By combining the associated flow rule and Hill's quadratic yield criteria, the stress triaxiality can be expressed as

$$\mu = \frac{\sigma_H}{\bar{\sigma}} = \frac{1+\alpha}{3\sqrt{1+\alpha^2-A\alpha}} = \frac{(1+\beta)(A+2)}{3\sqrt{(2-A)^2(1-\beta)^2+(2-A)(2\beta+A)(2+A\beta)}} \tag{4.10}$$

where parameters A, B , β, α are defined as:

$$A = \frac{2R}{R+1} \tag{4.11}$$

$$B = \sqrt{\frac{(2+2R)(2+R)}{(3+6R)}} \tag{4.12}$$

$$\beta = \frac{\varepsilon_2}{\varepsilon_1} \tag{4.13}$$

$$\alpha = \frac{\sigma_2}{\sigma_1} = \frac{2\beta+A}{2+A\beta} \tag{4.14}$$

where *R* is the coefficient of normal anisotropy, σ_1 and σ_2 are the principal stress, ε_1 and ε_2 are the major and minor principal strains.

For example, if one chooses the Oyane fracture criteria, the fracture integration equation in FE model is usually rewritten in the form of Equation (4.15) to judge the occurrence of fracture by the integral value I_F. If integral value of an element in the trimming zone reaches the critical damage value where the integral value I_F is equal to 1, the element is removed from the mesh.

$$\frac{1}{C_1}\int_0^{\bar{\varepsilon}_f}\left(\frac{\sigma_H}{\bar{\sigma}} + C_2\right)\mathrm{d}\bar{\varepsilon} = I_F \tag{4.15}$$

4.10. Implementation of VUMAT subroutine

One of the problems in FE modelling is that the above fracture criteria, Hill's quadratic yield criterion and constitutive equations are not provided in ABAQUS finite element program. Correct implementation of the proposed method and materials model in FE model is perhaps the most difficult and challenging part in FE modelling. Fortunately, ABAQUS provides a series of interfaces that allow users to implement suitable constitutive equations for their specific problems that are not available in the standard material library of ABAQUS. The user-defined material behavior sub-routine for ABAQUS/Explicit is called VUMAT. As an important technique, VUMAT makes it possible to define any constitutive model or yield criterion in FE model. The input variables of materials properties of VUMAT subroutine for the FE model of trimming process of AZ31 and ZEK100 are listed in Table 4-3, and the state variables which are updated in each increment are presented in Table 4-4.

Table 4-3. Input variables employed in VUMAT subroutine.

Input variables	**Description**
Props(1)	Young's modulus
Props(2)	Poisson's ratio
Props(3-7)	The constant parameters of stress-strain curves
Props(8-9)	The constant parameters of fracture criteria
Props(10)	Temperature

Table 4-4. State variables in VUMAT subroutine.

State variables	**Description**
SDV 1	Equivalent plastic strain
SDV 2	Strain rate
SDV 3	Material point deletion state variable (0/1)
SDV 4	Fracture criteria integration value
SDV 5	Ratio (The form of the ratio depends on the fracture criteria)
SDV 6	Yield strength
SDV 7	Hydrostatic stress

In the present work, for implementing the material model, constitutive equation and the various fracture criteria, a VUMAT subroutine was written in Fortran. A computation flow chart (or scheme) of VUMAT subroutine in the FE model is presented in Figure 4-3, and the interface pertaining to this subroutine is provided in Appendix B.

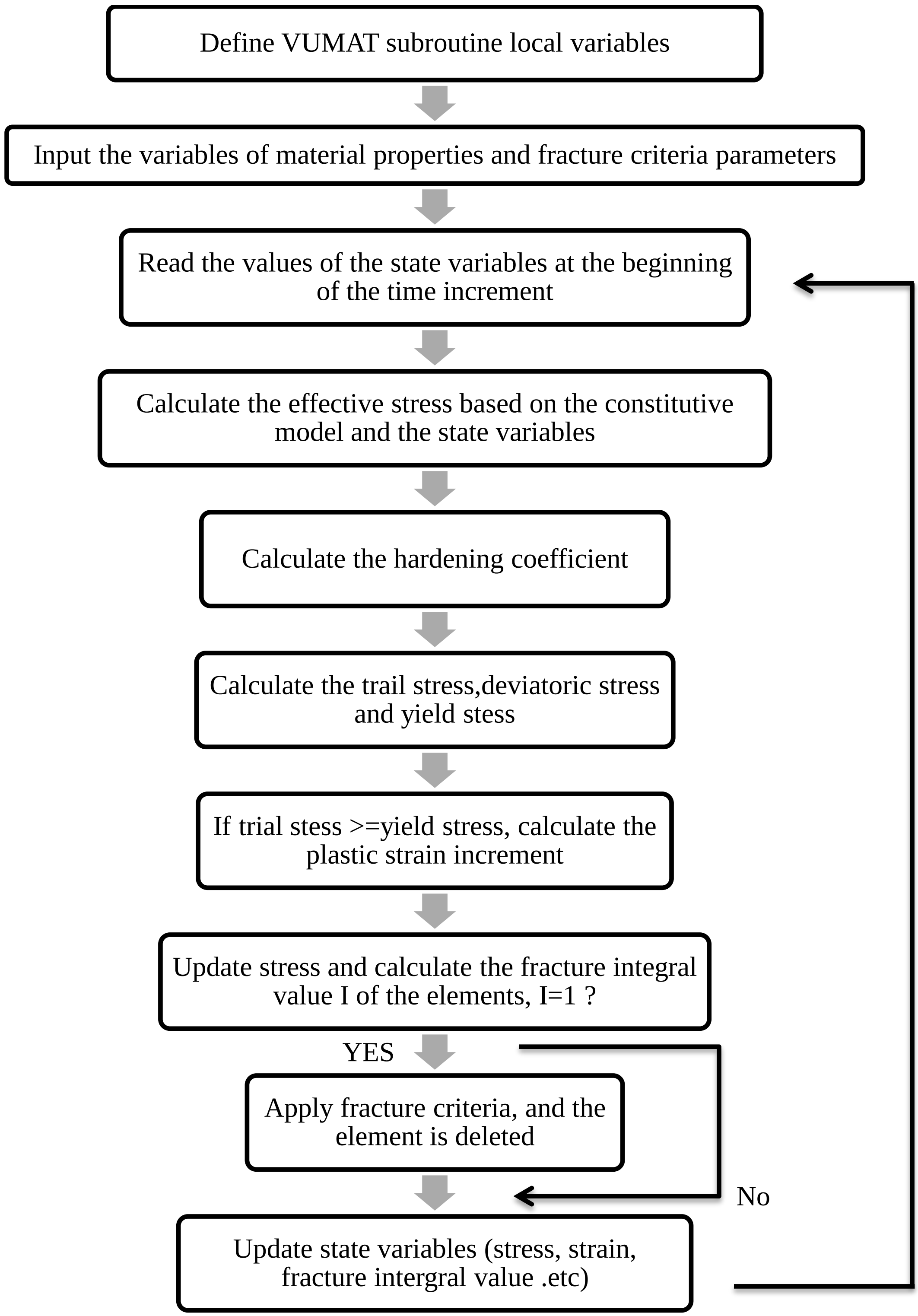

Figure 4-3. Flow chat of VUMAT subroutine.

4.11. Summary

This chapter presented the procedural details of material constitutive model, the tool geometric variables and the loading conditions of the experiments to build a Finite Element model of trimming process for AZ31 and ZEK100 materials. There has been four meshing methods and mass scaling factors and five different empirical fracture criteria (uncoupled damage model) and microstructure-based fracture criteria (coupled damage model) via VUMAT subroutine implemented in FE model, so that optimal modelling parameters for FE model were obtained, and correspondingly, the more accurate trimmed edge parameters and profile could be predicted as shown in Chapter 5. Trimmed edge parameters are considered the most significant attributes of a trimming process and its predictions via FE model can be useful in improving the industrial trimming process for magnesium alloy sheet.

Chapter 5. Experimental and Finite Element Simulation Results

In this chapter, experimental and simulation results from the trimming test and simulations for AZ31 and ZEK100 Magnesium alloy sheets are presented and compared. Experimental and simulation results pertaining to the effect of various factors such as test speed, clearance, tool set-up or configuration, sheet orientation with respect to the trim line (i.e., parallel or perpendicular) and sheet thickness on the trimming punch load-displacement curves and quality of trimmed edge are presented.

5.1. Experimental Results

5.1.1. Punch Load versus Displacement Curves

The punch load versus displacement curves are useful indicators of macroscopic material flow characteristics in metal forming processes.

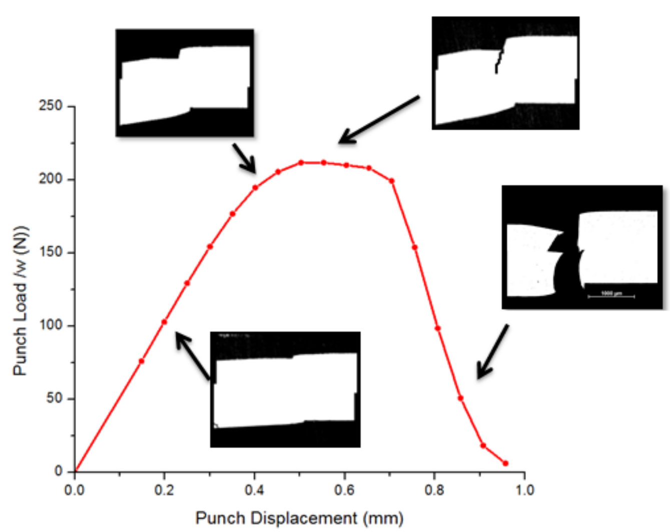

Figure 5-1. Typical stages of trimming process.

Figure 5-1 shows the characteristic feature of punch load-displacement curve from the sheet trimming process. The figure is accompanied by corresponding images in the various stages of trimming.

As shown in Figure 5-1, the trimming process can be divided into four successive steps as follows:

Step 1: Sheet material experiences elastic deformation as shown by the early linear stress-strain response.

Step 2: After elastic deformation, the material in the trimming zone yields and undergoes work hardening that is associated with plastic deformation. The work hardening causes the punch load to non-linearly increase to the peak load.

Step 3: Cracks initiate in the trimming zone when the punch force begins to decrease.

Step 4: Macroscopic crack develops that leads to final rupture making the part and offal separate from each other. Rapid load drop occurs at this stage.

5.1.1.1. Effect of trimming speed

The punch load-displacement curves for AZ31 and ZEK100 sheet with respect to different trimming speed are presented in Figure 5-2 (a, b) respectively. It is to be noted that in Figure 5-2 as well as in all subsequent punch load-displacement curves, the load has been normalized with specimen width to yield load per unit width of sheet. Similar to Figure 5-1, the punch load increases with increase in punch displacement until a peak load is reached, then begins to drop.

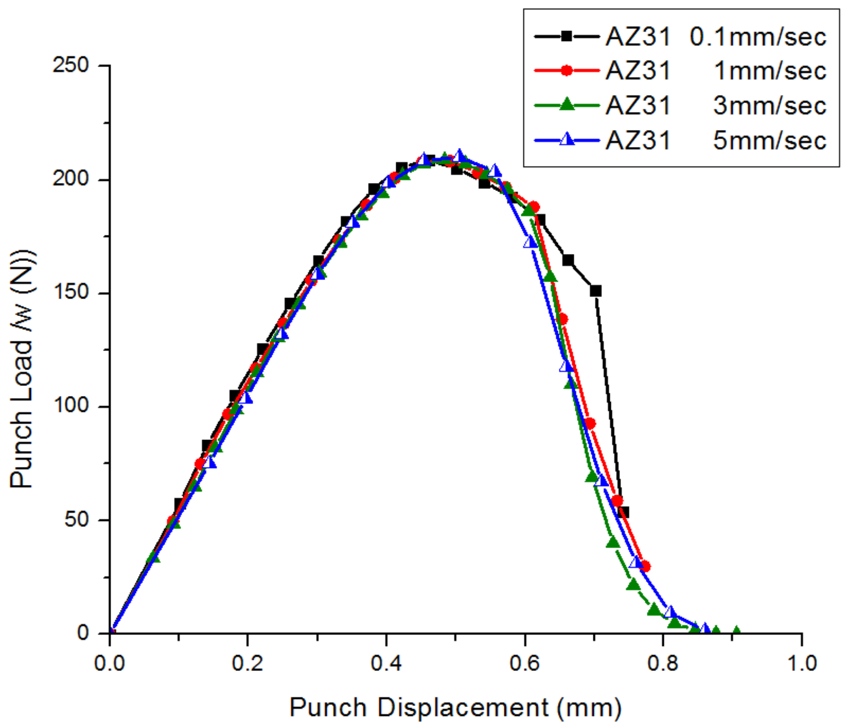

(a). AZ31

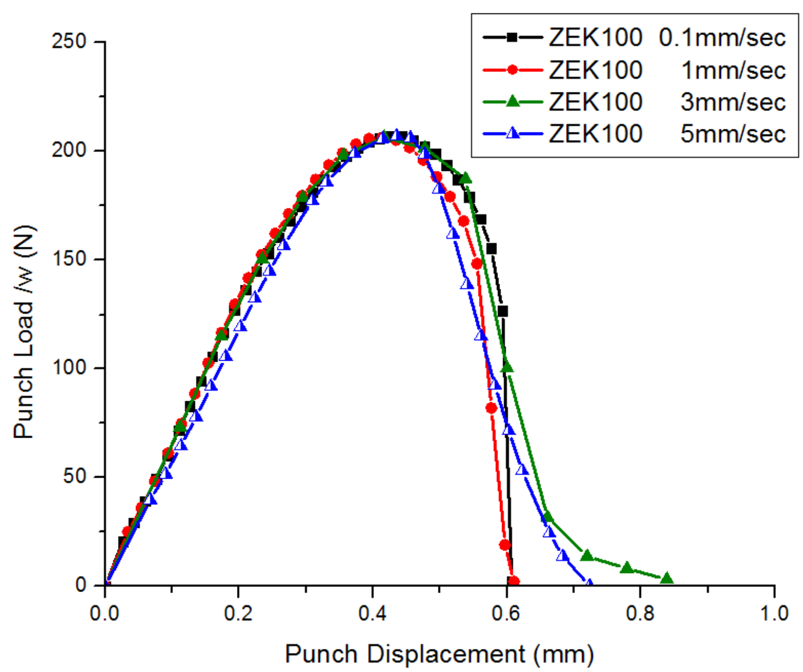

(b). ZEK100

Figure 5-2. Effect of trimming speed on punch load-displacement curves (tool setup without cushion, clearance: 11%, sheet orientation: RD).

As indicated in Figure 5-2 (a-b), for both AZ31 and ZEK100 sheets, trimming speed did not have a large influence on the peak load. Both materials exhibited a somewhat sharper load drop at higher punch speeds. This suggests that a higher trimming speed will produce a faster crack propagation and perhaps a slightly less work will be done in the trimming process. This may yield a slight reduction in the area under punch load-displacement curve at higher punch speeds.

5.1.1.2. Effect of clearance

Figure 5-3 (a-b) shows the plots of punch load versus displacement with respect to four different clearances. The trends consistently reveal an increase in the peak punch load and increase in the slope of the rising part of the curve with a decrease in the clearance between the punch and the die.

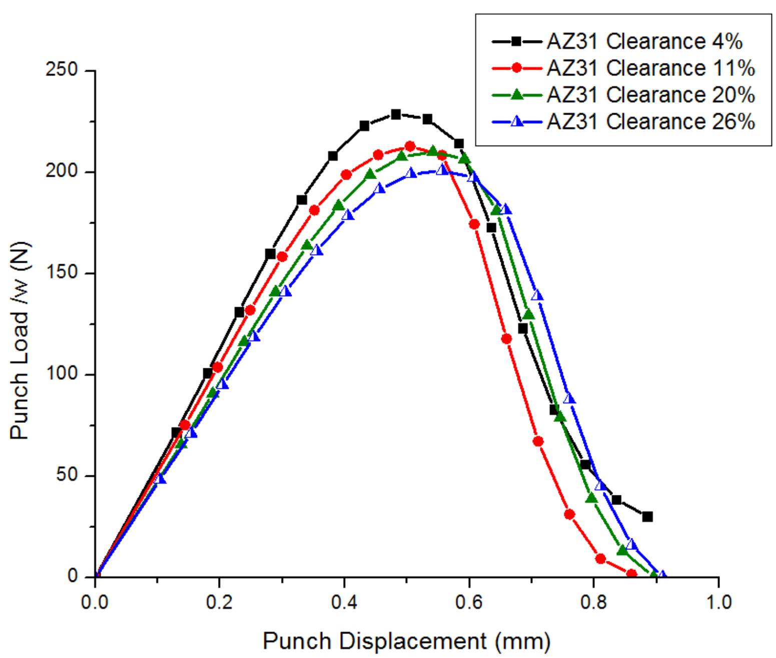

(a). AZ31

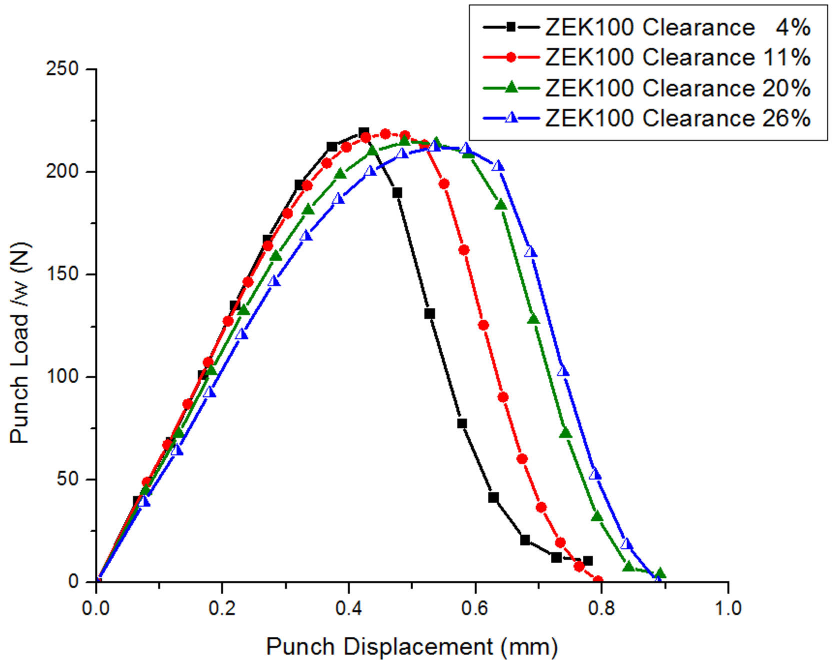

(b). ZEK100

Figure 5-3. Effect of clearance on punch load-displacement curves (tool setup configuration without cushion, trimming speed: 5 mm/sec, sheet orientation: RD).

For both AZ31 and the ZEK100 sheet materials, the punch load-displacement curves show the same trend, i.e., the load peak (maximum load) drops with increase of clearance, and, for smaller clearances, the trimming load decreases rapidly, but for the larger clearance, the decrease in trimming load is not so rapid. For larger clearances, the material dissipates more plastic strain energy (increased work done) and the crack initiates later. According to the area under the punch load-displacement curves, the clearance increases, the more mechanical work is required to complete the trimming process. While trimming is largely a through-thickness shearing process, sheet bending, tension and compression in the trimming zone are also involved. The offal will rotate during the trimming process and a larger clearance is expected to produce more bending effect and more offal rotation, and therefore, more punch penetration and increased plastic deformation will be required for crack initiation to complete the trimming process.

5.1.1.3. Effect of tool setup configuration

Figure 5-4 (a-b) shows the effect of tool setup configuration on the shape of punch load-displacement curves for AZ31 and ZEK100 sheet materials respectively. As shown, the curves are nearly identical for both materials except for the peak load which was higher when a cushion was utilized in trimming. This is because the sheet material is supported from both sides when a cushion is engaged and additional compressive force is required to compress the elastic cushion, and especially the EVA-foam material of the cushion. Reduced rotation of the material in the trimmed zone is expected when a cushion is utilized and this is consistent with reduced plastic work and punch penetration, as well as more rapid rate of load drop past the peak load when the cushion is utilized.

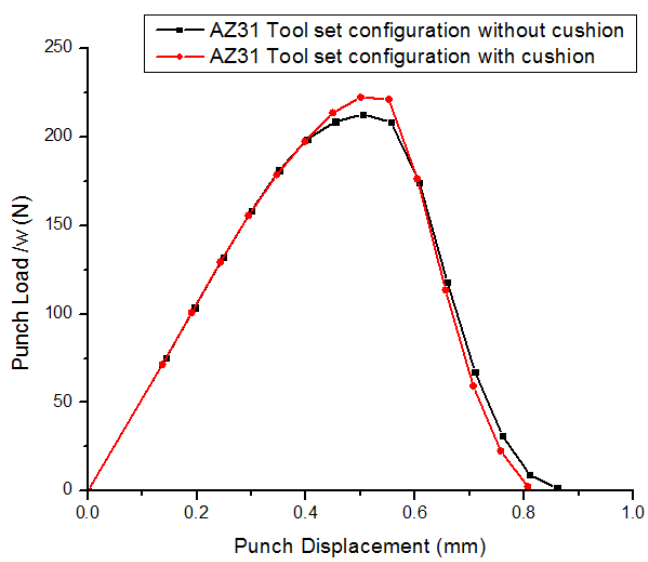

(a). AZ31

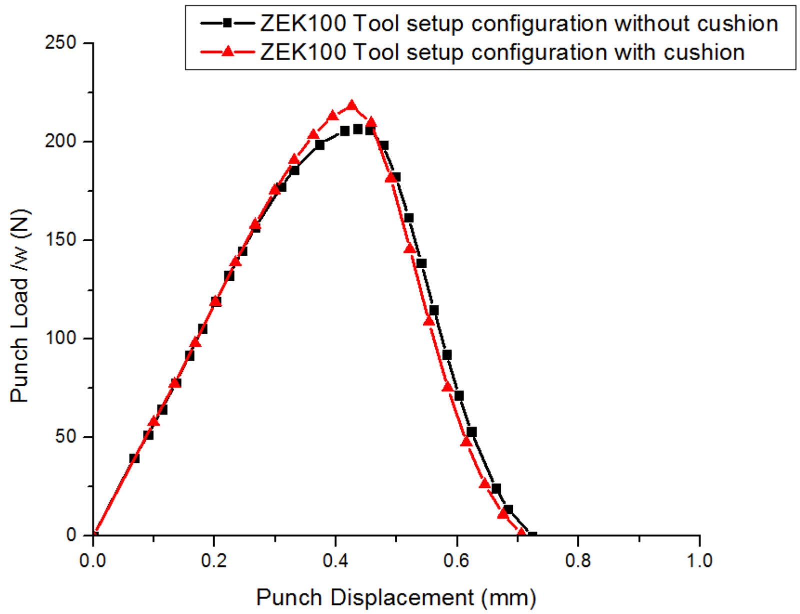

(b). ZEK100

Figure 5-4. Effect of tool setup configuration on punch load-displacement curves (clearance: 11%, trimming speed: 5 mm/sec, sheet orientation: RD).

5.1.1.4. Effect of sheet orientation

The punch load-displacement curves for AZ31 and ZEK100 sheets with different orientation are presented in Figure 5-5(a-b). Both materials exhibit very similar features with respect to the peak load which remains independent of the specimen orientation (with respect to the trimming line). However, a rather large plateau or load saturation is observed for the transverse (or TD) specimens compared to the rolling direction (RD) specimens. This means that crack initiation and fracture is delayed in the transverse specimens and more plastic work is required to complete the trimming process. As mentioned in Chapter 3, both AZ31 and ZEK100 sheets exhibited significant anisotropy (see Figure 3-9) , the flow stress-strain curves and work-hardening capacity along RD and TD were different (see Figure 3-8), and that is why the response of the punch load - displacement curves are also quite different.

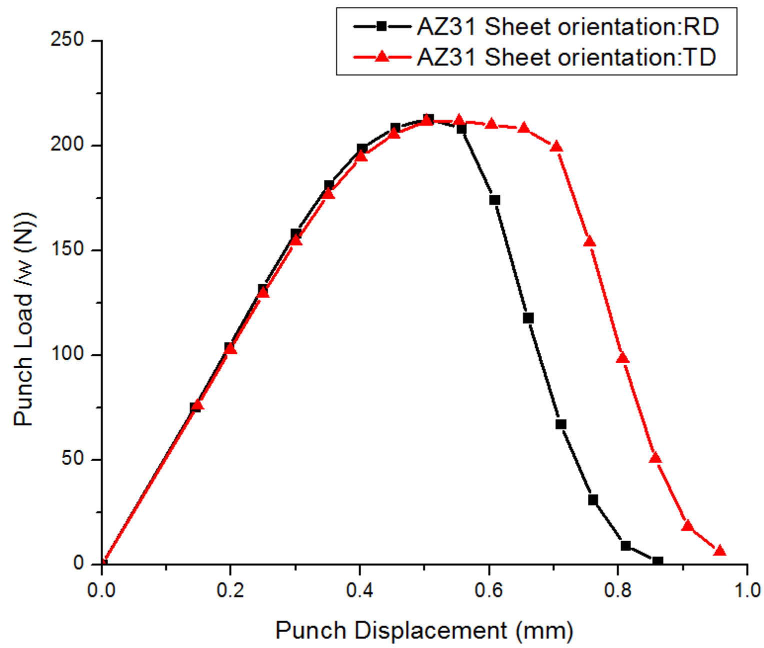

(a). AZ31

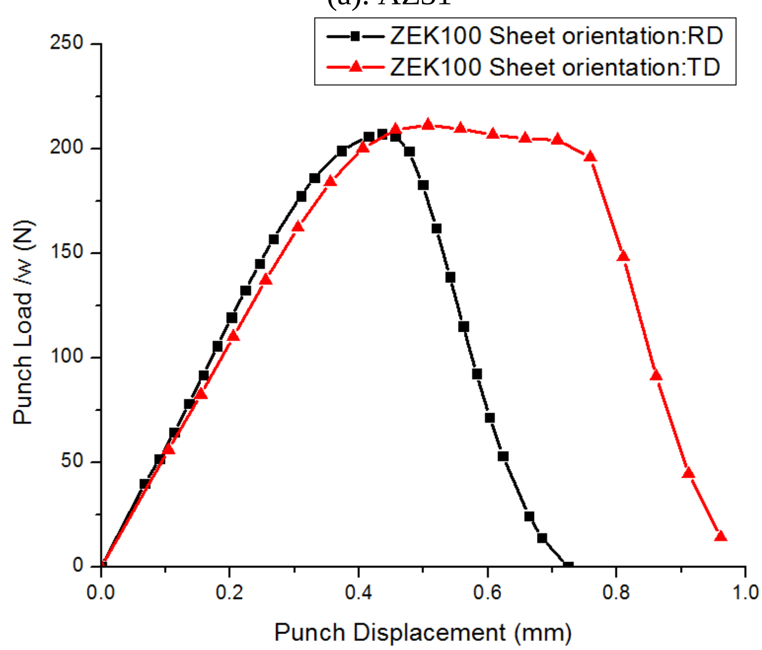

(b). ZEK100

Figure 5-5. Effect of sheet orientation on punch load-displacement curves (tool setup configuration without cushion, clearance: 11%, trimming speed: 5 mm/sec).

5.1.1.5. Effect of sheet thickness

Figure 5-6 presents the punch load-displacement curves for AZ31 sheet for sheet thicknesses of 1.58 mm and 3.20 mm. The peak load with thickness of 3.2 mm is about twice that of the 1.58 mm thickness sheet. This is to be expected as the curves have not been normalized by the sheet thickness. However, the punch displacement at peak load is larger when the sheet thickness is higher. This is because the punch penetration where crack initiates is expected to be proportional to thickness of the sheet. The thicker sheet is subjected to more work and increase punch penetration is required to complete trimming process.

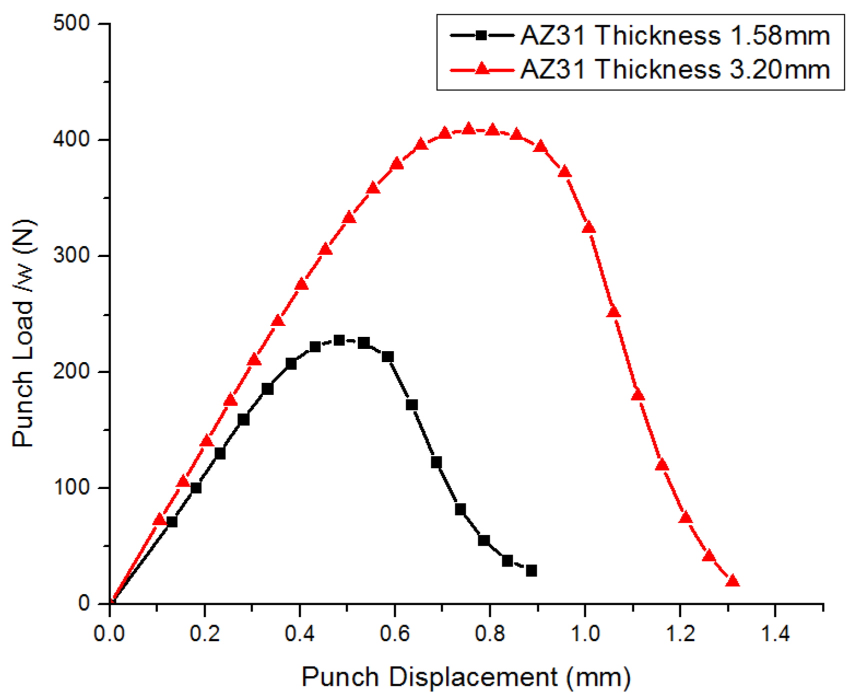

Figure 5-6. Effect of sheet thickness on punch load-displacement curves (tool setup configuration without cushion, clearance: 4%, trimming speed: 5 mm /sec, sheet orientation: RD).

5.1.1.6. AZ31 versus ZEK100 Magnesium alloy sheet

Earlier punch load-displacement curves for AZ31 and ZEK100 sheets for the same trimming condition are re-plotted on the same graph in Figures 5-7 and 5-8 in order to compare the characteristic features of two materials. For this comparison, 2 specific experiment results with the following experimental parameters are utilized; (i) tool setup configuration without cushion and clearance of 4%, and (ii) tool setup configuration with cushion and a clearance of 11%. The results in Figure 5-7 and 5-8 are representative of the other experimental conditions. For example, the peak load for AZ31 is higher and load saturation is larger than that for ZEK100. Also, the punch load drops more rapidly after peak load for ZEK100 compared to AZ31 sheet, which means, for ZEK100, the crack initiates earlier than AZ31.

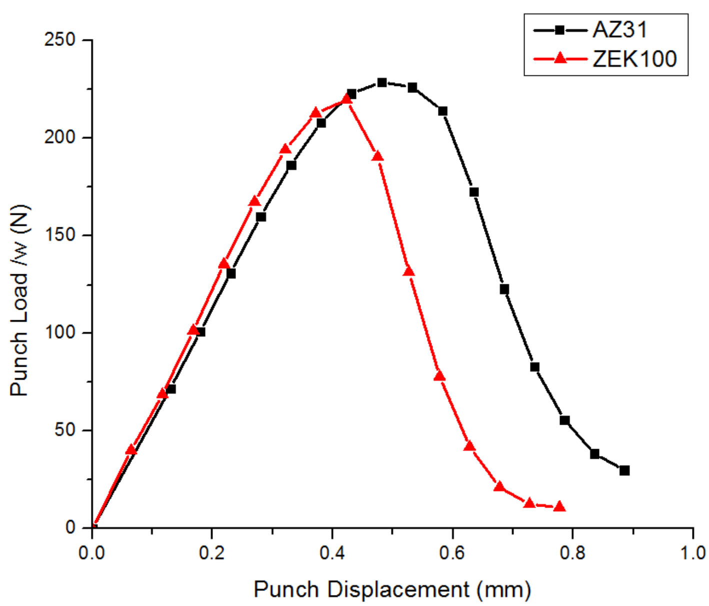

Figure 5-7. Comparison of AZ31 and ZEK100 (tool setup configuration: without cushion, clearance: 4%, trimming speed: 5 mm /sec, sheet orientation: RD).

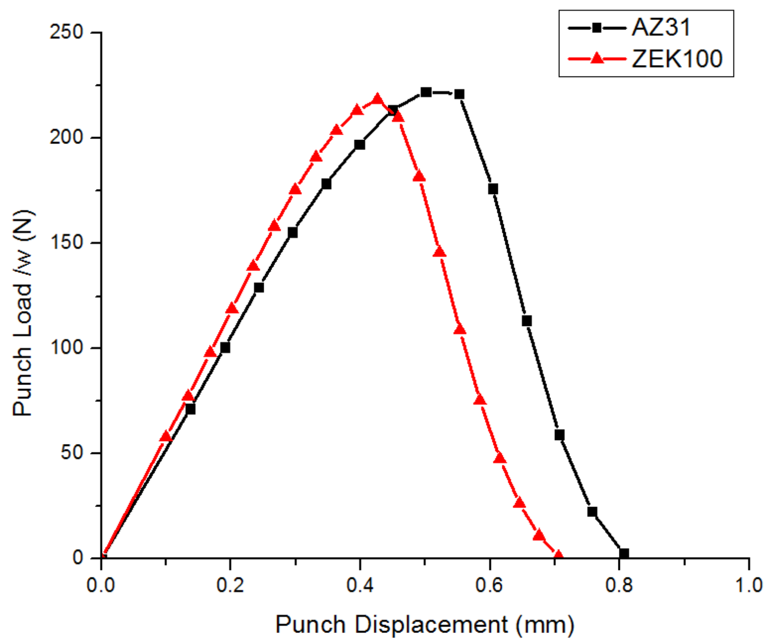

Figure 5-8. Comparison of AZ31 and ZEK100 (tool setup configuration with cushion, clearance: 11%, trimming speed: 5 mm /sec, Sheet orientation: RD).

5.1.2. Parameters affecting trimmed edge quality

In this section, the results focus on the trimmed edge quality, experimentally measured by a specific set of parameters described earlier in Chapter 3 (also see Figure 5-9 below), as a function of trimming process parameters. As mentioned in Chapter 3, the trimmed edge shown in Figure 5-9 is divided into four zones: rollover zone, burnish zone, fracture zone and burr, which are perhaps the most important parameters used to assess the quality of trimmed edge. All trimmed edge parameters (rollover depth, burnish depth and fracture depth and burr height) are measured and presented as graphs in various figures in this sub-section. It is to be noted that above edge parameters are relative values expressed as a percentage of the initial sheet thickness.

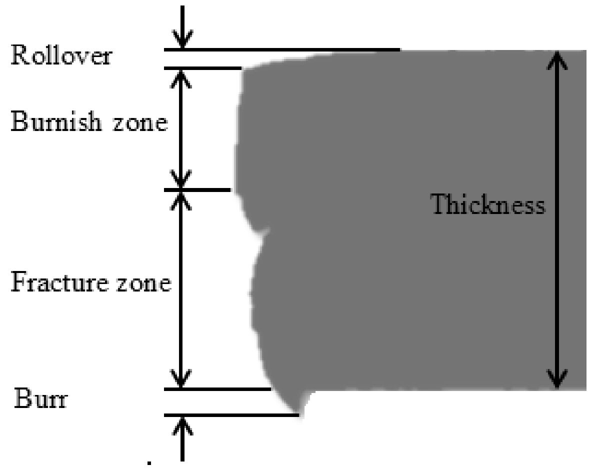

Figure 5-9. Typical profile of trimmed edge for metal sheets.

5.1.2.1. Effect of trimming speed

Figure 5-10 shows the images of the profiles of trimmed edge obtained by optical microscope with respect to different trimming speeds for AZ31 and ZEK100 sheets. In general, for both sheet materials, the quality of trimmed edge improves with increase in trimming speed. Quantitative data on effect of trimming speed on the trimmed edge parameters is presented in Appendix Table A-1 and Figure 5-11. Tables A-1 to A-12 in the Appendix A include repeatability errors from 4 or 5 repeat tests under each of the test conditions.

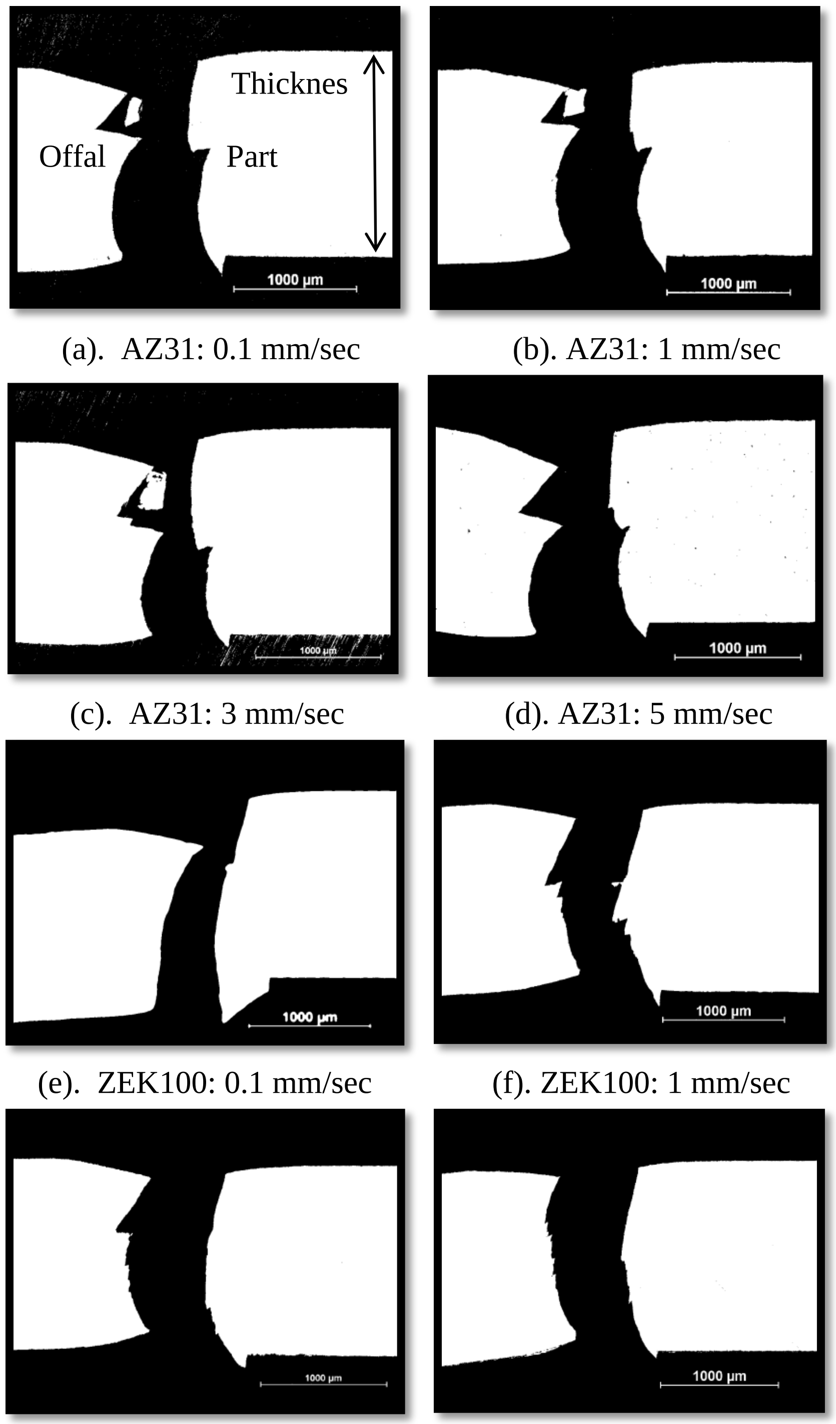

(a). AZ31: 0.1 mm/sec (b). AZ31: 1 mm/sec

(c). AZ31: 3 mm/sec (d). AZ31: 5 mm/sec

(e). ZEK100: 0.1 mm/sec (f). ZEK100: 1 mm/sec

(g). ZEK100: 3 mm/sec (h). ZEK100: 5 mm/sec

Figure 5-10. Profiles of trimmed edges of AZ31 and ZEK100 for different trimming speeds (tool setup configuration without cushion, clearance 11%, sheet orientation: RD).

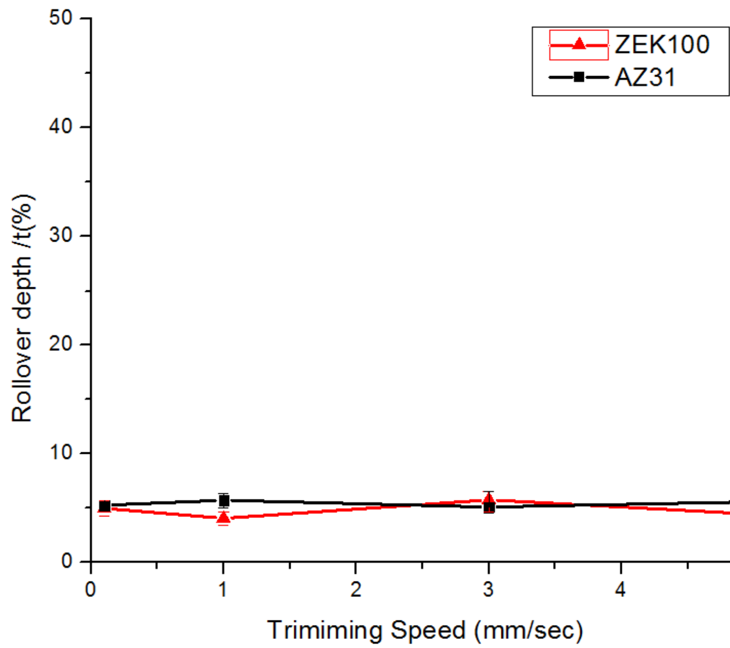

(a). Rollover depth

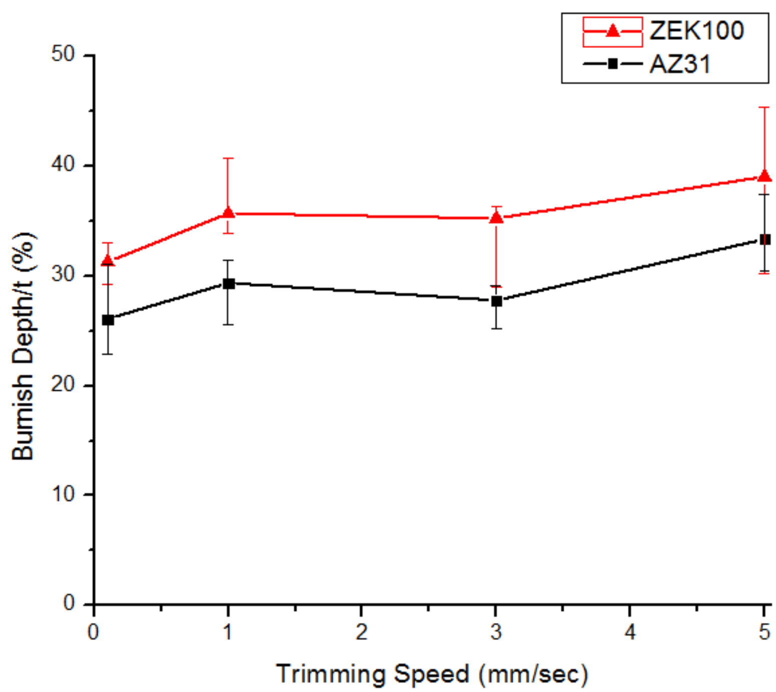

(b). Burnish depth

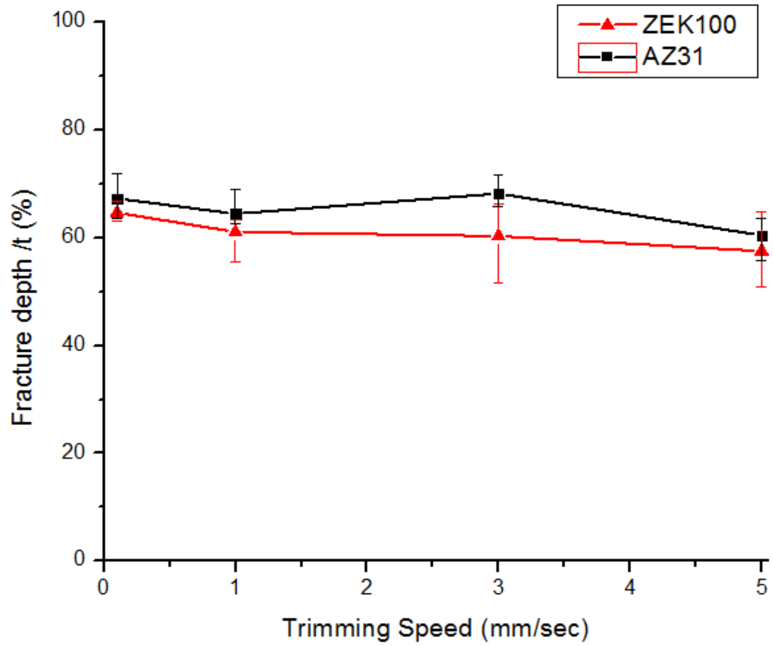

(c). Fracture depth

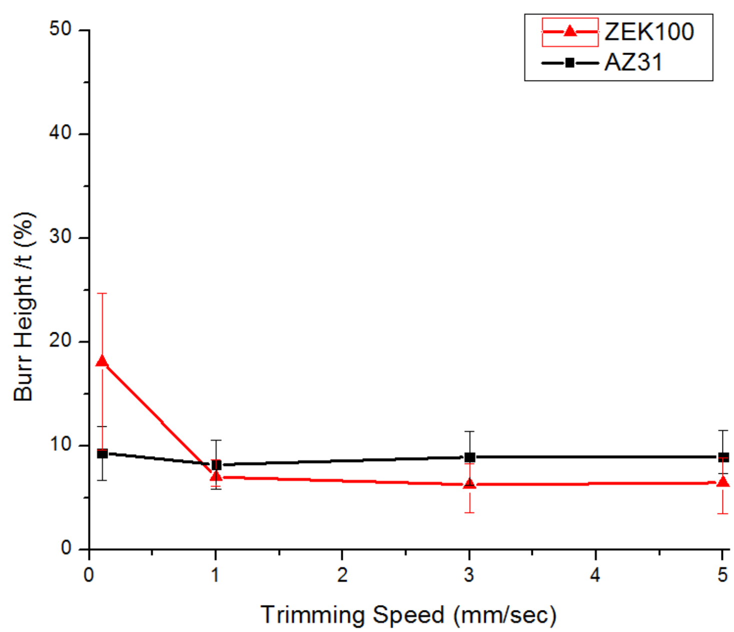

(d). Burr height

Figure 5-11. A plot of trimmed edge parameters as a function of trimming speed.

As indicated in Figure 5-11, both AZ31 and ZEK sheets show the same general trend; burnish depth increases with an increase in trimming speed, because trimmed edge is mainly composed of the burnish zone and fracture zone, so the fracture depth usually shows the opposite trend to the burnish depth . As for rollover, it remains almost constant with increase in trimming speed. Lastly, the burr height for ZEK100 decreases with increase of trimming speed at lower trimming speeds but becomes constant at higher speeds. On the other hand, the burr height for AZ31 remains almost constant in the entire range of experimental trimming speeds. A comparison of trimmed edge quality between AZ31 and ZEK100 reveals that the rollover depth for both AZ31 and ZEK100 are almost the same, but the burnish depth for ZEK100 is higher than that for AZ31, whereas the fracture shows the opposite trend. The burr height for ZEK100 is higher than that for AZ31 in the range of higher trimming speeds. Therefore, it can be concluded that the trimming quality of ZEK100 is generally better than that of AZ31.

5.1.2.2. Effect of clearance

Figure 5-12(a-h) show the images of the profiles of trimmed edge of AZ31 and ZEK100 sheets with respect to different clearances. It is obvious that, for the both materials, the quality of trimmed edge progressively decreases with an increase in clearance. The measurements of trimmed edge parameters are presented in Appendix Table A-2 , and the corresponding plots of trimmed edge parameters as a function of clearance are provided in Figure 5-13.

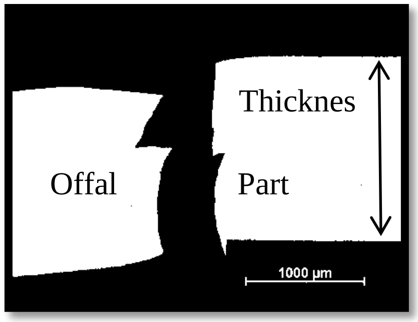

(a). AZ31 - Clearance 4%

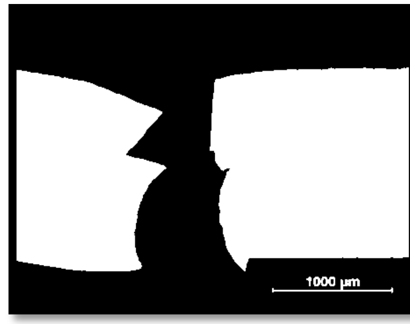

(b). AZ31 – Clearance 11%

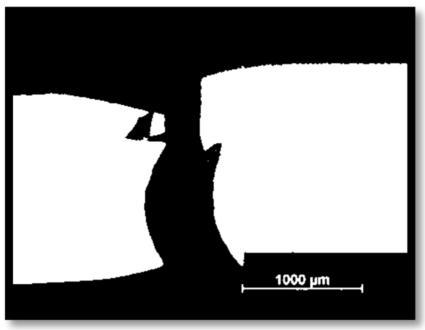

(c). AZ31 - Clearance 20%

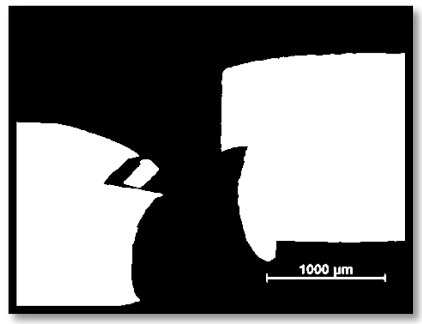

(d). AZ31 – Clearance 26%

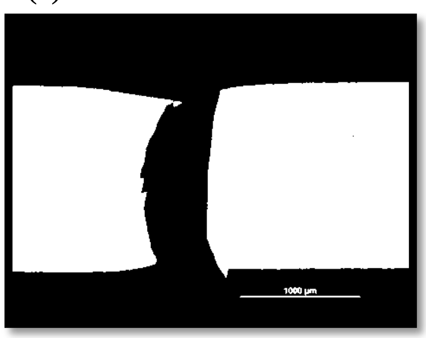

(e). ZEK100 - Clearance 4%

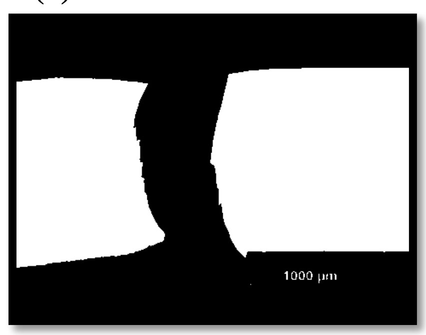

(f). ZEK100 – Clearance 11%

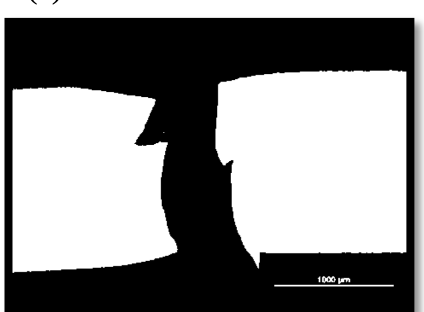

(g). ZEK100 - Clearance 20%

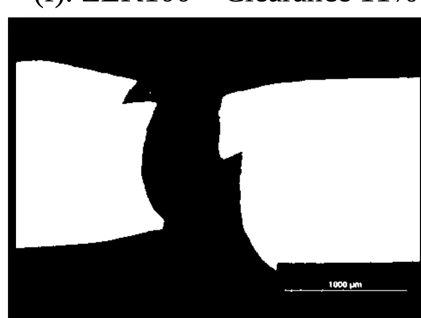

(h). ZEK100 – Clearance 26%

Figure 5-12. Profile of trimmed edge of AZ31 and ZEK100 for different clearances (tool setup configuration without cushion, trimming speed 5 mm/sec, sheet orientation: RD).

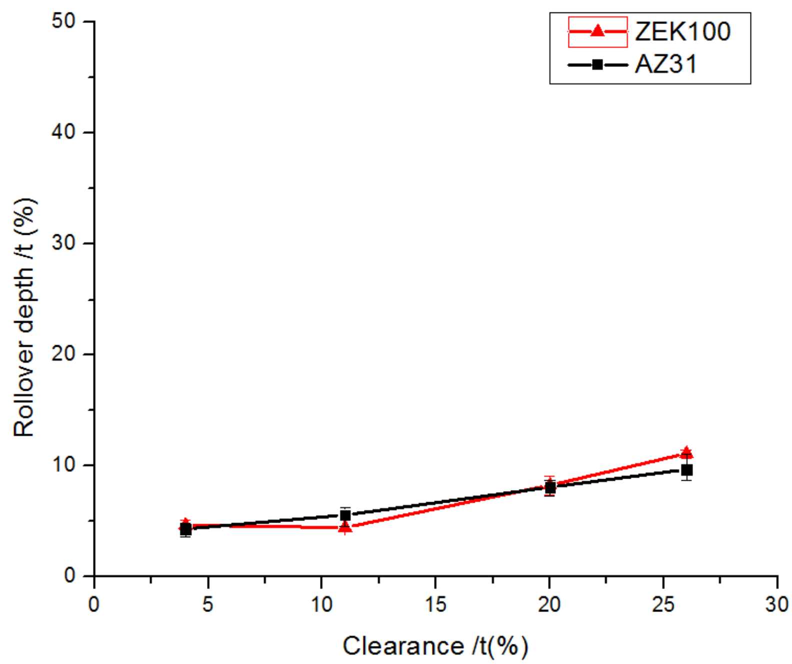

(a). Rollover depth

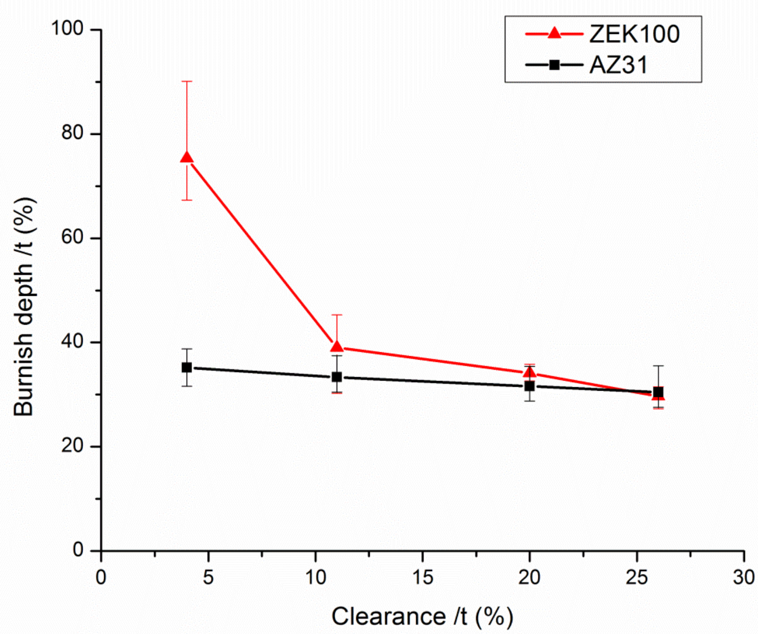

(b). Burnish depth

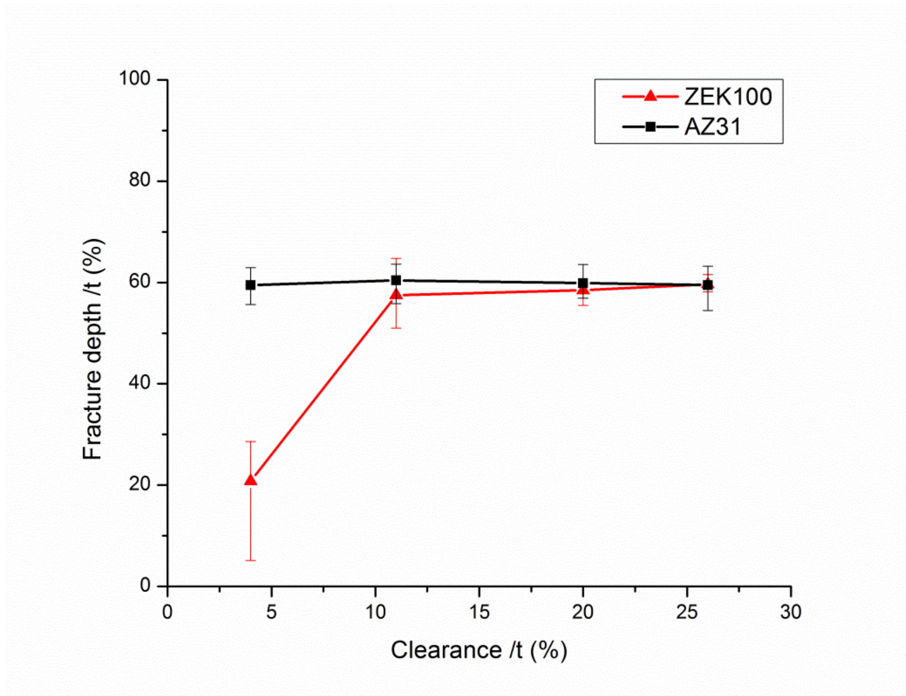

(c). Fracture depth

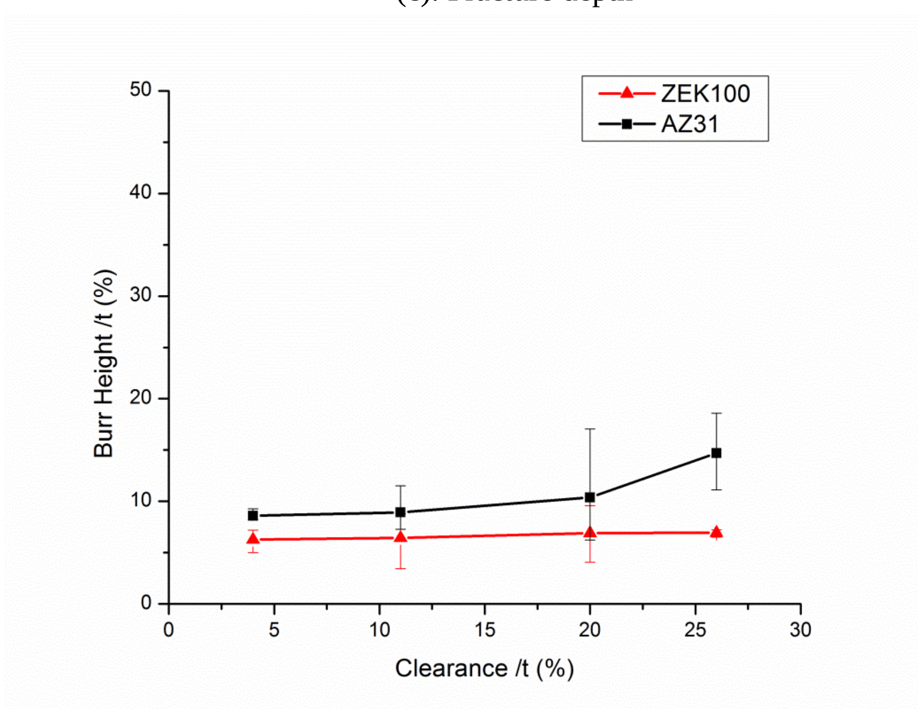

(d). Burr height

Figure 5-13. A plots of trimmed edge parameters as a function of clearance.

Figure 5-13(a-d) compares the trimmed edge quality between AZ31 and ZEK100 with respect to different clearances. For rollover, both materials show the same trend; the rollover depth decreases with increasing clearance, and for identical clearance, there is no significant difference between AZ31 and ZEK100 sheets. The burnish depth for ZEK100 is much higher than that for AZ31 in the range of small clearance (up to 11%), but for clearances above 11%, the burnish depth for both AZ31 and ZEK100 tend to evolve to a similar value. The fracture depth exhibits an opposite trend to burnish depth. Lastly, for the burr height, ZEK100 remains almost constant within the entire range of clearances while the burr height increases with increase of clearance for AZ31. Especially, at large clearances, the trimming zone is wider and this region will encounter more bending. Consequently, the burnish zone is reduced while fracture zone is increased, the burr height and size becomes larger, and the precision and quality of trimmed edge decreases. From a comparison of results between AZ31 and ZEK100 for different clearances, one can conclude that the trimming quality of ZEK100 is better than that of AZ31. Moreover, there is dramatic change of trimmed edge quality for ZEK100 in the range of small clearance, this is because the ZEK100 is much more ductile compared to AZ31, it can be concluded that the trimmed edge quality of ZEK100 sheet material is much more sensitive at small clearances compared to AZ31 sheet.

5.1.2.3. Effect of tool setup configuration

Figure 5-14 shows the profile of trimmed edge of AZ31 and ZEK100 sheets obtained using two different tool setup configurations described earlier. From Figure 5-14, the burr size is clearly more visible for the conventional tool setup configuration (i.e., without cushion) than with the tool setup configuration with cushion. The quantified parameters of trimmed edge are listed in Appendix Table A-3 and are plotted in Figure 5-15 to compare the effect of tool setup configuration on the trimmed edge quality.

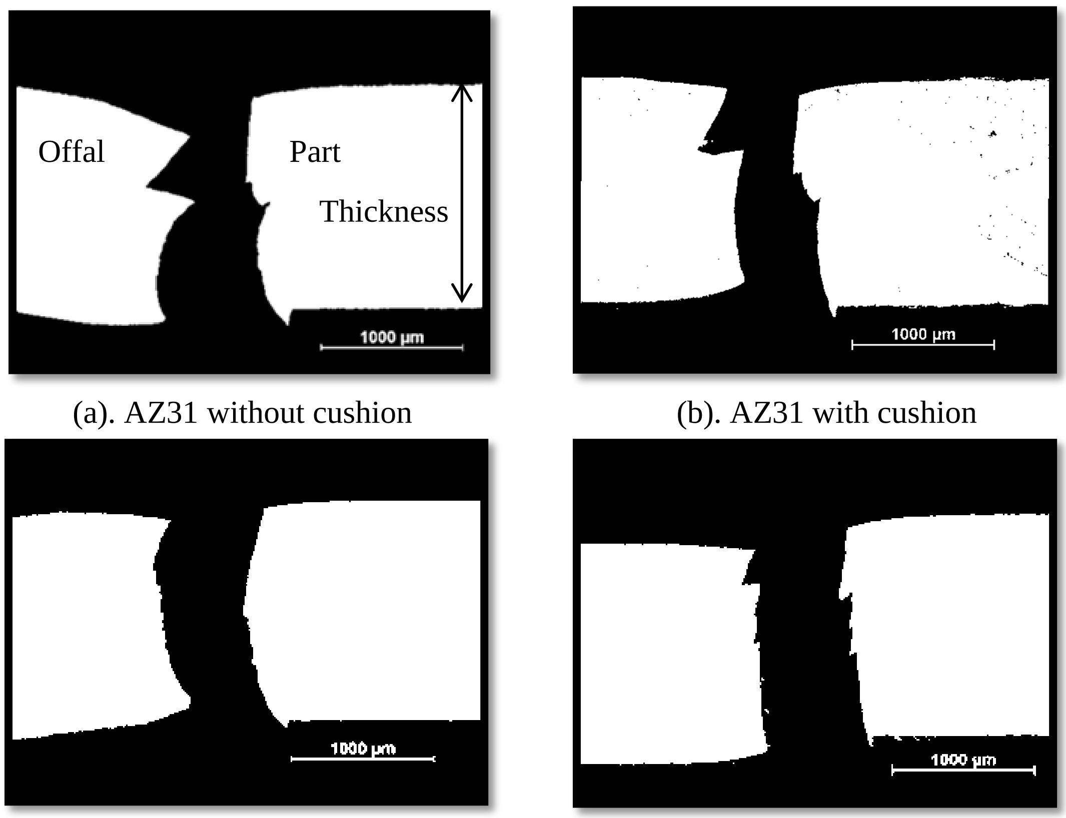

(a). AZ31 without cushion (b). AZ31 with cushion

(c). ZEK100 without cushion (d). ZEK100 with cushion

Figure 5-14. Profiles of trimmed edges of AZ31 and ZEK100 specimens obtained using different tool setup configuration (trimming speed: 5 mm/sec, clearance 11% , sheet orientation: RD).

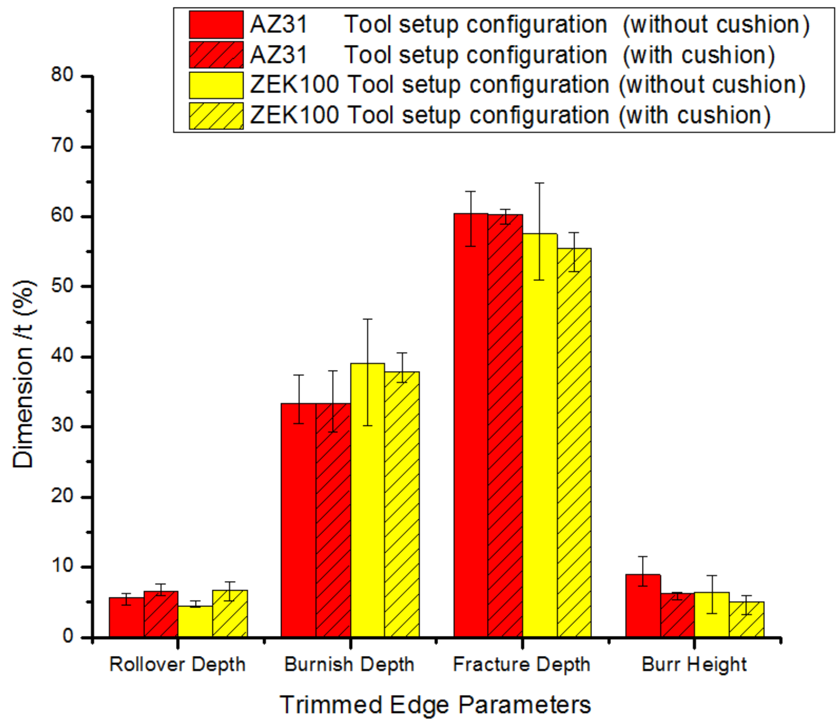

Figure 5-15. Comparisons of effect of tool setup configuration on trimmed edge quality.

As shown in Figure 5-15, for both AZ31and ZEK100, the rollover depth for tool set configuration with cushion is slightly larger than that for tool setup configuration without cushion, this is because with the use of cushion, more punch penetration are required to overcome resistance of cushion, and correspondingly, there is more compression and tension in the trimmed zone that can possibly contribute to larger rollover depth. The burr height, on the other hand, decreases with the use of cushion because the cushion prevents the offal from rotation and bending at the bottom area of the trimming zone. Lastly, the burnish and fracture depth appear to be almost the same for AZ31 and ZEK100. In general, comparing the overall quality of the trimmed edge from the 2 different tool configurations, the use of cushion not only keeps the burnish depth to same extent, but also can effectively reduce the burr size and improve the quality and precision of trimmed edge. Also, in majority of the test conditions involving two different tool setup configurations, the rollover depth, fracture depth and burr height of ZEK100 is smaller than that of AZ31, so, in general, ZEK100 sheet shows better trimming quality than AZ31.

5.1.2.4. Effect of Sheet Orientation

Figure 5-16 presents the profiles of trimmed edge of AZ31 and ZEK100 sheets with two different sheet orientations, longitudinal and transverse to the trim line direction. The corresponding trimmed edge parameters are presented in Appendix A, Table A-4, and plotted in Figure 5-17. The trend is similar for both AZ31 and ZEK100 in that the sheet orientations have no large influence on the rollover depth. However, the burnish depth and burr height of the sheet with RD orientation is larger than that of the sheet with TD orientation whereas the fracture depth shows the opposite trend as the burnish depth. The different profile and quality of trimmed edge result from anisotropy of the two materials with the different microstructures, R values and stress-strain behavior along rolling and transverse directions (see earlier Figure 3-8 in Chapter 3).

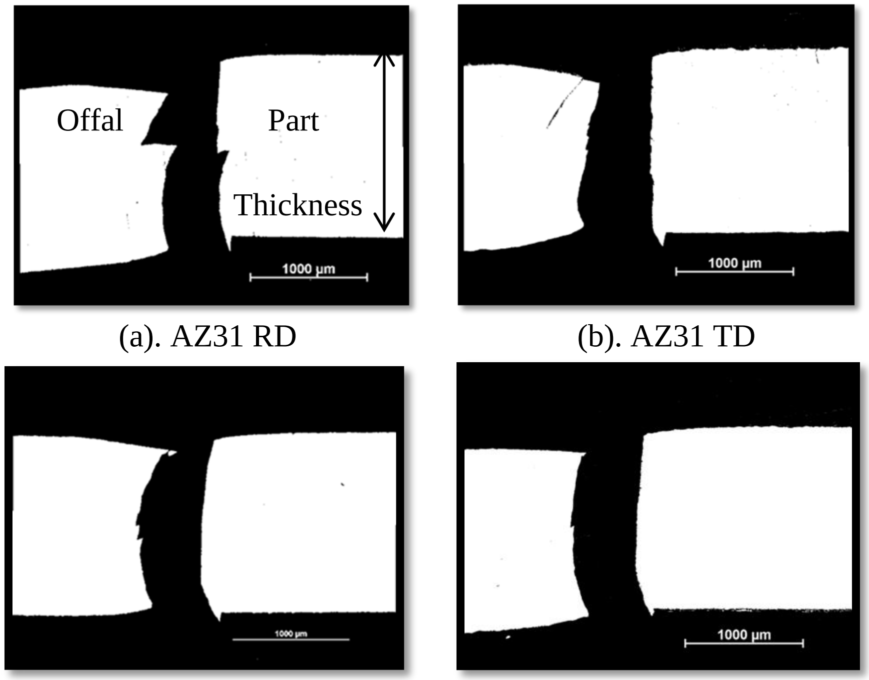

(a). AZ31 RD (b). AZ31 TD

(c). ZEK100 RD (d). ZEK100 TD

Figure 5-16. The profile of trimmed edge of AZ31 and ZEK100 sheets with two different sheet orientations (tool setup configuration without cushion, trimming speed: 5 mm/sec, clearance 4%).

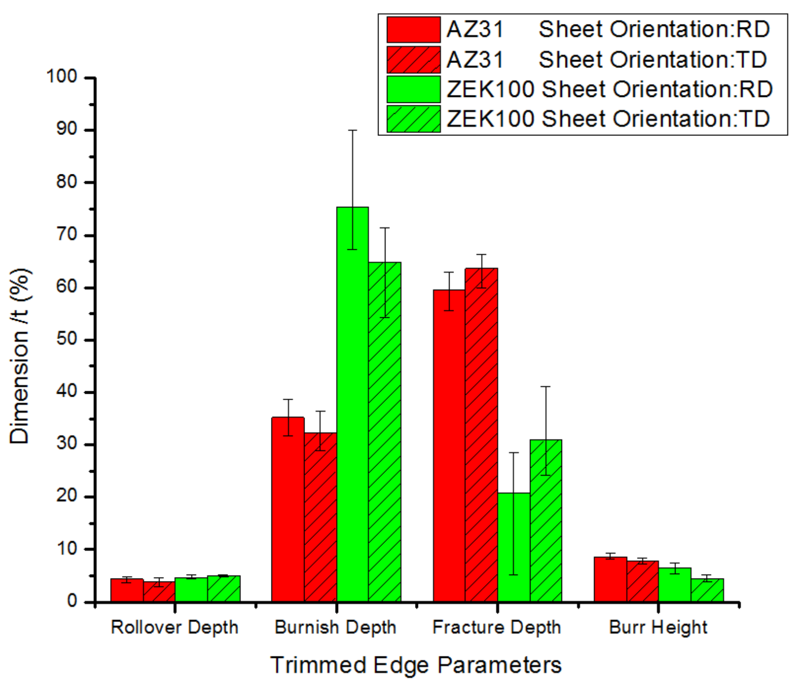

Figure 5-17. Comparisons of effect of sheet orientation on trimmed edge quality.

5.1.2.5. Effect of sheet thickness

To evaluate the effect of sheet thickness on the trimmed edge, two different sheet thicknesses with only one clearance between die and punch of 0.062 mm were utilized. Figure 5-18 shows the profile of trimmed edge of AZ31 sheet where it is clearly seen that trimming of thin sheet is a better than a thick one. The quantified parameters of trimmed edge are listed in Appendix A, Table A-5, and corresponding comparison of effect of sheet thickness on the trimmed edge quality is presented in Figure 5-19.

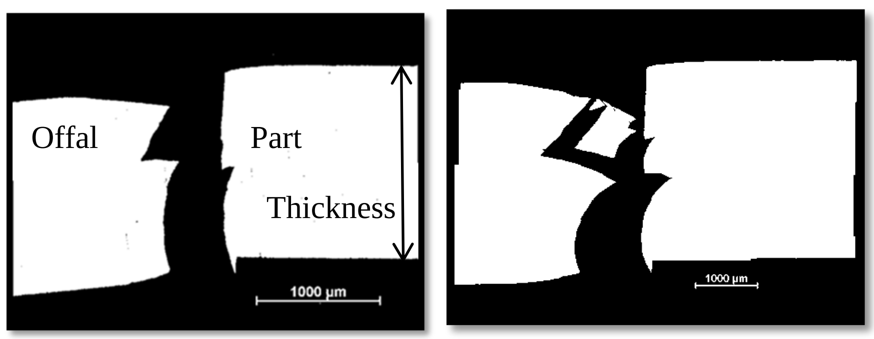

(a). Sheet thickness: 1.58 mm (b). Sheet thickness: 3.2 mm

Figure 5-18. Profile of trimmed edges of AZ31 sheet with different sheet thicknesses (tool setup configuration without cushion, trimming speed: 5 mm/sec, clearance: 0.062 mm).

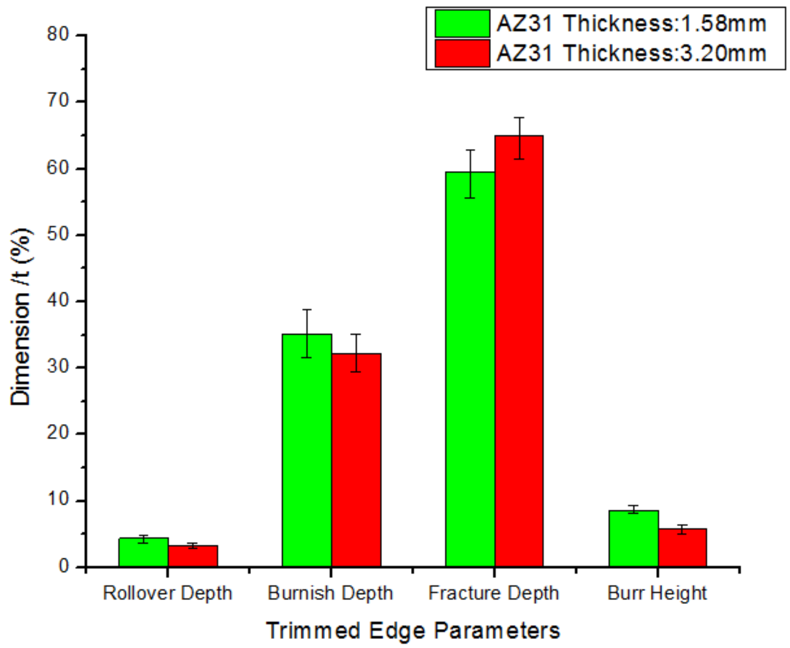

Figure 5-19. A comparison of effect of sheet thickness on trimmed edge quality.

As shown in Figure 5-19, under the same trimming conditions, the thick sheet shows good performance in term of the lower rollover length and burr height compared to the thin sheet. However, thick sheet exhibited poor performance as it yielded a smaller burnish zone and a larger fracture zone. A clearance of 0.062 mm is reasonable clearance (about 4% of thickness) for the thin sheet but not so for the thick sheet (about 2% of thickness). When the clearance is too small, the cracks originating from the top and bottom of the trim zone do not meet each other during crack propagation, and the middle part between the top crack and the bottom crack is sheared the second time resulting in a second burnish zone (see Figure 5-18). Therefore, for a metal sheet with certain thickness, there must be an optimal clearance that allows the crack from the two sides to meet as easily as possible and minimum secondary shearing takes place.

5.2. Finite Element Simulation Results

As mentioned in Chapter 4, as a parallel study, FE simulation of the laboratory based trimming tests were carried out to analyze the effect of trimming conditions on the punch load versus displacement response as well as the response of trimmed edge quality. FE modelling method was improved up and refined by carrying out separate investigations of the effect of choice of available continuum-based ductile fracture criteria, meshing method, mass scaling method and friction coefficient. All of the above methods have certain influence on the simulation results. In this section, the effects of these methods on the FE simulation results are presented first and compared with the experimental results where possible and then justification for the selection of optimal parameter(s) for each method are provided. Finally, a simulation matrix very similar to the experimental one is utilized to obtain all numerical results for comparison with the experimental results presented earlier in this chapter.

5.2.1. Effect of modelling methods on the FE results

In order to analyze the effect of different fracture criteria, mass scaling and meshing methods on the simulation results, all simulations were conducted for tool setup configuration without cushion, punch-die clearance of 11%, trimming speed of 5 mm/sec and RD sheet orientation. A description of the different fracture criteria utilized in the present work was provided earlier in Table 4-2.

5.2.1.1. Effect of different fracture criteria

The profile of trimmed edge from different fracture criteria are presented in Figure 5-20 (a-f) for AZ31 and Figure 5-20(g-l) for ZEK100 respectively, the corresponding trimmed edge parameters are listed in Appendix A, Table A-6, and plotted in Figure 5-21. The profile predicted by simulation shows the similar characteristic zones (rollover, burnish zone, fracture zone and burr) as the trimmed edge observed in experiment.

AZ31 (a). Experiment (b). Oyane (c). C-L

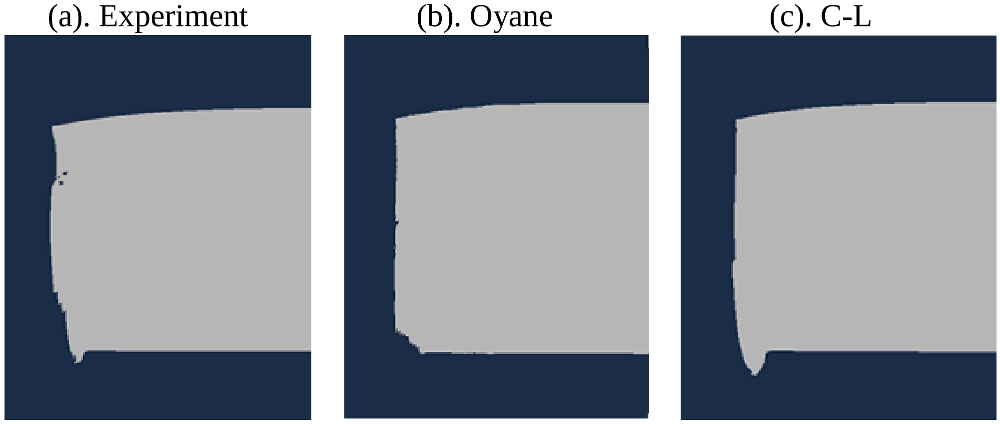

AZ31 (d). Brozzo (e). Clift (f). Rice-Tracy(R-T)

ZEK100 (g). Experiment (h). Oyane (i). C-L

ZEK100 (j). Brozzo (k). Clift (l). Rice-Tracy(R-T)

Figure 5-20. Profiles of trimmed edge of AZ31 and ZEK100 obtained from experiment and FE model using different fracture criteria, (a-f) AZ31, and (g-l) ZEK100 specimen.

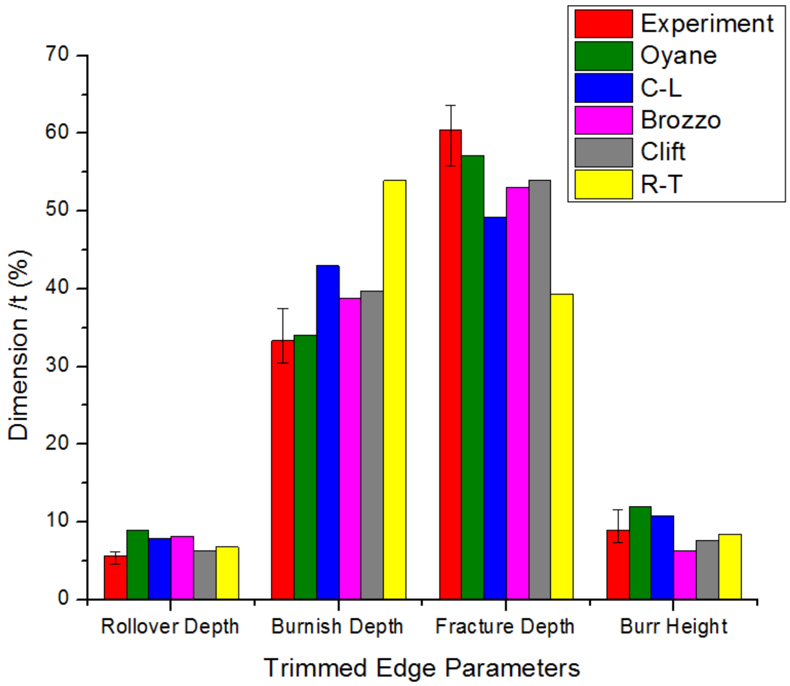

(a). AZ31

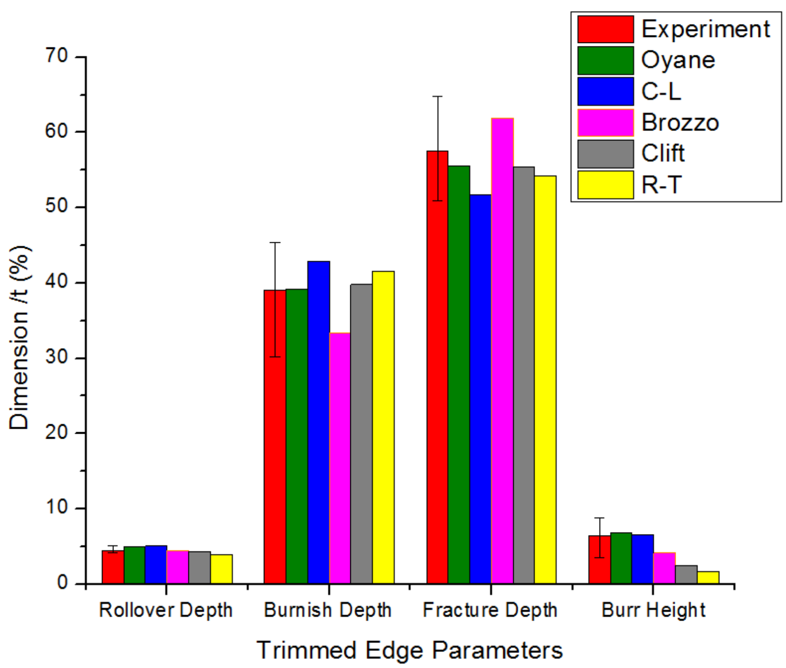

(b). ZEK100

Figure 5-21. Comparisons of trimmed edge parameters of AZ31and ZEK100 between experiment and simulation using different fracture criteria.

As indicated in Figure 5-21(a), the burnish and fracture depths and burr height of AZ31 predicted by Oyane fracture criteria are in good agreement with experimental result. The rollover predicted is somewhat higher than that from the experiment. For C-L, Brozzo, Clift and R-T fracture criteria, there are large differences between simulation and experiment results. Considering all of the trimmed edge parameters predicted by simulations into consideration, Oyane fracture criteria appeared to be the most suitable one among the five chosen fracture criteria to predicted the trimming process of AZ31 magnesium alloy sheet.

For ZEK100 magnesium sheet, as shown in Figure 5-20 (g-l) and Figure 5-21 (b), all five fracture criteria have good general agreement with the experimental results except for the burr height predicted by the Brozzo, Clift and Rice-Tracy. Oyane fracture criteria still appeared to be the closest to experimental results in all cases. Therefore, all of simulations results in the following sections were based on Oyane fracture criteria.

5.2.1.2. Effect of mass scaling

ZEK100 sheet was chosen for analyzing the effect of mass scaling. The profile of trimmed edge obtained from experiment and FE model using mass scaling are presented in Figure 5-22, and the corresponding trimmed edge parameters are listed in Appendix Table A-7, and plotted in Figure 5-23. It can been seen from Figure 5-22 that the profiles of trimmed edge obtained by FE model using different mass scaling factors (MSFs) are almost same.

(a). Experiment (b). MSF 100 (c). MSF 900

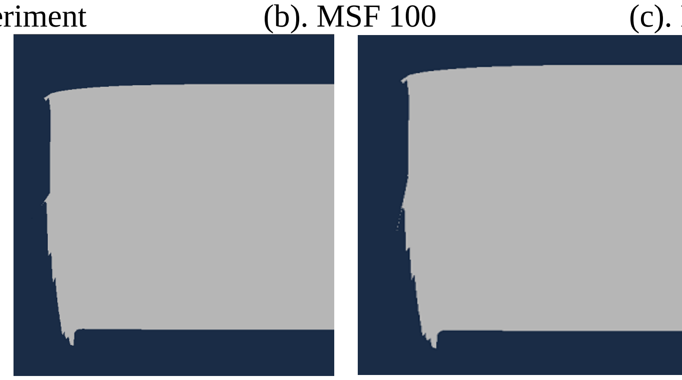

(d). MSF 2500 (e). MSF 10000

Figure 5-22. Profiles of trimmed edges obtained from experiment and FE models using various mass scaling factors.

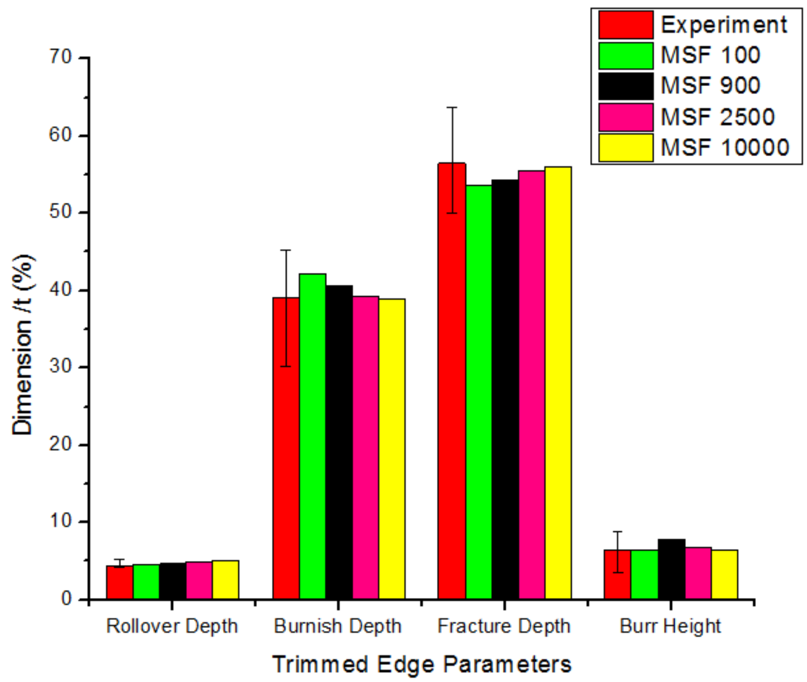

Figure 5-23. A comparison of trimmed edge parameters between experiment and simulation using different mass scaling factors.

From the quantitative analysis shown in Figure 5-23, the trimmed edge parameters predicted by the FE model using different mass scaling factors (100, 900, 2500 and 10,000) agreed well with the experimental results within some error band. As mentioned in Section 4.8, when too large a mass scaling factor is used, the dynamic effects will increase and may cause incorrect simulation results. The dynamic effect of mass scaling factors of 2500 and 10000 were therefore analyzed, and the corresponding evolution of ratio of total kinetic energy to total internal energy is shown in Figure 5-24. At the initiation of trimming process there were some oscillations in the ratio of total kinetic energy to total internal energy, this was because there of a sudden contact between the punch and sheet at the beginning of trimming process, which resulted in the system as a whole becoming unstable. After about 0.4-0.5 seconds, however, the system did become stable, and the ratio of total kinetic energy to total internal energy was reduced to below 10%. Under such conditions, the dynamic effects could be negligible and the simulations results were acceptable. Based on above analysis, the mass scaling factors of 10000 and 2500 were chosen for various trimming process models for AZ31 and ZEK100 respectively to improve the computational efficiency while not introducing significant errors into the analysis.

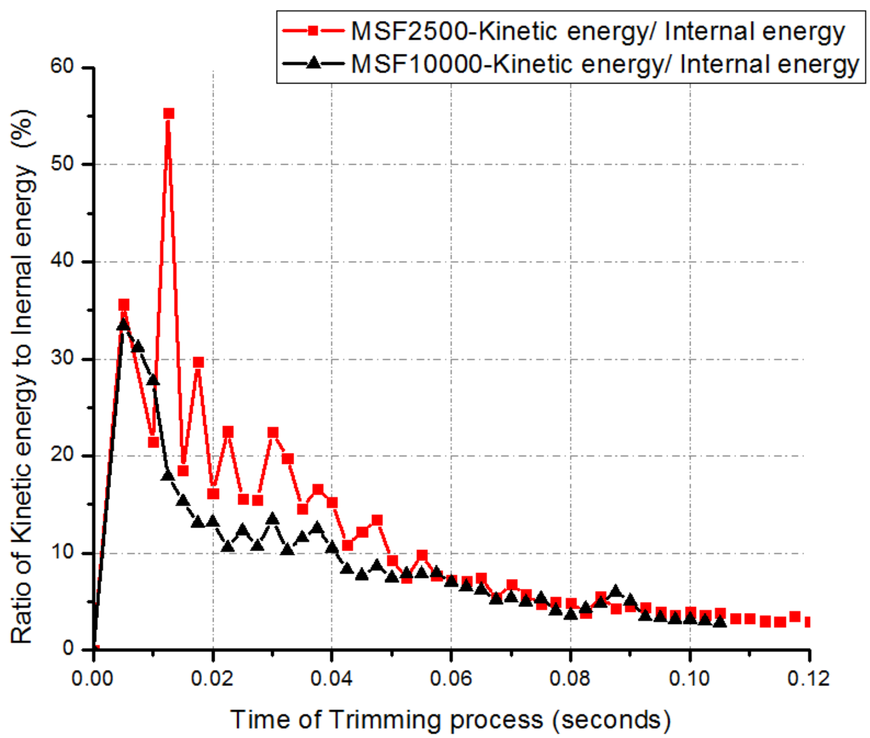

Figure 5-24. The evolution of ratio of the total kinetic energy to the total internal energy with trimming time in the FE simulations.

5.2.1.3. Effect of different meshing methods

ZEK100 sheet was chosen for analyzing the effect of different meshing methods. The profile of trimmed edge obtained from experiment and FE model using different mesh size (MS) without adaptive meshing are presented in Figure 5-25(a-d) while the one predicted by FE model using adaptive re-meshing(ALE) is shown in Figure 5-25(e), the corresponding trimmed edge parameters are listed in Appendix A, Table A-8, and plotted in Figure 5-26.

(a). Experiment (b). MS 0.01 x 0.01 (c). MS 0.02 x 0.02

(d). MS 0.03 x 0.03 (e). MS 0.02 x 0.02 (Adaptive re-meshing)

Figure 5-25. Profiles of trimmed edges obtained from experiment and FE model using different meshing methods (mesh size is abbreviated here as MS, dimension in mm).

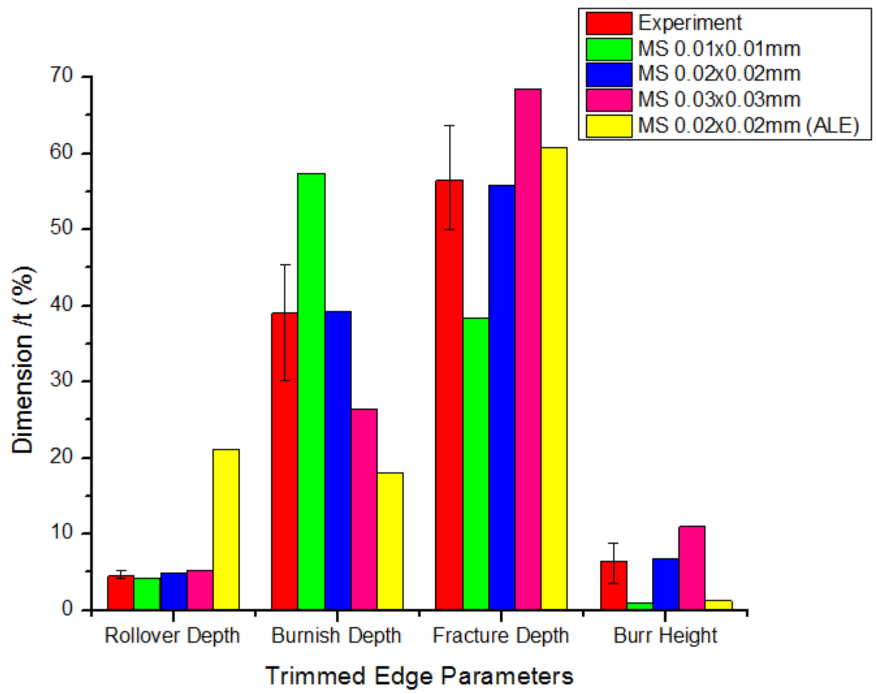

Figure 5-26. Comparisons of trimmed edge parameters between experiment and simulations using different meshing methods.

As shown in Figure 5-25 and Figure 5-26, the profiles of trimmed edges and the corresponding trimmed edge parameters predicted by mesh size 0.02 x 0.02 mm without adaptive re-meshing method are most close to the experimental results in all cases. The burr height, however, showed large differences between the experiment results and simulation results using either smaller or larger mesh sizes. This is perhaps because when smaller mesh size of 0.01 x 0.01 mm was used, it was faster for each element to reach the critical fracture integration value after a small deformation and rotation of offal side before fracture, while the larger mesh size of 0.03 x 0.03 mm showed the opposite phenomenon.

In adaptive re-meshing method the primary advantage of its capability is that a smoother mesh is generated at regular intervals to reduce element distortion in the nonlinear simulations where the material undergoes large deformation. As shown in Figure 5-27, for mesh size of 0.02 x 0.02 mm, the nodes and their connectivity did not change, but they were adjusted automatically into much smaller ones with increase in strain and stress concentration at the contact point between sheet and punch and die. Because adaptive re-meshing avoided excessive distortion of element by adjusting the mesh size into smaller elements, more punch penetration was required to sufficiently deform the elements to reach the critical fracture integration value. Therefore, the rollover depth predicted by this method was unrealistically large. Based on above analysis, a mesh size of 0.02 x 0.02 mm without adaptive re-meshing was found to be the most suitable method to predict the trimming behavior.

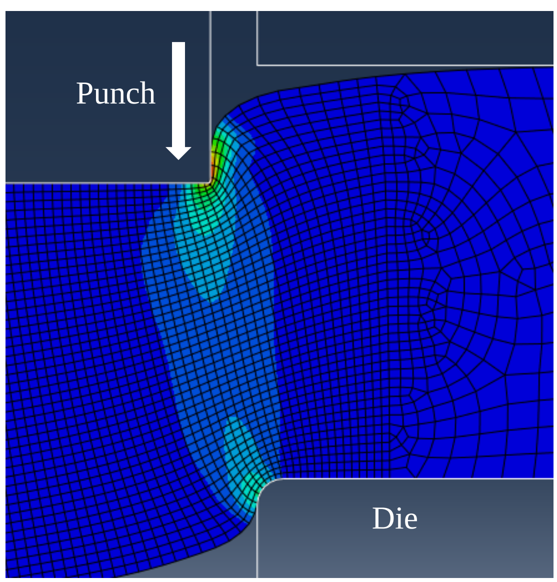

Figure 5-27. Adaptive re-meshing with ALE formulation during FE simulations of trimming.

5.2.2. Finite Element model results

In order to further verify the validity of FE model of the trimmng process for AZ31 and ZEK100 sheets, additional simulations under different trimming condition, similar to the experimental test matrix, were conducted. For example, two different trimming speeds, clearances, tool setup configurations were applied to the FE model, and the corresponding results were compared with the experimental results. In the following sub-sections, the results of predicted punch load-displacement curve are presented first. This is followed by a comparison of the FE predicted and experimental trimmed edges profiles.

5.2.2.1. Effect of trimming speed

The FE simulation of trimming process were conducted at trimming speed of 3 mm/sec and 5 mm/sec for AZ31 sheet, 1 mm/sec and 5mm/sec for ZEK100 sheet with a clearance of 11%, tool setup configuration without cushion and sheet orientation of RD. The simulation results of punch load-displacement curve with respect to the above trimming speed are shown in Figure 5-28. The trend in the punch load-displacement curves for both AZ31 and ZEK100 sheets are same as in earlier experimental results (see Figure 5-2) where trimming speed has no big influence on the peak load with the trimming speed, and the sharper the curve around the load peak the more dramatic is the load drop and faster is the crack propagation. There are some differences in the shape of punch load-displacement curves for both AZ31 and ZEK100 sheet between simulation and experiment results. These will be analyzed and discussed in Chapter 6.

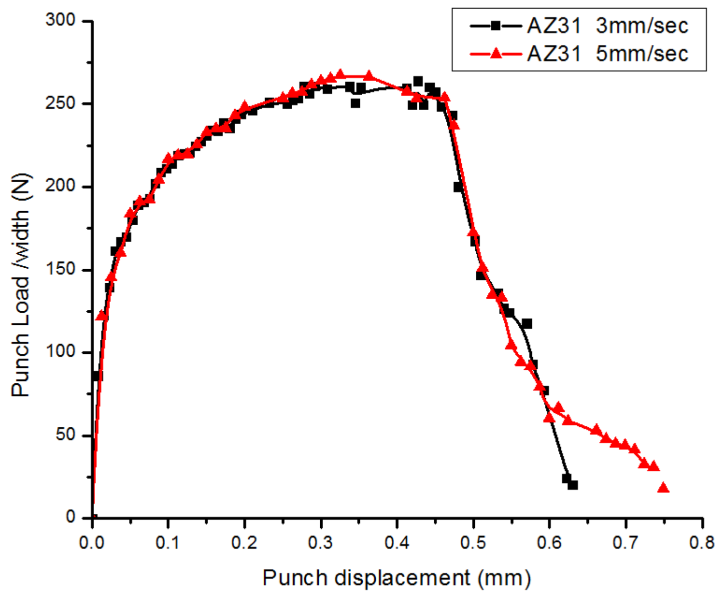

(a). AZ31

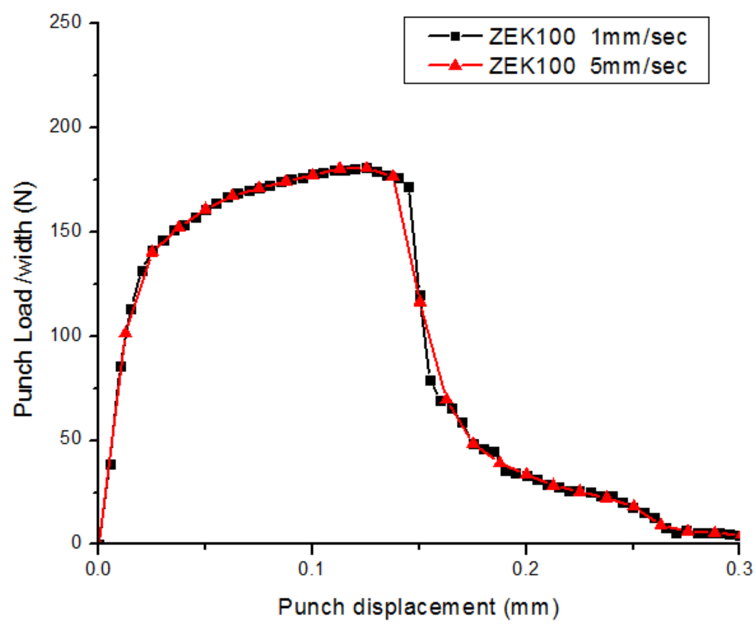

(b). ZEK100

Figure 5-28. Punch load-displacement curves for different trimming speeds as predicted by FE model (a). AZ31, (b). ZEK100 sheets.

The profiles of trimmed edges of AZ31 and ZEK100 sheet obtained from experiment and FE model with respect to different trimming speed are shown in Figure 5-29, the corresponding trimmed edge parameters are presented in Appendix A, Table A-9, and plotted in Figure 5-30.

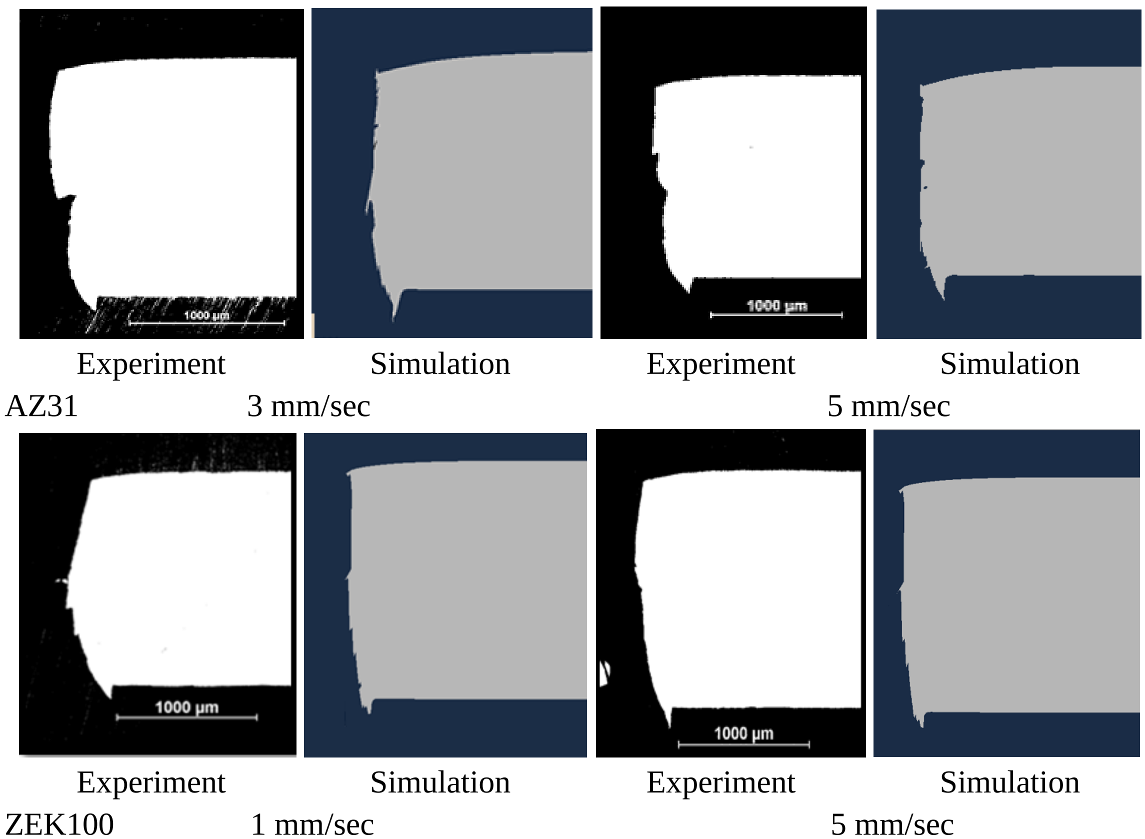

Figure 5-29. Comparisons of profiles of trimmed edges obtained from experiments and FE simulations for 2 different trimming speeds for AZ31 and ZEK100 sheets.

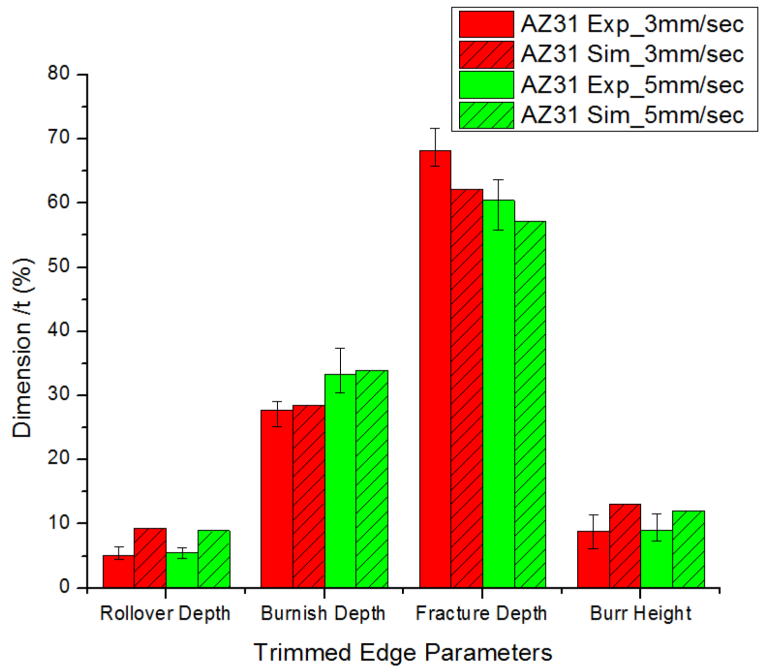

(a). AZ31

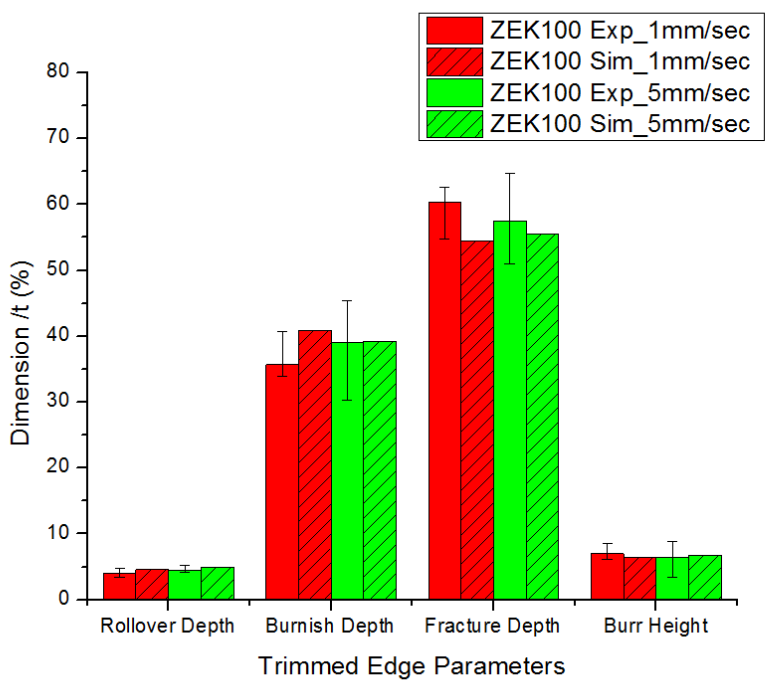

(b). ZEK100

Figure 5-30. Comparisons of trimmed edge parameters between experiment and simulation for 2 different trimming speeds.

The predicted trimmed edge parameters in Figure 5-30 show the same trend as observed in experiment where burnish depth increases with increase of trimming speed while the fracture depth shows the opposite trend. The rollover remains largely constant and the burr height decrease slightly with increase in trimming speed. For AZ31, the burnish depth, fracture depth and burr height predicted by FE model close to that obtained from experiment, but the rollover depth is higher than that in the experiment. For ZEK100, in all cases, the simulation results match the experimental results rather well.

5.2.2.2. Effect of clearance

The punch load-displacement curves for 2 different clearances as predicted by FE model for AZ31 and ZEK100 sheet are shown in Figure 5-31. Once again, same trend is observed in the simulation results as in the experiments (see earlier Figure 5-2). The peak load drops and crack initiates at a later stage with an increase in clearance. Also, at the same clearance, the crack for ZEK100 initiates earlier that that for AZ31. The profiles of trimmed edges as obtained from experiment and FE model for the 2 clearances are shown Figure 5-32, the corresponding trimmed edge parameters are presented in Appendix A, Table A-10, and plotted in Figure 5-33.

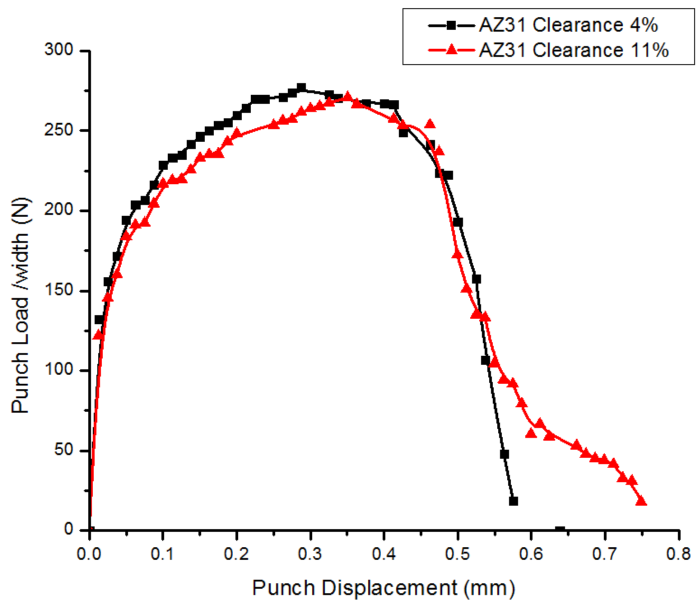

(a). AZ31

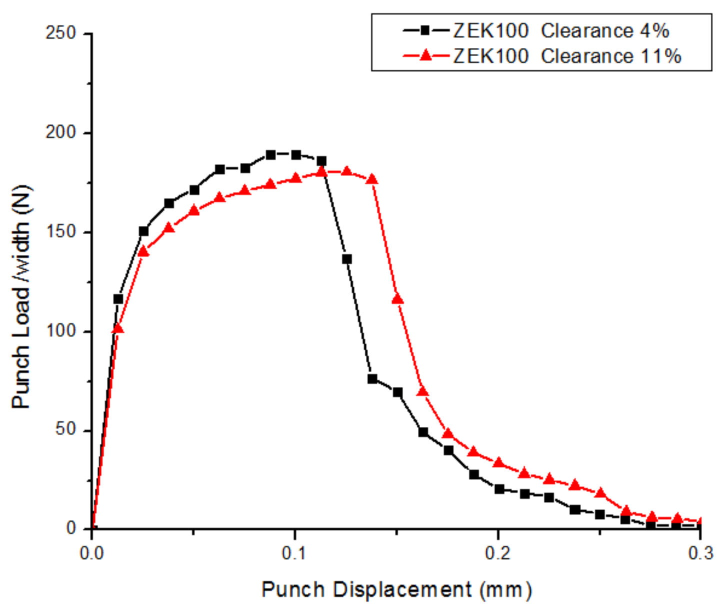

(b). ZEK100

Figure 5-31. Punch load-displacement curves for 2 different clearances as predicted by FE model (tool setup configuration without cushion, trimming speed of 5 mm/sec and sheet orientation RD).

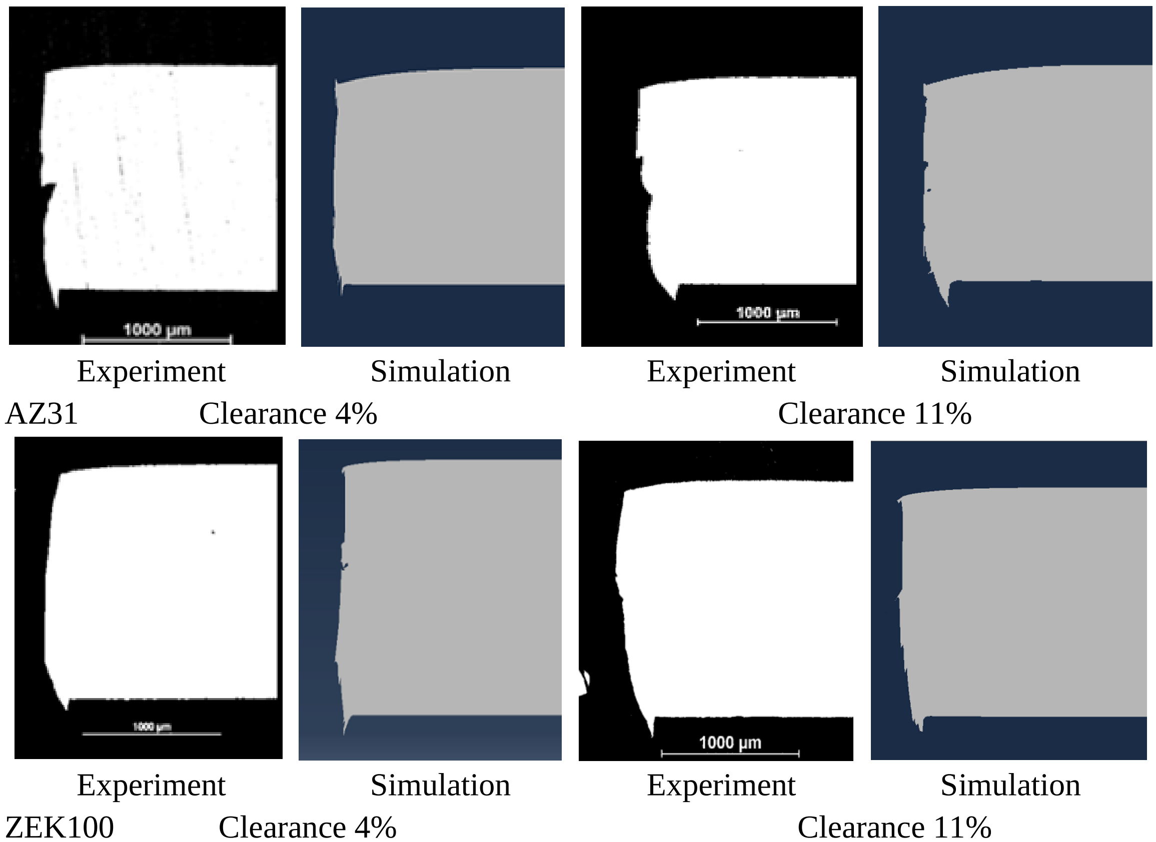

Figure 5-32. Comparisons of profiles of trimmed edges obtained from experiments and FE models for 2 different punch-die clearances.

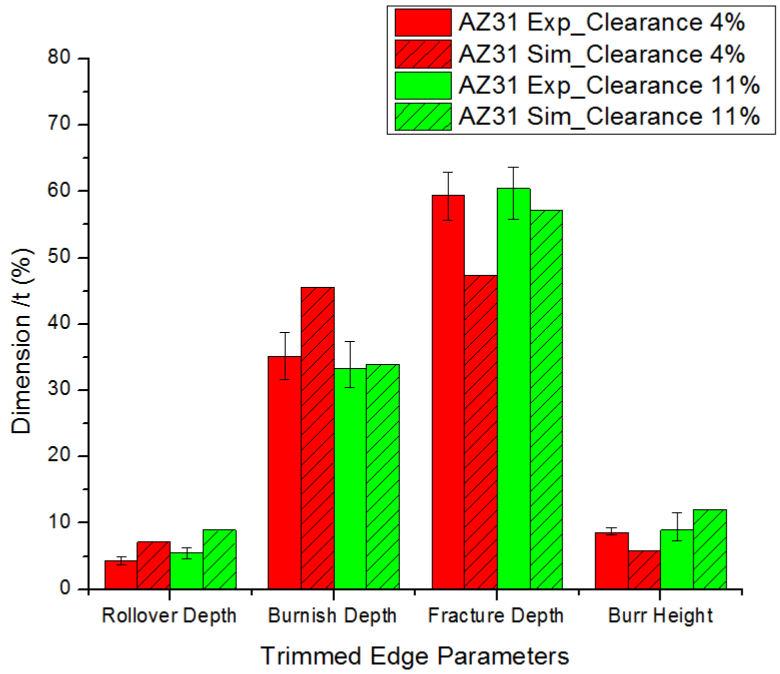

(a). AZ31

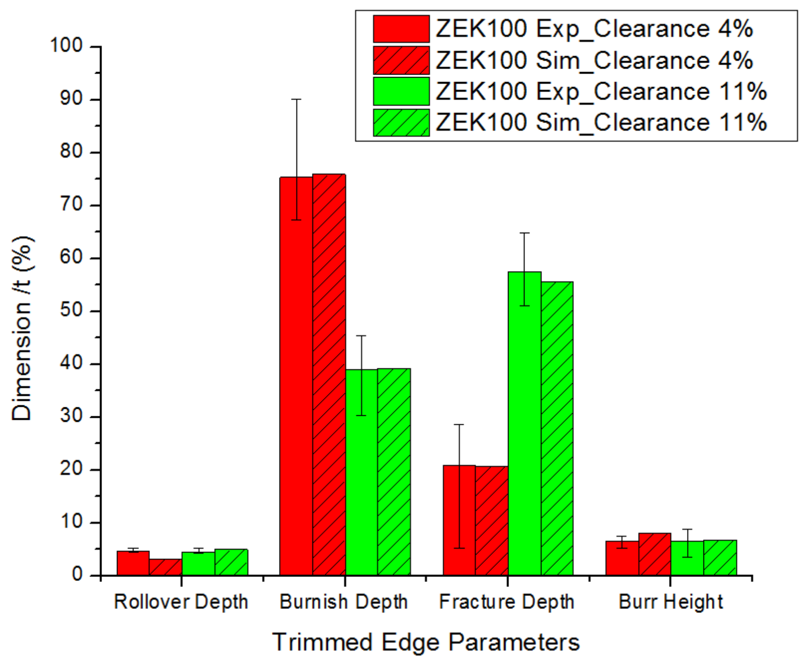

(b). ZEK100

Figure 5-33. Comparisons of various trimmed edge parameters between experiments and FE simulations for 2 different clearances.

From the quantitative trimmed edge parameters shown in Figure 5-33, it can be been that the trimmed edge parameters of AZ31 and ZEK100 as predicted by FE model shows the same trend as observed in experiments where burnish depth decreases with an increase in clearance, whereas the fracture depth, rollover depth and burr height show an opposite trend to the burnish depth. For AZ31, there are some differences between the value of trimmed edge parameters predicted by FE model and obtained from experiment. However, for ZEK100, in nearly all cases, the simulation results have good agreement with the experimental results.

5.2.2.3. Effect of tool setup configuration

The punch load-displacement curves for 2 different tool setup configurations as predicted by FE model for the 2 sheet materials are shown in Figure 5-34. Once again, the predictions yields trends similar to those observed earlier in the experiments (see Figure 5-2). With the use of the cushion, the punch load-displacement curves are higher compared to the conventional tool setup configuration without the cushion. The profiles of trimmed edges obtained from experiments and FE simulations for the 2 tool setup configurations are show in Figure 5-35, the corresponding trimmed edge parameters are presented in Table A-11and plotted in Figure 5-36.

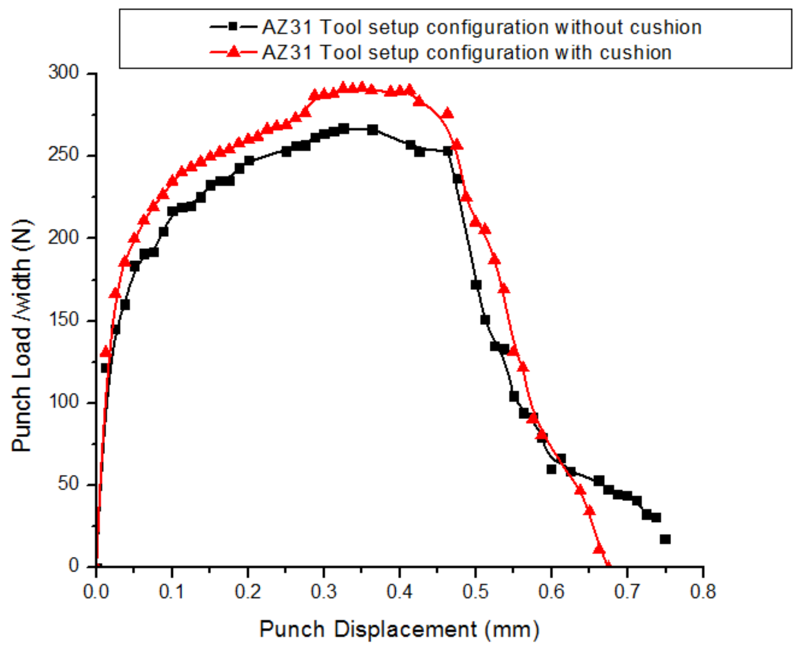

(a) AZ31

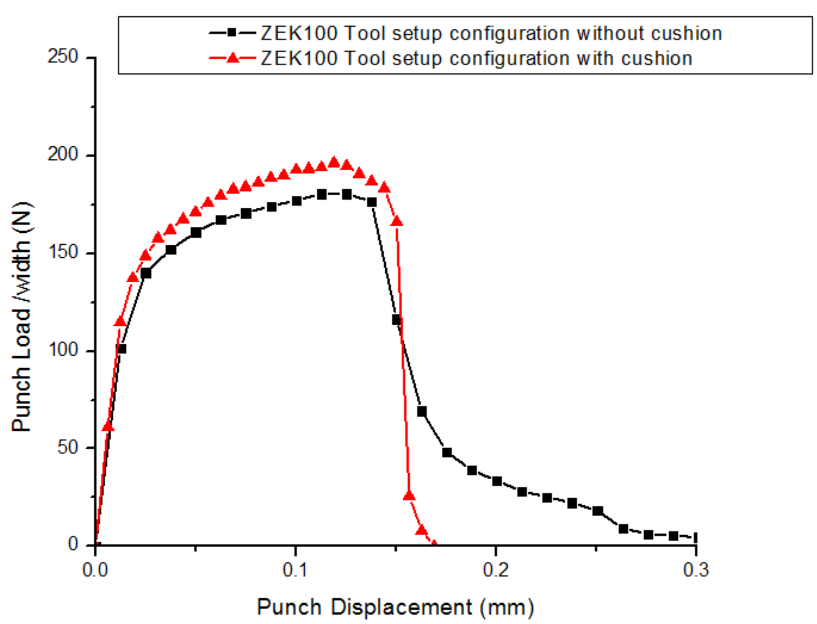

(b) ZEK100

Figure 5-34. Punch load-displacement curves predicted by FE model for 2 different tool setup configuration (trimming speed of 5 mm/sec, clearance of 11% and sheet orientation RD).

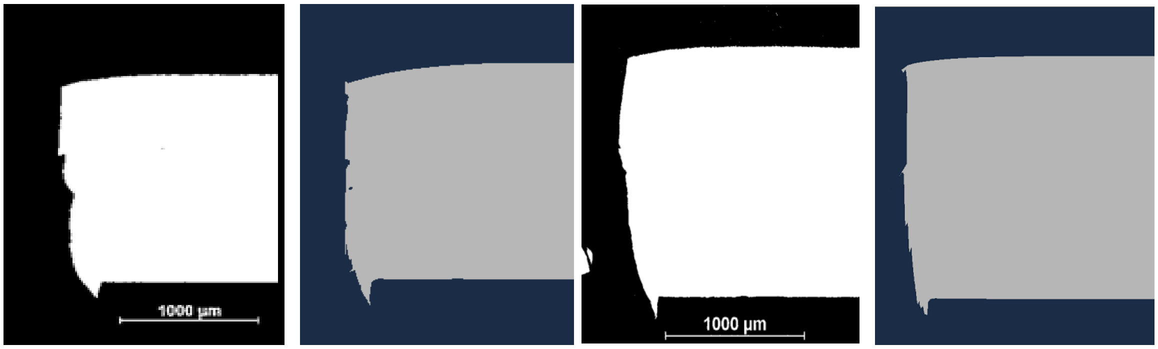

Experiment Simulation Experiment Simulation

AZ31 ZEK100

Tool setup configuration without cushion

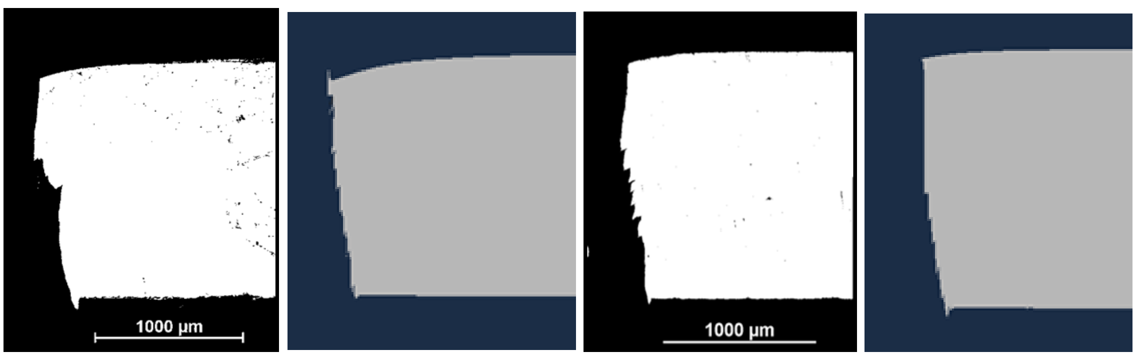

Experiment Simulation Experiment Simulation

AZ31 ZEK100

Tool setup configuration with cushion

Figure 5-35. Comparisons of the profiles of trimmed edges obtained from experiment and FE simulations for 2 different tool setup configurations.

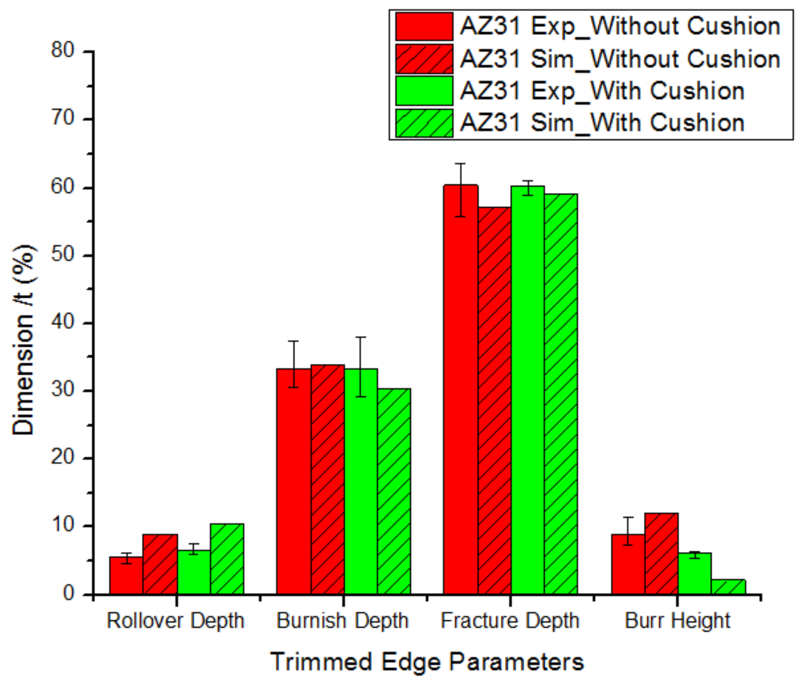

(a). AZ31

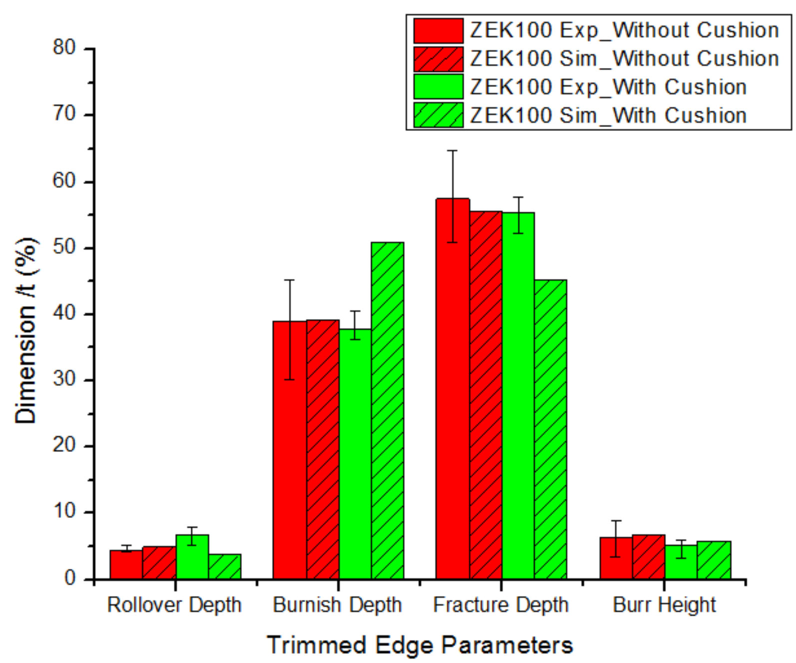

(b). ZEK100

Figure 5-36. Comparisons of trimmed edge parameters between experiment and simulation with respect to different tool setup configuration.

From Figure 5-36(a) for AZ31, the trimmed edge parameters are not identical in both tool setup configurations. However, the results show the same trend as observed in experiment, the burr height can be effectively reduced using tool setup configuration with cushion. Similar results were obtained for ZEK100. As shown in Figure 5-36(b), in general, the trimmed edge parameters predicted by FE model agree well with the experiments.

In summary, the effect of various factors (trimming speed, clearance, tool setup configuration, sheet orientation and thickness) on the punch load-displacement and the quality of trimmed edge are described, and corresponding Finite Element simulation results are compared with the experiment results. Even though, some discrepancies are observed, the FE simulation results have good general agreement with experimental results.

5.2.2.4. Effect of friction

All of the above FE simulations results were based on the assumption that friction coefficient between various tools and sheet was 0.1, and both the profile and parameters of trimmed edge predicted by FE model agree well with the experiment results within a small error band. The effect of different friction conditions on trimming behavior of Magnesium alloy sheets could not be easily observed in experiment, but they could be predicted via FE simulations. In this section, the effect of different friction coefficients (μ=0.1, 0.2, 0.3, 0.5) is presented and compared. ZEK100 sheet was chosen for analyzing the effect of friction. The simulation results of punch load-displacement curve with respect to the above different friction coefficients are shown in Figure 5-37.

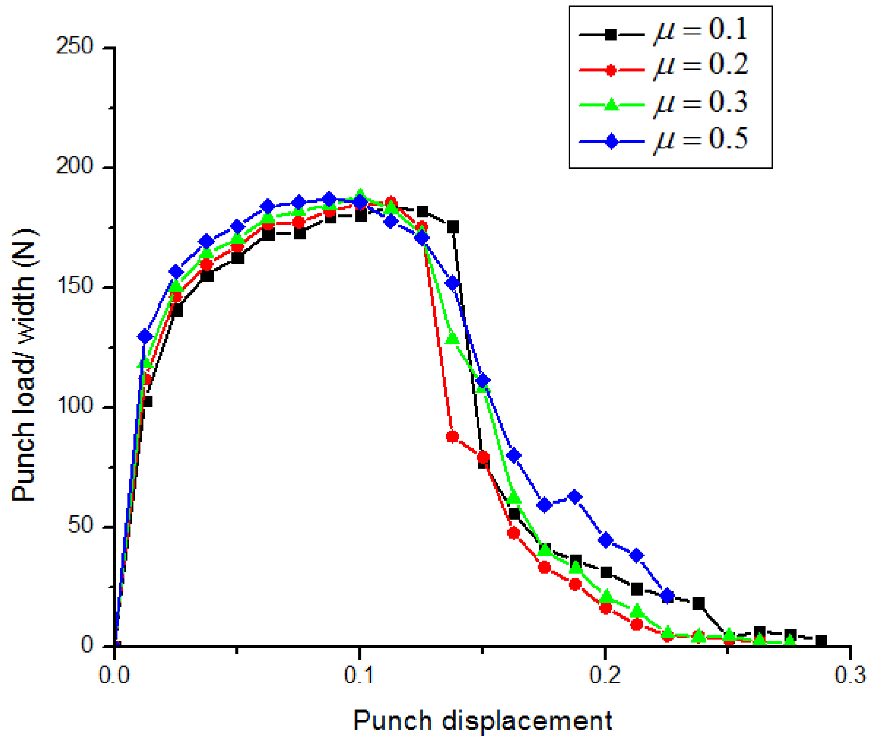

Figure 5-37. Punch load-displacement curves for 4 different friction coefficients as predicted by FE model (tool setup configuration without cushion, trimming speed of 5 mm/sec and sheet orientation RD).

It can be seen that the maximum punch load increases slightly with increase in friction coefficient. This trend is same as Maiti's simulation results for steels (Maiti et al. 2000). Also, it appears that a larger friction coefficient value results in an earlier initiation of crack. The profile of trimmed edge obtained from experiment and FE model using different friction coefficients are presented in Figure 5-38, the corresponding trimmed edge parameters are listed in Appendix A, Table A-12, and plotted in Figure 5-39.

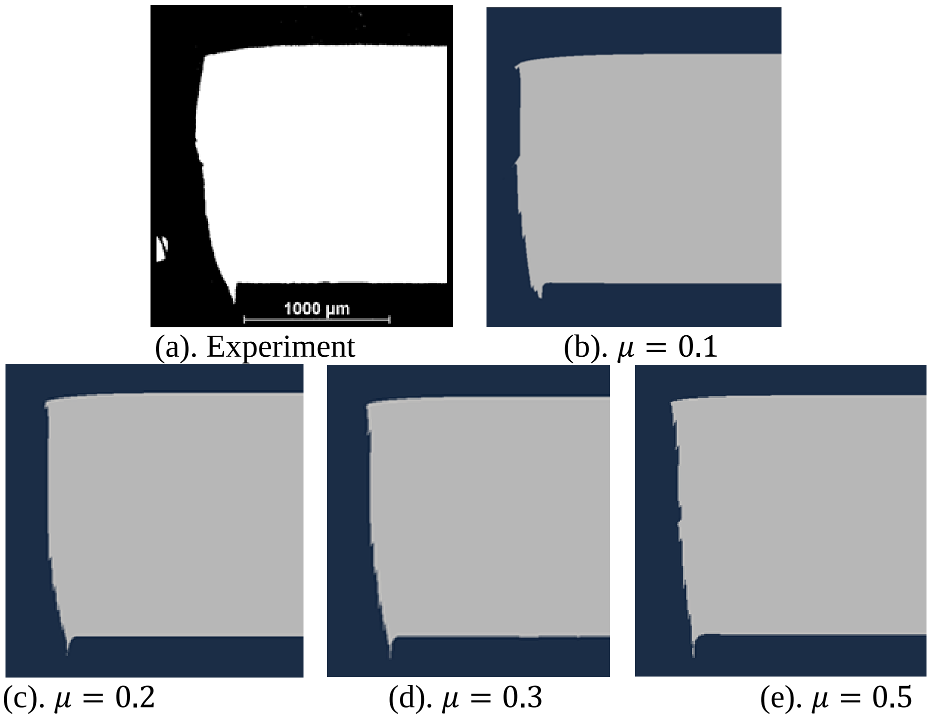

Figure 5-38. Comparisons of profiles of trimmed edges obtained from experiments and FE models for 4 different friction coefficients.

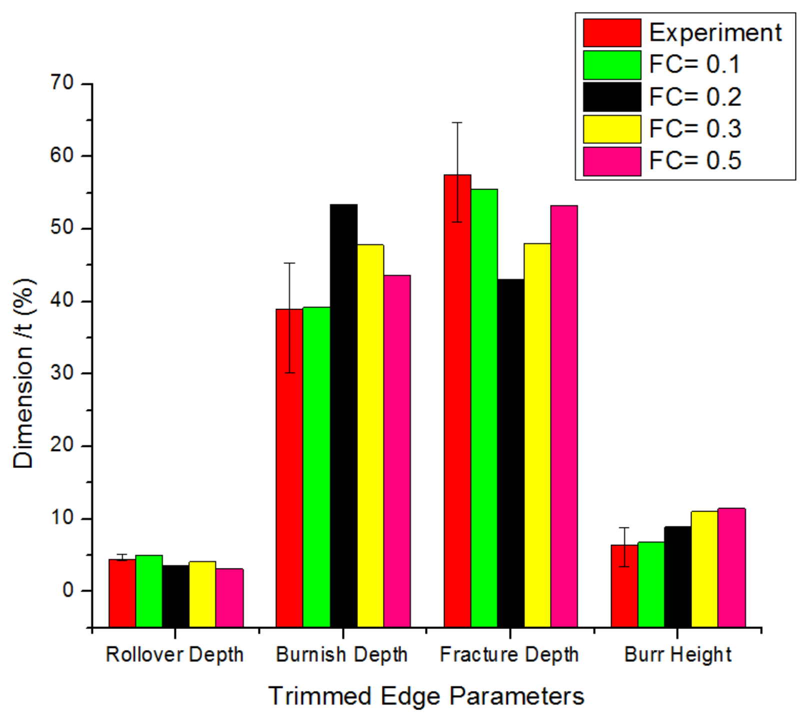

Figure 5-39. Comparisons of trimmed edge parameters between experiments and simulations using different friction coefficients.

From the quantitative analysis shown in Figure 5-39, the burnish zone increases with increase in friction coefficient from 0.1 to 0.2 and then begins to decrease, whereas the fracture zone shows the opposite trend. Also, the rollover depth decreases and burr height increases with increase in friction value. This may be attributed to increased plastic deformation in the trimming zone when friction coefficient is higher.

5.3. Summary

This chapter presented and compared the punch load-displacement curves and profile and parameters of trimmed edge from experiments and FE models under various trimming conditions for AZ31 and ZEK100. In general, the FE simulation results have good agreement with experimental ones with minor discrepancies in the two sets of results. These discrepancies tend to be somewhat larger for AZ31 compared to ZEK100 and will be discussed in Chapter 6. There are more significant differences in the peak load and corresponding peak displacements between model predictions and experiments. Possible reasons for such a discrepancy will be discussed in the Chapter 6.

Chapter 6. Discussion

In Chapter 5, laboratory-based experimental results and FE simulation results for AZ31 and ZEK100 automotive magnesium sheet materials were presented. The experiment results of trimming test on the effect of trimming speed, clearance between die and punch, tool setup configuration, sheet orientation and sheet thickness were presented and compared with the corresponding results predicted from FE simulations. Some discussion of the relevant results was included in individual sub-sections in the last chapter. In this rather short chapter, the critical trimming process parameters affecting the trimmed edge quality are further discussed with some supporting microstructural observations. Also, the origin of the differences in the performance between AZ31 and ZEK100 during the trimming process is further discussed. Lastly, the difference between experimental and FE simulation results are discussed from the perspective of trimming experimental set-up and constitutive material model limitations.

6.1. Experimental and material aspects

6.1.1. Trimming process parameters

The interrupted trimming test where the test was stopped prior to complete separation were conducted at a trimming speed of 0.01mm/sec to examine the development of crack and the mechanism of burr formation. This is shown in Figure 6-1.

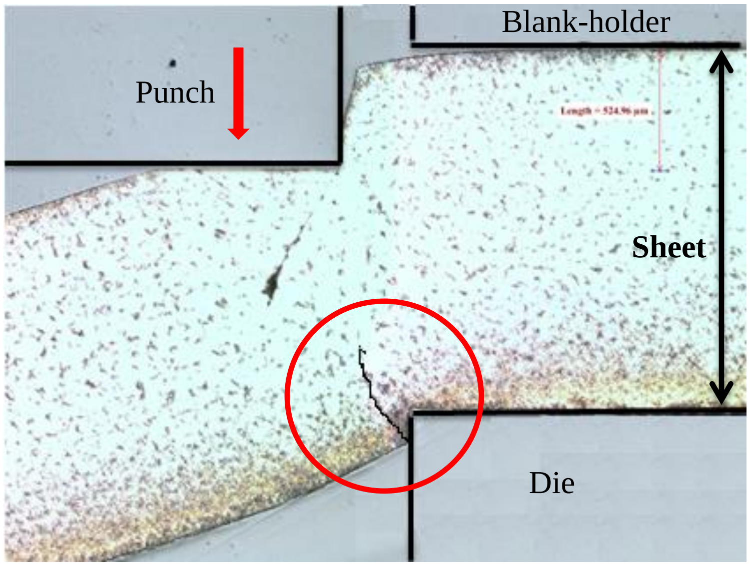

Figure 6-1. Crack initiation and propagation and the mechanism of burr formation in AZ31 (tool setup configuration without cushion, clearance 11%, sheet orientation: RD).

From Figure 6-1, it appears that trimming process is not a pure shearing process, but a rather complex shear process accompanied with bending, compression and tension. During the trimming process, the offal rotates when punch moves down, and the crack at the bottom of trimming zone initiates from the lower point of sheet where the die first indents the material, but not the point adjacent to die tip, so the crack propagation path results in the burr being formed on the part. Understanding the development of crack and mechanism crack of formation in different zones in the trimmed edge is useful for the manufacturing engineer to choose the optimal trimming process parameters.

6.1.1.1. Trimming speed

For the trimming speeds from 0.1 mm/sec up to 5 mm/sec, it is to be noted that trimming speed has no significant influence on peak trimming load for both AZ31 and ZEK100 sheets (see earlier Figure 5-2), but the trimmed edge quality and production efficiency can be improved with increase in trimming speed (see Figure 5-10) because higher trimming speed can reduce the bending effect in the trimming zone. However, a higher trimming speed will also increase the tool wear and reduce the life of tools. In industry, larger trimming speed such as 50 mm/sec might be applied where the rise of temperature in trimming zone may not be negligible. Therefore, the temperature effects on the trimming performance of AZ31 and ZEK100 sheet materials have to be taken into account. However, this was not the focus of the present work due to the speed limitations of the laboratory based experimental set-up. This will also introduce additional complexity in the FE modeling of the trimming process.

6.1.1.2. Clearance

As a process parameter in the trimming process, clearance between die and punch has the most significant influence on the trimmed edge profile and the dimensional precision of trimmed edge (see Figure 5-12). The trimmed edge quality will become poor with increase in punch-die clearance, this is because larger clearance increases the bending effect in the trimming zone. Therefore, choosing a reasonable clearance plays an important role in controlling the quality of trimmed edge. For AZ31 and ZEK100, clearances in the range 4%-11% is reasonable. For those work-pieces with less stringent requirement of quality or precise dimension of trimmed edge, larger clearance can be chosen because the trimming peak load is smaller (see Figure 5-3). This will reduce the friction between tools and sheet and tool wear and consequently increase tool life.

6.1.1.3. Tool setup configuration

In practice, the negative effect of burr formation is much more than that of fracture and rollover because burr on a trimmed part might scratch a smooth surface of another part on contact and sliding but also lead to early onset of fracture when the part with burr is subjected to deformation in a subsequent forming operations. Burr is essentially a highly work hardened material that has very limited capacity for further work hardening. As shown in Figure 6-1, the excessive rotation of offal will produce large burr. A tool setup configuration with cushion can support the sheet and restrict the excessive rotation of the offal to reduce the burr height.

6.1.2. Relative trimming behavior of magnesium and other new automotive sheet materials

6.1.2.1. Comparison of AZ31 and ZEK100 Mg alloy sheet

AZ31 and ZEK100 are new automotive sheet materials that are not yet commonly available on the market. There have been very few studies of trimming behavior of these alloys. In fact, no studies are available in published literature for ZEK100. The chemical compositions of AZ31 and ZEK100 magnesium sheets (see earlier Table 3-1) as well as processing of these two materials are different, and, therefore, microstructure of these two materials are expected to be different. The microstructure plays an important role in inititating void formation and its subsequent growth and coalescence to a macroscopic fracture. The mechanical behavior such as flow stress-strain curves along different orientation of specimen are also different. Therefore, the two materials are expected to yield a different punch load-displacement response as well as quality of trimmed edge.

ZEK is an improved version of the AZ31 alloy and is more formable than AZ31 as established by their respective forming limit diagrams (Antoniswamy et al. 2013). The ultimate tensile strength of AZ31 is also higher than that of ZEK100. In general, a more formable materials is expected to result in better trimmed edge quality (Grünbaum et al. 1996). Additionally, it should be noted that the peak punch load for AZ31 is higher and the crack initiates later than that for ZEK100 (see Figure 5-7 and 5-8). One reason for this is because the thickness of AZ31 in the present work was about 0.05 mm larger that of ZEK100.

6.1.2.2. Comparison of magnesium and aluminum alloys

Similar to automotive magnesium sheets, automotive aluminum sheet materials are also newer materials. The typical profile of trimmed edge of aluminum alloy AA6111-T4 at a clearance of 10% and AZ31 and ZEK100 Magnesium alloy sheets at a clearance 11% are shown in Figure 6-2. It can be seen that there are significant difference between the two types of sheet materials. For aluminum alloy AA6111-T4 sheet as shown in Figure 6-2(a) (Golovashchenko 2006), the trimmed edge consists of straight burnish zone on the top and curved fracture surface at the bottom, whereas both AZ31 and ZEK100 have straight burnish zone and curved fracture surface with a jagged fracture (see circle in Figure 6-2(b-c)). This type of fracture for ZEK100 is less than that in AZ31 sheet.

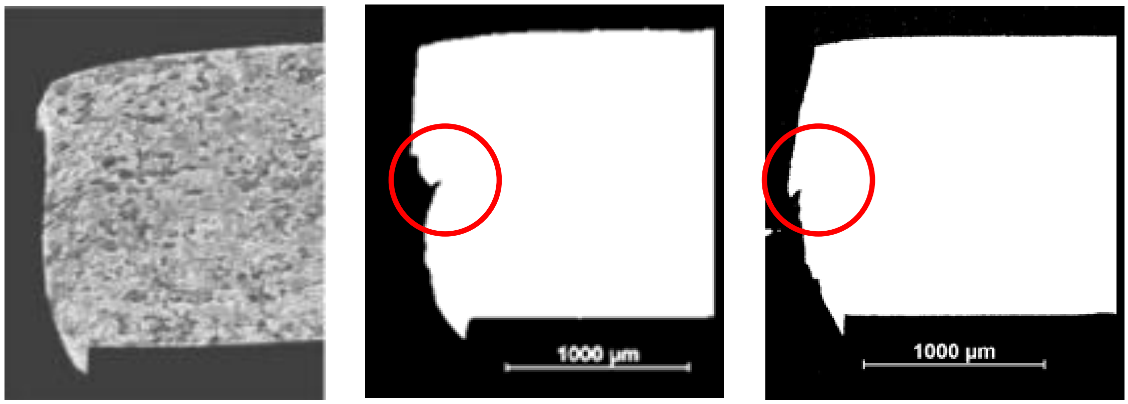

(a). AA6111-T4 (b). AZ31 (c). ZEK100

Figure 6-2. Typical profile of trimmed edge for different mrtal alloys. Figure (a) is take from Golovashchenko (2006)

The differences in profiles of trimmed edges of different materials is because of different chemical composition, different anisotropic nature of the materials at the crystal level, and microstructure and mechanical behavior differences. These basic properties result in different crack propagation paths and shear band development. These are often observed in interrupted trimming process such as in Figure 6-3. For aluminum alloy AlAA6111-T4, the dash line in Figure 6-3(a) is the possible crack path (Li, 2000b) where an almost straight crack propagation path is formed from the tip of punch to the initial indentation point at the bottom die. However, compared to aluminum alloy, the shear bands in AZ31 and ZEK100 were larger, and the crack propagation path were also different (see Figure 6-3 (b-c)). The dashed line in Figure 6-3 (b-c) shows the local shear plastic flow direction and the possible crack propagation path. The crack from punch tip and the crack at the initial indentation point at the bottom die did not coincide but propagated along different directions. Also, there was evidence of internal crack formation in the shear band for AZ31 as shown by the red circle in Figure 6-3(b). Different crack propagation path and complex local shear band resulted in the jagged fracture profile for AZ31 and ZEK100.

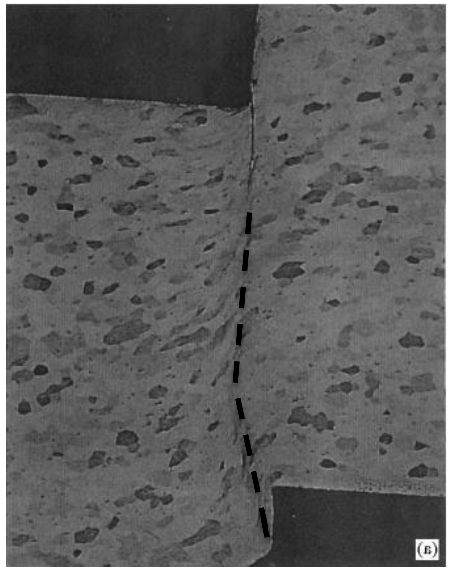

(a). Al-AA6111-T4

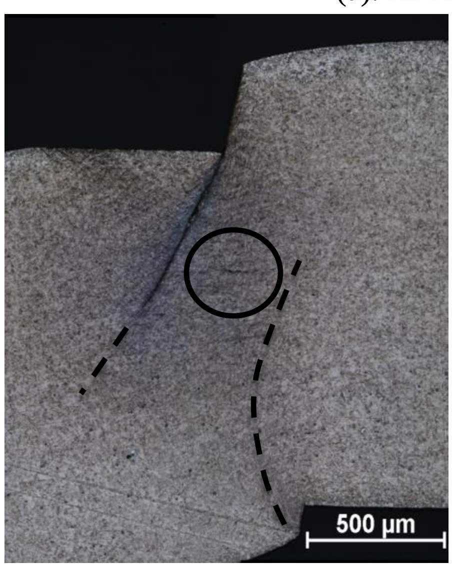

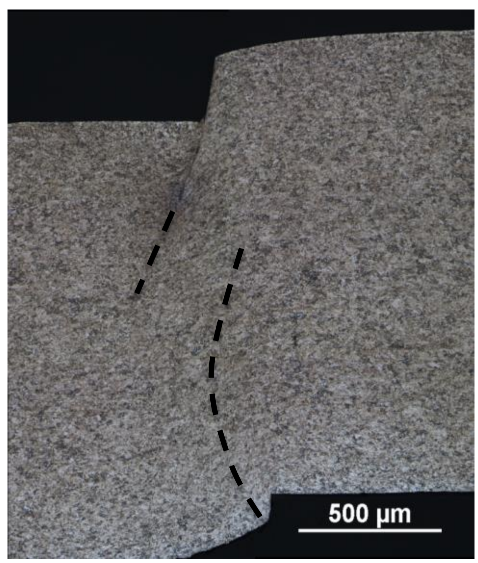

(b). AZ31 (c). ZEK100

Figure 6-3. Crack propagation path and local plastic shear band formation in (a). Al-AA6111-T4 (Li, 2000b), (b). AZ31, and (c). ZEK100.

Even though AZ31 and ZEK100 both show the same shear band formation and crack propagation in the trimming zone, the profile and quality of trimmed edge are different between them. The jagged fracture of ZEK100 was smaller than that of AZ31 and corresponding quality of trimmed edge for ZEK100 was better than that of AZ31 for the same trimming conditions. This can be easily explained from Figure 6-3(b-c), where it can be seen that the angle of crack path to vertical direction for AZ31 is larger than that for ZEK100 sheet.

6.2. Finite Element Modelling

In Chapter 5, results of FE simulations of trimming of AZ31 and ZEK100 Mg sheets materials using FE code ABAQUS/Explicit FE code were presented. A large number of FE models capturing a range of experimental trimming conditions were developed. Also, similar output to that from experimental trimming work was generated from the simulation runs. In general, the experimental profiles of trimmed edge and various quantified trimmed edge parameters (rollover, burnish depth, fracture depth and burr height) were predicted rather well by the simulations for the entire range of experimental trimming conditions. However, there were still some differences between the simulations and experiments in terms of punch load-displacement curves, trimmed edge profile and parameters of trimmed edge. The differences between FE simulation and experiment result from two main sources; experimental limitations and errors and choice of constitutive material model for AZ31 and ZEK100 materials in the FE code. Both of these discrepancies are discussed below.

Figure 6-4 shows representative punch load-displacement curves obtained from FE model and experiment for tool setup configuration without cushion, clearance of 11%, trimming speed of 5 mm/sec and sheet orientation along rolling direction. Although the peak loads in the model and experiments are not very different, position of peak load is much earlier in the FE model (punch displacement 0.15 mm) compared to the experiments (0.45 mm). In other words, the shape of punch load-displacement curves are quite different for the two cases. In reality, the real punch displacement where peak punch load occurs in experiment is about 0.22 mm as observed in the interrupted trimming test (the test was stopped at load peak) as shown in Figure 6-5 which is much closer to the simulation result.

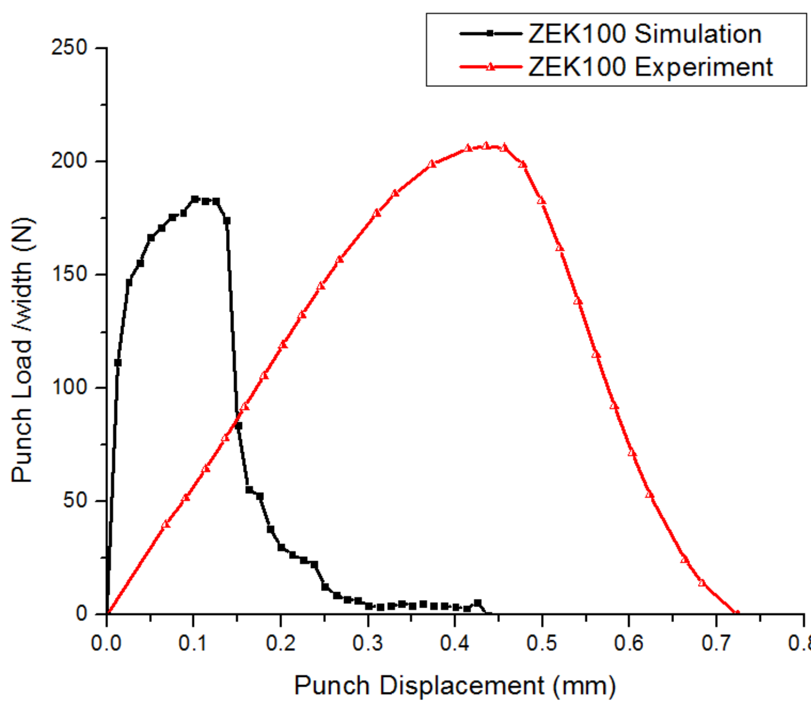

Figure 6-4. Punch load-displacement curve obtained from experiment and FE model.

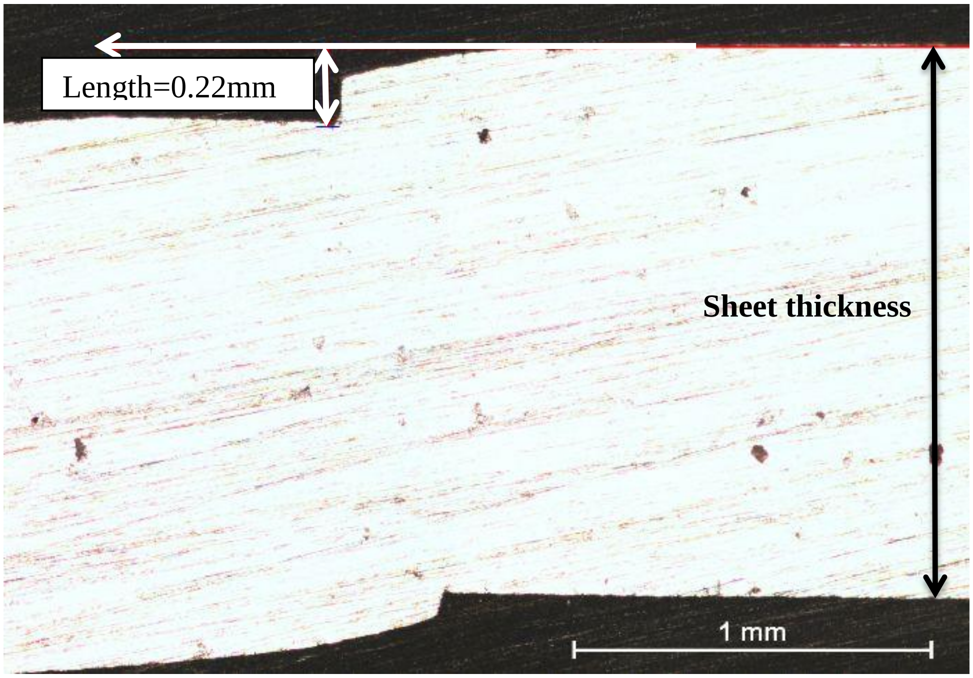

Figure 6-5. Punch displacement at punch load peak.

The reason for difference in the punch displacements corresponding to the peak load in experiments is that the experimental trimming test system turned out to be far more compliant than originally designed. As shown in Figure 6-6, the parts connecting the compression plate and the bottom plate for mounting the trimming tool setup are connected to the INSTRON 10 KN mechanical test system by pins but not threads (see red and blue circle in Figure 6-6), so it was unavoidable to eliminate small gaps between the connecting parts. At the beginning of trimming test, before the load could be effectively transferred to the test specimen, the slack in the load train from grip rotation had to be eliminated. This effectively decreased the slope of the rising part of the load-displacement curve.

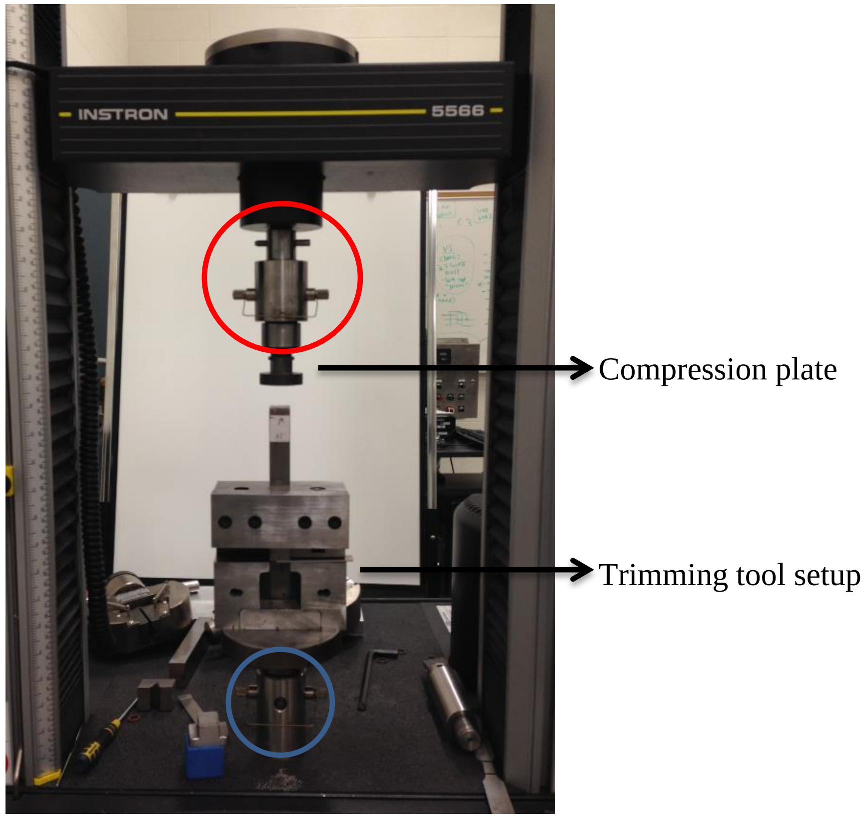

Figure 6-6. INSTRON 10 kN mechanical test system for trimming test.

The other source of error in the experimental and predicted response could be attributed to the constitutive material model. As mentioned earlier in sub-section 6.1.1, trimming process is not pure shearing process in the though-thickness direction, but a complex shearing process accompanied with bending, tension and compression. Both AZ31 and ZEK100 sheets are anisotropic materials, which means the mechanical behavior such as flow stress-strain curves are not identical in all directions (see Figure 3-8 and Figure 3-9). Therefore, it is rather simplistic to simply use one stress-strain curve obtained from tensile, compression or shear test to describe the flow stress-strain behavior during the trimming process. In this thesis, in order to simplify the problem, the flow stress-strain along RD obtained from uniaxial tensile test is implemented in FE model when simulating the trimming of specimen with sheet orientation of RD. In fact, the flow stress-strain curves obtained from compression test along thickness, uniaxial tensile test along RD and TD and shear test along thickness were all tried in the FE model, and the results predicted by FE model using flow stress-strain obtained from uniaxial tensile test were found to have better agreement with the experiment. The Hill quadratic yield criteria is also strictly applicable to materials that exhibit tension compression symmetry. It is now well known that magnesium alloys exhibit significant tension compression asymmetry at room temperature due to twinning and different slip systems that become active in tension and compression. The development of a suitable anisotropic yield criteria for magnesium is a subject of intense current research in the literature and no generally acceptable yield criteria is yet available for use in a general purpose FE code to simulate sheet metal forming processes. Also, all of the ductile failure criteria considered in this work were phenomenological in nature and did not incorporate any microstructural heterogeneity in the analysis. The inaccuracies in yield criteria, hardening law and fracture criteria are expected to manifest in prediction errors in peak punch load and profile of the rimmed edge. In spite of the approximations of the constitutive models, a reasonably good agreement has been obtained between the FE models and experiments.

Chapter 7. Conclusions

The effect of various factors such as trimming speed, clearance, tool setup configuration, sheet orientation and thickness on the trimming behavior of AZ31 and ZEK100 magnesium sheets was systematically investigated, analyzed and discussed by using a laboratory-based experimental method and complementary Finite Element (FE) simulations of the lab-based experiments. In general, the FE simulation results have good agreement with the experiment in terms of trimmed edge profile and quantified parameters of the trimmed edge.

The following conclusions were drawn from experimental and numerical study:

1. Trimming speed up to 5 mm/sec has no significant influence on the peak punch load, and the trimmed edge quality can be improved with increase of trimming speed.
2. Clearance between punch and die has the most significant influence on the trimming behavior of AZ31 and ZEK100, both the punch load peak and quality of trimmed edge decrease with increase of clearance. The larger is the clearance, the later the crack initiates. ZEK100 is much more sensitive to smaller clearance compared to AZ31.
3. The tool setup configuration with cushion consistently resulted in better trimmed edge quality and especially the burr height which is a key parameter for assessing the quality of the trimmed edge.
4. Sheet orientations did not have a large influence on the peak punch load, but did an influence on the shape of punch load-displacement curves where the load

saturation region for the sheet oriented along transvers direction (TD) is much larger and the fracture occurs later than that along the rolling direction (RD).

5. The trimmed edge quality for ZEK100 was consistently better than that of AZ31 and could be partially attributed to its superior formability compared to AZ31 sheet.
6. The profile of trimmed edge for AZ31 and ZEK100 is quite different from that of aluminum sheet materials. The two materials result in the quite different crack propagation paths and local shear bands.
7. Among the five different phenomenological ductile fracture criteria examined in the present work, Oyane fracture criteria most closely predicted the trimming behavior of AZ31 and ZEK100 when compared to the experiments.
8. The profile of trimmed edge predicted by FE model using mesh size of 0.02 mm x 0.02 mm without adaptive re-meshing method are closest to the experimental observations.

Chapter 8. Suggestions for Future Work

The following suggestions for future work are being made to further improve the understanding of trimming behavior of AZ31 and ZEK100 magnesium sheet materials:

1. In industry, the trimming speed is up to 50 mm/sec or more. Therefore, higher strain rate and temperature effect in the trimming of AZ31 and ZEK100 magnesium alloy should be further investigated.
2. Friction condition is another factor that can affect the trimmed edge quality and trimming force. Different lubrication between the punch and sheet is should be studied. It is to be noted that there may be pre-existing lubricant on blanks from the previous forming process.
3. In order to obtain better trimmed edge quality and reduce or eliminate the slivers during the trimming process, the trimming with a proper angle, as proposed by Li (2003) for aluminum sheet, should be attempted for trimming of magnesium sheets.
4. The flow stress-strain is complex in the trimming zone for the anisotropic materials: AZ31 and ZEK100. As the most important part in the FE model, the flow stress-strain constitutive model in trimming process should be further explored to improve the accuracy of FE model.
5. Element deletion method used in FE model results in mass loss that can affect the accuracy of simulation results, so another more challenging method of node separation should be assessed for trimming of magnesium sheet materials.

6. Better re-meshing technique should be explored that not only reduces the excessive distortion of elements at large strains, but also maintain the accuracy of simulation results
7. The current FE model should be extended to three dimensions and to curved trim lines to have a broader understanding of trimming behavior of AZ31 and ZEK100 magnesium alloy sheets for more industrially relevant applications.

References

Abaqus/CAE User's Manual (6.12), 2012,Dassault Systèmes Simulia Corp., Providence, RI, USA.

Antoniswamy, A.R.,Carpenter, A. J.,Carter, J.T.,Hector, L.G. and Taleff, E.M., 2013. Forming-Limit Diagrams for Magnesium AZ31B and ZEK100 Alloy Sheets at Elevated Temperatures. *Journal of Materials Engineering and Performance,* 22(11), pp.3389–3397.

Atkins, A.G., 1996. Fracture in forming. *Journal of Materials Processing Technology*, 56(1-4), pp.609–618.

Ayada, M., Higashino, T. and Mori, K., 1987. Central bursting in extrusion of inhomogeneous materials. *Advanced technology of plasticity lange, K. Springer-Verlag, Berlin*, pp.553–558.

Boba, M., Worswick, M.J. ,Mishra, R. and Carter, J., 2012. Formability of AZ31B and ZEK100 Magnesium alloy sheets at elevated temperatures. *In Mg2012: 9th International Conference on Magnesium Alloys and their Applications.* Vancouver, pp. 397–402.

Broek, D., 1971. A study on ductile failure. Ph.D. thesis, Delft University of Technology, TheNetherlands.

Brokken, D., Brekelmans, W.A.M and Baaijens, F.P.T., 1998. Numerical modelling of the metal blanking process. *Journal of Materials Processing Technology* vol. 83 (1-3), pp.192–199.

Brokken, D., Brekelmans, W.A.M. and Baaijens, F.P.T., 2000. Predicting the shape of blanked products : a finite element approach. *Journal of Materials Processing Technology*, 103, pp.51 – 56.

Brozzo, P., Deluca, B. and Redina, R. A., 1972,A new method for the prediction of the formability limits of metals sheets, *Proc. 7th Biennial Conf. Int. Deep Drawing Research Group.*

Chang, T.M. and Swift, H.W., 1950. Shearing of metal bars. *Journal of Institute of Metals*, 78, pp.119–146.

Clift, S.E., Hartley, P., Strugess, C.E.N and Rowe, G.W., 1990. Fracture prediction in plastic deformation processes. *International Journal of Mechanical Sciences*, 32(1), pp.1–17.

Cockroft, M.G. and Latham, D.J., 1968. Ductility and the Workability of Metals. *Jouranl of The Institute of Metals*, 96, pp.33–39.

Fang, G., Zeng, P. and Lou, L., 2002. Finite element simulation of the effect of clearance on the forming quality in the blanking process. *Journal of Materials Processing Technology*, 122(2-3), pp.249–254.

Faura, F., García, A. and Estrems, M., 1998. Finite element analysis of optimum clearance in the blanking process. *Journal of Materials Processing Technology*, 80-81, pp.121–125.

Freudenthal, F.A., 1950. The Inelastic Behaviors of Solid [M] New York :Wiley.

Ghosh, S., Li, M. and Khadke, A., 2005. 3D modeling of shear-slitting process for aluminum alloys. *Journal of Materials Processing Technology*, 167(1), pp.91–102.

Goijaerts, A.M., 1999. Prediction of Ductile Fracture in Metal Blanking. *Ph.D. thesis* Eindhoven University of Technology.

Goijaerts, A.M., Govaert, L.E. and Baaijens, F.P.T., 2001. Evaluation of ductile fracture models for different metals in blanking. *Journal of Materials Processing Technology*, 110(3), pp.312–323.

Golovashchenko, S.F., 2006. A study on trimming of aluminum autobody sheet and development of a new robust process eliminating burrs and slivers. *International Journal of Mechanical Sciences*, 48(12), pp.1384–1400.

Golovashchenko, S.F., 2008. Quality of Trimming and its Effect on Stretch Flanging of Automotive Panels. *Journal of Materials Engineering and Performance*, 17(3), pp.316–325.

Grünbaum, M., Breitling, J. and Altan, T., 1996. Influence of high cutting speeds on the quality of blanked parts, Report No. ERC/NSM - S-96-19, Columbus, Ohio.

Gurson, A.L., 1977. Continuum theory of ductile rupture by void nucleation and growth : Pat I - Yield criteria and flow rules for porous ductile media. *Journal of Engineering Materials and Technology*, 99, pp.2–15.

Gwynne, B. and Lyon, P., 2007. Magnesium Alloys in Aerospace Applications, Past Concerns, Current Solutions. In *Triennial International Aircraft Fire & Cabin Safety Research Conference*.

Hatanaka, N., Yamaguchi, K. and Takakura, N., 2003. Finite element simulation of the shearing mechanism in the blanking of sheet metal. *Journal of Materials Processing Technology*, 139(1-3), pp.64–70.

Huo, T. and Nakamachi, E., 1995. Evaluation of the dynamic explicit/elastoviscoplastic finite-element method in sheet-forming simulation. *Journal of Materials Processing Technology*, 50(1-4), pp.180–196.

Husson, C., Correia, J.P.M., Daridon, L.and Ahzi, S., 2008. Finite elements simulations of thin copper sheets blanking: Study of blanking parameters on sheared edge quality. *Journal of Materials Processing Technology*, 199(1-3), pp.74–83.

Jain, M., Allin, J. and Lloyd, D.J., 1999. Fracture limit prediction using ductile fracture criteria for forming of an automotive aluminum sheet. *International Journal of Mechanical Sciences*, 41(10), pp.1273–1288.

Johnson, W. and Mellor, P.B., 1973. Engineering plasticity, London,Van Nostrand Reinhold Company LTD.

Komori, K., 2005. Ductile fracture criteria for simulating shear by node separation method. *Theoretical and Applied Fracture Mechanics*, 43(1), pp.101–114.

Komori, K., 2013. Simulation of crack arrest in blanking using the node separation method. *International Journal of Mechanical Sciences*, 68, pp.150–159.

Komori, K., 2001. Simulation of shearing by node separation method. *Computers & Structures*, 79(2), pp.197–207.

Krrabaj, S., Bytyqi, B. and Osmani, H., 2011. Influence of Cutting Speed on the Quality of Blanked Parts. In *15th International research/Expert conference:Trends in the development of machinery and associated technology*. Prague, Czech Repubilc, pp. 817–820.

Lemiale, V., Chambert, J. and Picart, P., 2009. Description of numerical techniques with the aim of predicting the sheet metal blanking process by FEM simulation. *Journal of Materials Processing Technology*, 209(5), pp.2723–2734.

Li, M., 2000a. An experimental investigation on cut surface and burr in trimming aluminum autobody sheet. *International Journal of Mechanical Sciences*, 42(5), pp.889–906.

Li, M., 2000b. Micromechanisms of deformation and fracture in shearing aluminum alloy sheet. *International Journal of Mechanical Sciences*, 42(5), pp.907–923.

Li, M., 2003. Sliver Generation Reduction in Trimming of Aluminum Autobody Sheet. *Journal of Manufacturing Science and Engineering*, 125(1), p.128.

Lin, Z.-C. and Chen, C.-C., 2007. Friction coefficient investigation on IC dam-bar trimming process by inverse method with experimental trimmed geometric profiles. *International Journal of Machine Tools and Manufacture*, 47(1), pp.44–52.

Maiti, S. Ambekar, A.A,Singh, U.P,Date, P.P and Narasimhan, K, 2000. Assessment of influence of some process parameters on sheet metal blanking. *Journal of Materials Processing Technology*, 102(1-3), pp.249–256.

Magnesium Elektron : http://www.magnesium-elektron.com/about-magnesium.asp?ID=1

McClintock, F.A., 1968. A Criteria for Ductile Fracture by the Growth of Holes. *Journal of Applied Mechanics*, 35(2), pp.363–371.

Needleman, A. and Tvergaard, V., 1984. An analysis of ductile rupture in notched bars. *Journal of the Mechanics and Physics of Solids*, 32(6), pp.461–490.

Norris, D.M., Reaugh, J. E., Moran, B. and Quiñones, D. F., 1978. A Plastic-Strain, Mean-Stress Criteria for Ductile Fracture. *Journal of Engineering Materials and Technology*, 100(3), pp.279–286.

Oyane, M., 1972. Criteria of Ductile Fracture Strain. *Bulletin of JSME*, 15(90), pp.1507–1513.

Prior, A.M., 1994. Applications of implicit and explicit finite element techniques to metal forming. *Journal of Materials Processing Technology*, 45(1-4), pp.649–656.

Quazi, P.T.Z. and Shaikh, R.S., 2012. An Overview of Clearance Optimization in Sheet Metal Blanking Process. *International Journal of Modern Engineering Research(IJMER)*, 2(6), pp.4547–4558.

Rachik, M., Roelandt, J.. and Maillard, A., 2002. Some phenomenological and computational aspects of sheet metal blanking simulation. *Journal of Materials Processing Technology*, 128(1-3), pp.256–265.

Rice, J.R. and Tracey, D.M., 1969. On the ductile enlargement of voids in triaxial stress fields∗. *Journal of the Mechanics and Physics of Solids*, 17(3), pp.201–217.

Samuel, M., 1998. FEM simulations and experimental analysis of parameters of influence in the blanking process. *Journal of Materials Processing Technology*, 84(1-3), pp.97–106.

Situ, Q., Bruhis, M. and Jain, M., 2005. Trimming of AA6111-T4 and AA5754-O Automotive Aluminum Sheet Materials. *International Journal of Forming Processes*, 8/4, pp.341–361.

Taupin, E., Breitling, J.,Wu, Wei-T. and Altan, T., 1996. Material fracture and burr formation in blanking results of FEM simulations and comparison with experiments. *Journal of Materials Processing Technology*, 59(1-2), pp.68–78.

Thipprakmas, S., Jin, M. and Tomokazu, K.,Katsuhiro, Y. and Murakawa, M., 2008. Prediction of Fineblanked surface characteristics using the finite element method (FEM). *Journal of Materials Processing Technology*, 198(1-3), pp.391–398.

Tvergaard, V., 1981. Influence of voids on shear band instabilities under plane strain conditions. *International Journal of Fracture*, 17(4), pp.389–407.

Tvergaard, V., 1982. On localization in ductile materials containing spherical voids. *International Journal of Fracture*, 18(4), pp.237–252.

Appendix

A. Experimentally obtained trimmed edge parameters

Table A-1. Trimmed edge parameters of AZ31and ZEK100 for different trimming speeds.

AZ31	**0.1 mm/sec**		**1 mm/sec**		**3 mm/sec**		**5 mm/sec**	
Trimmed edge Parameters /t (%)	Value	Error	Value	Error	Value	Error	Value	Error
Rollover Depth	5.28	$^{+0.34}_{-0.27}$	5.74	$^{+0.65}_{-0.72}$	5.11	$^{+1.40}_{-0.56}$	5.59	$^{+0.63}_{-1.04}$
Burnish Depth	26.07	$^{+5.03}_{-3.18}$	29.36	$^{+2.10}_{-3.81}$	27.78	$^{+1.34}_{-2.64}$	33.35	$^{+4.09}_{-2.84}$
Fracture Depth	68.65	$^{+4.62}_{-3.60}$	64.90	$^{+4.40}_{-2.41}$	67.11	$^{+3.10}_{-2.41}$	61.06	$^{+3.23}_{-4.60}$
Burr Height	9.31	$^{+2.55}_{-2.62}$	8.17	$^{+2.32}_{-2.39}$	8.91	$^{+2.46}_{-2.73}$	8.9	$^{+2.60}_{-1.63}$
ZEK	**0.1 mm/sec**		**1 mm/sec**		**3 mm/sec**		**5 mm/sec**	
Trimmed edge Parameters /t (%)	Value	Error	Value	Error	Value	Error	Value	Error
Rollover Depth	5.00	$^{+0.66}_{-0.75}$	4.08	$^{+0.63}_{-0.63}$	5.78	$^{+0.77}_{-1.07}$	4.56	$^{+0.71}_{-0.22}$
Burnish Depth	31.28	$^{+1.73}_{-2.09}$	35.70	$^{+5.02}_{-1.80}$	35.23	$^{+1.04}_{-6.19}$	39.03	$^{+6.30}_{-8.78}$
Fracture Depth	63.72	$^{+2.15}_{-1.68}$	60.22	$^{+2.23}_{-5.60}$	60.31	$^{+6.04}_{-8.74}$	56.41	$^{+7.27}_{-6.53}$
Burr Height	18.07	$^{+6.60}_{-8.48}$	6.98	$^{+1.65}_{-0.87}$	6.25	$^{+1.98}_{-2.73}$	6.44	$^{+3.35}_{-2.98}$

Table A-2. Trimmed edge parameters for different punch-die clearances.

AZ31	**4%**		**11%**		**20%**		**26%**	
Trimmed edge Parameters /t (%)	Value	Error	Value	Error	Value	Error	Value	Error
Rollover Depth	4.34	$^{+0.53}_{-0.68}$	5.60	$^{+0.63}_{-1.04}$	8.10	$^{+0.58}_{-0.79}$	9.71	$^{+1.40}_{-1.03}$
Burnish Depth	35.18	$^{+3.57}_{-3.58}$	33.35	$^{+4.09}_{-2.84}$	31.61	$^{+3.84}_{-2.80}$	30.47	$^{+5.07}_{-2.89}$
Fracture Depth	60.48	$^{+3.49}_{-3.80}$	61.05	$^{+3.70}_{-2.98}$	60.29	$^{+3.70}_{-2.98}$	59.82	$^{+3.76}_{-5.01}$
Burr Height	8.60	$^{+0.68}_{-0.38}$	8.93	$^{+2.60}_{-1.63}$	10.38	$^{+6.66}_{-4.14}$	14.69	$^{+3.89}_{-3.56}$
ZEK100	**4%**		**11%**		**20%**		**26%**	
Trimmed edge Parameters /t (%)	Value	Error	Value	Error	Value	Error	Value	Error
Rollover Depth	4.68	$^{+0.50}_{-0.28}$	4.56	$^{+0.71}_{-0.22}$	8.29	$^{+0.81}_{-0.91}$	11.14	$^{+0.31}_{-0.47}$
Burnish Depth	75.35	$^{+14.76}_{-8.06}$	39.03	$^{+6.30}_{-8.78}$	34.14	$^{+1.67}_{-1.50}$	29.69	$^{+1.81}_{-2.38}$
Fracture Depth	19.97	$^{+7.79}_{-15.66}$	56.41	$^{+7.27}_{-6.53}$	57.77	$^{+1.38}_{-2.95}$	59.17	$^{+1.96}_{-1.49}$
Burr Height	6.26	$^{+0.94}_{-1.24}$	6.44	$^{+3.35}_{-2.98}$	6.90	$^{+2.67}_{-2.82}$	6.93	$^{+0.28}_{-0.42}$

Table A-3. Trimmed edge parameters obtained using two different tool setup configurations.

Material	**AZ31**				**ZEK100**			
Tool setup configuration	**without cushion**		**with cushion**		**without cushion**		**with cushion**	
Trimmed edge Parameters /t (%)	Value	Error	Value	Error	Value	Error	Value	Error
Rollover Depth	5.60	$^{+0.63}_{-1.04}$	6.48	$^{+1.12}_{-0.55}$	4.56	$^{+0.71}_{-0.22}$	6.75	$^{+1.09}_{-1.53}$
Burnish Depth	33.35	$^{+4.09}_{-2.84}$	33.35	$^{+4.63}_{-4.05}$	39.03	$^{+6.30}_{-8.78}$	37.84	$^{+2.78}_{-1.51}$
Fracture Depth	61.05	$^{+3.70}_{-2.98}$	60.17	$^{+0.67}_{-1.46}$	56.41	$^{+7.27}_{-6.53}$	55.41	$^{+2.29}_{-3.22}$
Burr Height	8.93	$^{+2.60}_{-1.63}$	6.17	$^{+0.27}_{-0.80}$	6.44	$^{+3.35}_{-2.98}$	5.12	$^{+0.76}_{-1.85}$

Table A-4. Trimmed edge parameters for AZ31 and ZEK100 from two different sheet orientations.

Material	**AZ31**				**ZEK100**			
Sheet Orientation	**RD**		**TD**		**RD**		**TD**	
Trimmed edge Parameters /t (%)	Value	Error	Value	Error	Value	Error	Value	Error
Rollover Depth	4.34	$^{+0.53}_{-0.68}$	3.84	$^{+0.73}_{-0.95}$	4.68	$^{+0.50}_{-0.28}$	5.03	$^{+0.16}_{-0.31}$
Burnish Depth	35.18	$^{+3.57}_{-3.58}$	32.33	$^{+4.02}_{-3.53}$	75.35	$^{+14.76}_{-8.06}$	64.79	$^{+6.56}_{-10.44}$
Fracture Depth	60.48	$^{+3.49}_{-3.80}$	63.83	$^{+2.57}_{-3.67}$	19.97	$^{+7.79}_{-15.66}$	30.18	$^{+10.29}_{-6.67}$
Burr Height	8.60	$^{+0.68}_{-0.38}$	7.80	$^{+0.57}_{-0.65}$	6.26	$^{+0.94}_{-1.24}$	4.45	$^{+0.73}_{-0.52}$

Table A-5 . Trimmed edge parameters of AZ31 from 2 different sheet thicknesses.

Material	**AZ31**			
Sheet Thickness	**1.58 mm**		**3.20 mm**	
Trimmed edge Parameters /t (%)	Value	Error	Value	Error
Rollover Depth	4.34	$^{+0.53}_{-0.68}$	3.27	$^{+0.41}_{-0.47}$
Burnish Depth	35.18	$^{+3.57}_{-3.58}$	32.14	$^{+2.92}_{-2.70}$
Fracture Depth	60.48	$^{+3.49}_{-3.80}$	64.59	$^{+2.84}_{-3.53}$
Burr Height	8.60	$^{+0.68}_{-0.38}$	5.69	$^{+0.62}_{-0.68}$

Table A-6. Trimmed edge parameters of AZ31 and ZEK100 for different fracture criteria.

AZ31	Experiment		Simulation				
Trimmed edge Parameters /t (%)	Parameters	Error	Oyane	C-L	Brozzo	Clift	R-T
Rollover depth	5.60	$^{+0.63}_{-1.04}$	8.92	7.85	8.16	6.30	6.78
Burnish depth	33.35	$^{+4.09}_{-2.84}$	33.99	42.97	38.73	39.75	53.92
Fracture depth	61.05	$^{+3.70}_{-2.98}$	57.09	49.18	53.10	53.95	39.29
Burr height	8.93	$^{+2.60}_{-1.63}$	12.03	10.82	6.27	7.59	8.48
ZEK100	Experiment		Simulation				
Trimmed edge Parameters /t (%)	Parameters	Error	Oyane	C-L	Brozzo	Clift	R-T
Rollover depth	4.56	$^{+0.71}_{-0.22}$	4.96	5.05	4.45	4.38	3.96
Burnish depth	39.03	$^{+6.30}_{-8.78}$	39.22	42.92	33.35	39.78	41.53
Fracture depth	56.51	$^{+7.27}_{-6.53}$	55.55	51.70	61.90	55.42	54.22
Burr height	6.44	$^{+3.35}_{-2.98}$	6.78	6.61	4.11	2.44	1.65

Table A-7. Trimmed edge parameters obtained from experiments and FE models using various mass scaling factors.

ZEK100	Experiment		Simulation				
Trimmed edge Parameters /t (%)	Vaule	Error	MS100	MS400	MS900	MS2500	MS10000
Rollover depth	4.46	$^{+0.72}_{-0.22}$	4.56	4.70	4.64	4.96	5.15
Burnish depth	39.03	$^{+7.20}_{-8.78}$	42.13	39.46	40.64	39.22	38.87
Fracture depth	56.51	$^{+7.27}_{-6.53}$	53.65	55.56	54.37	55.55	55.98
Burr height	6.44	$^{+2.35}_{-2.98}$	6.36	7.55	7.88	6.78	6.42

Table A-8. Trimmed edge parameters obtained from experiment and FE model using different meshing methods.

ZEK100	Experiment		Simulation			
Trimmed edge Parameters /t (%)	Value	Error	MS (mm) 0.01x0.01	MS(mm) 0.02x0.02	MS(mm) 0.03x0.03	MS(mm)0.02x0.02 (Adaptive Meshing)
Rollover depth	4.46	$^{+0.72}_{-0.22}$	4.56	4.70	4.64	21.11
Burnish depth	39.03	$^{+7.20}_{-8.78}$	42.13	39.46	40.64	18.04
Fracture depth	56.51	$^{+7.27}_{-6.53}$	53.65	55.56	54.37	60.85
Burr height	6.44	$^{+2.35}_{-2.98}$	6.36	7.55	7.88	1.24

Table A-9. Trimmed edge parameters of AZ31 and ZEK100 obtained from experiments and FE simulations.

AZ31	Trimming speed 3 mm/sec			Trimming speed 5 mm/sec		
Trimmed edge Parameters /t (%)	Experiment		Simulation	Experiment		Simulation
	Value	Error	Value	Value	Error	Value
Rollover depth	5.11	$^{+1.40}_{-0.56}$	9.37	5.60	$^{+0.63}_{-1.04}$	8.92
Burnish depth	27.78	$^{+1.34}_{-2.64}$	28.48	33.35	$^{+4.09}_{-2.84}$	33.99
Fracture depth	68.21	$^{+3.40}_{-2.41}$	62.15	61.05	$^{+3.70}_{-2.98}$	57.09
Burr height	8.91	$^{+2.46}_{-2.73}$	13.04	8.93	$^{+2.60}_{-1.63}$	12.03
ZEK100	Trimming speed 1 mm/sec			Trimming speed 5 mm/sec		
Trimmed edge Parameters /t (%)	Experiment		Simulation	Experiment		Simulation
	Value	Error	Value	Value	Error	Value
Rollover depth	4.08	$^{+0.63}_{-0.63}$	4.62	4.56	$^{+0.71}_{-0.22}$	4.96
Burnish depth	35.70	$^{+5.02}_{-1.80}$	40.88	39.03	$^{+6.30}_{-8.78}$	39.22
Fracture depth	60.32	$^{+2.22}_{-5.60}$	54.50	56.51	$^{+7.27}_{-6.53}$	55.55
Burr height	6.98	$^{+1.65}_{-0.87}$	6.51	6.44	$^{+3.35}_{-2.98}$	6.78

Table A-10. Trimmed edge parameters of AZ31 and ZEK100 from experiments and FE simulations.

AZ31	Clearance 4%			Clearance 11%		
Trimmed edge Parameters /t (%)	Experiment		Simulation	Experiment		Simulation
	Value	Error	Value	Value	Error	Value
Rollover depth	4.34	$^{+0.53}_{-0.68}$	7.15	5.60	$^{+0.63}_{-1.04}$	8.92
Burnish depth	35.18	$^{+3.57}_{-3.58}$	45.53	33.35	$^{+4.09}_{-2.84}$	33.99
Fracture depth	59.45	$^{+3.49}_{-2.80}$	47.32	61.05	$^{+3.70}_{-2.98}$	57.09
Burr height	8.60	$^{+0.68}_{-0.38}$	5.92	8.93	$^{+2.60}_{-1.63}$	12.03
ZEK100	Clearance 4%			Clearance 11%		
Trimmed edge Parameters /t (%)	Experiment		Simulation	Experiment		Simulation
	Value	Error	Value	Value	Error	Value
Rollover depth	4.68	$^{+0.50}_{-0.28}$	3.07	4.56	$^{+0.71}_{-0.22}$	4.96
Burnish depth	75.35	$^{+14.76}_{-8.06}$	75.94	39.03	$^{+6.30}_{-8.78}$	39.22
Fracture depth	20.79	$^{+7.79}_{-15.66}$	20.73	56.51	$^{+7.27}_{-6.53}$	55.55
Burr height	6.26	$^{+0.94}_{-1.24}$	8.14	6.44	$^{+3.35}_{-2.98}$	6.78

Table A-11. Trimmed edge parameters of AZ31 and ZEK100 as obtained from experiments and FE simulations for two different tool setup configurations.

AZ31	Tool setup without cushion			Tool setup with cushion		
Trimmed edge Parameters /t (%)	Experiment		Simulation	Experiment		Simulation
	Value	Error	Value	Value	Error	Value
Rollover depth	5.60	$^{+0.63}_{-1.04}$	8.92	6.48	$^{+1.12}_{-0.55}$	10.44
Burnish depth	33.35	$^{+4.09}_{-2.84}$	33.99	33.35	$^{+4.63}_{-4.05}$	30.38
Fracture depth	61.05	$^{+3.70}_{-2.98}$	57.09	60.31	$^{+0.67}_{-1.46}$	59.18
Burr height	8.93	$^{+2.60}_{-1.63}$	12.03	6.17	$^{+0.27}_{-0.80}$	2.15
ZEK100	Tool setup without cushion			Tool setup with cushion		
Trimmed edge Parameters /t (%)	Experiment		Simulation	Experiment		Simulation
	Value	Error	Value	Value	Error	Value
Rollover depth	4.56	$^{+0.71}_{-0.22}$	4.96	6.75	$^{+1.09}_{-1.53}$	3.73
Burnish depth	39.03	$^{+6.30}_{-8.78}$	39.22	37.84	$^{+2.78}_{-1.51}$	50.98
Fracture depth	56.51	$^{+7.27}_{-6.53}$	55.55	55.41	$^{+2.29}_{-3.22}$	45.29
Burr height	6.44	$^{+3.35}_{-2.98}$	6.78	5.12	$^{+0.76}_{-1.85}$	5.82

Table A-12. Trimmed edge parameters obtained from experiment and FE model using different friction coefficients.

ZEK100	Experiment		Simulation			
Trimmed edge Parameters /t (%)			Friction coefficient			
	Value	Error	0.1	0.2	0.3	0.5
Rollover depth	4.46	$^{+0.72}_{-0.22}$	4.56	3.54	4.11	3.14
Burnish depth	39.03	$^{+7.20}_{-8.78}$	42.13	53.40	47.84	43.59
Fracture depth	56.51	$^{+7.27}_{-6.53}$	53.65	43.06	48.05	53.27
Burr height	6.44	$^{+2.35}_{-2.98}$	6.36	8.89	11.05	11.47

B. User-defined material VUMAT subroutine interface

(Run in ABAQUS/Explicit 12.1)

```
subroutine vumat(
C Read only -
    1 nblock, ndir, nshr, nstatev, nfieldv, nprops, lanneal,
    2 stepTime, totalTime, dt, cmname, coordMp, charLength,
    3 props, density, strainInc, relSpinInc,
    4 tempOld, stretchOld, defgradOld, fieldOld,
    5 stressOld, stateOld, enerInternOld, enerInelasOld,
    6 tempNew, stretchNew, defgradNew, fieldNew,
C Write only -
    7 stressNew, stateNew, enerInternNew, enerInelasNew )
C     implicit none
      include 'vaba_param.inc'
C       dimension props(nprops), density(nblock),
    1 coordMp(nblock,*),
    2 charLength(*), strainInc(nblock,ndir+nshr),
    3 relSpinInc(*), tempOld(nblock),
    4 stretchOld(*), defgradOld(nblock, ndir+nshr),
    5 fieldOld(nblock,nfieldv), stressOld(nblock,ndir+nshr),
    6 stateOld(nblock,nstatev), enerInternOld(*),
    7 enerInelasOld(*), tempNew(nblock),
    8 stretchNew(*), defgradNew(nblock, ndir+nshr),
    9 fieldNew(nblock,nfieldv),
    1 stressNew(nblock,ndir+nshr), stateNew(nblock,nstatev),
    2 enerInternNew(*), enerInelasNew(*)
C
      character*80 cmname
C
      do 100 km = 1,nblock
        user coding
  100 continue
      return
      end
```

C. Input file of FE model of trimming process for ZEK100

(Run in ABAQUS/Explicit 12.1)

Trimming conditions: Tool setup configuration without cushion, Clearance of 11% thickness, Trimming speed of 5 mm/sec, Sheet orientation of RD.

*Heading
** Job name: ZEKRD_Oyane_G1C10M002 Model name: ZEKRD_Oyane_G1C10M002Standard
** Generated by: Abaqus/CAE 6.12-1
*Preprint, echo=NO, model=NO, history=NO, contact=NO
**
**** PARTS** **(Part definition)**
**
*Part, name=Blank
*Node (Node definition)
*Element, type=CPE4R (Element definition)
*Element, type=CPE3
*Nset, nset=_PickedSet2, internal, generate
1, 7479, 1
*Elset, elset=_PickedSet2, internal, generate
1, 7337, 1
** Section: BlankSection
*Solid Section, elset=_PickedSet2, material=ZEK100
,
*End Part
**
*Part, name=Die
*End Part
**
*Part, name=Holder
*End Part
**
*Part, name=Punch
*End Part
**
**
**** ASSEMBLY** **(Assembly definition)**
**
*Assembly, name=Assembly

```
**
*Instance, name=Punch-1, part=Punch
-0.0900000000000007,       16.531,           0.
*Node
      1,         -20.,  8.43614868e-31,           0.
*Nset, nset=Punch-1-RefPt_, internal
1,
*Surface, type=SEGMENTS, name=PunchSurf
START,         -20.,          55.
 LINE,           0.,          55.
 LINE,           0., 0.0499999271359704
 CIRCL, -0.0499999274239325,           0., -0.0500000000000035,         0.05
 LINE,         -20.,           0.
 LINE,         -20.,          55.
*Rigid Body, ref node=Punch-1-RefPt_, analytical surface=PunchSurf
*End Instance
**
*Instance, name=Blank-1, part=Blank
        5.09,        11.58,           0.
*End Instance
**
*Instance, name=Die-1, part=Die
*Node
      1, 0.0900000036,  -19.9099998,           0.
*Nset, nset=Die-1-RefPt_, internal
1,
*Nset, nset=_PickedSet6, internal
 1,
*Surface, type=SEGMENTS, name=DieSurf
START, 0.090000000000005,       -19.91
 LINE, 0.0900000000000007, 14.9500000729419
 CIRCL, 0.139999929064499,          15., 0.140000000000001,        14.95
 LINE,          55.,          15.
*Rigid Body, ref node=Die-1-RefPt_, analytical surface=DieSurf
*Element, type=HEATCAP, elset=_PickedSet6_Inertia-1_
1, 1
*Heat Cap, elset=_PickedSet6_Inertia-1_
1.,
*End Instance
**
*Instance, name=Holder-1, part=Holder
0.0899999999999978,        16.53,           0.
*Node
      1,  -3.36777865e-15,         27.5,           0.
```

```
*Nset, nset=Holder-1-RefPt_, internal
1,
*Surface, type=SEGMENTS, name=HolderSurf
START,         55.,          0.
 LINE,          0.,          0.
 LINE,          0.,         55.
*Rigid Body, ref node=Holder-1-RefPt_, analytical surface=HolderSurf
*End Instance
**
*Nset, nset=Refpunch, instance=Punch-1
 1,
*Nset, nset=RefDie, instance=Die-1
 1,
*Nset, nset=RefHolder, instance=Holder-1
 1,
*Nset, nset=Center, instance=Blank-1
   5,   6, 344, 345
*Elset, elset=Center, instance=Blank-1
 5828, 5832, 5928
*Nset, nset=_PickedSet33, internal, instance=Holder-1
 1,
*Nset, nset=_PickedSet45, internal, instance=Punch-1
 1,
*Nset, nset=_PickedSet47, internal, instance=Holder-1
 1,
*Nset, nset=_PickedSet50, internal, instance=Die-1
 1,
*Nset, nset=_PickedSet110, internal, instance=Blank-1
   7,   8, 429
*Elset, elset=_PickedSet110, internal, instance=Blank-1
 6636, 6742
*Nset, nset=SetTotalNode, instance=Blank-1, generate
    1,  7479,     1
*Elset, elset=_BlankTop_S2, internal, instance=Blank-1
*Elset, elset=_BlankTop_S3, internal, instance=Blank-1
*Elset, elset=_BlankTop_S1, internal, instance=Blank-1
*Elset, elset=_BlankTop_S4, internal, instance=Blank-1
*Surface, type=ELEMENT, name=BlankTop
_BlankTop_S2, S2
_BlankTop_S3, S3
_BlankTop_S4, S4
_BlankTop_S1, S1
*Elset, elset=_BlankBot_S4, internal, instance=Blank-1
*Elset, elset=_BlankBot_S2, internal, instance=Blank-1
```

```
*Elset, elset=_BlankBot_S3, internal, instance=Blank-1
*Surface, type=ELEMENT, name=BlankBot
_BlankBot_S4, S4
_BlankBot_S2, S2
_BlankBot_S3, S3
*Elset, elset=_BlankTopLeft_S2, internal, instance=Blank-1
*Elset, elset=_BlankTopLeft_S3, internal, instance=Blank-1
*Elset, elset=_BlankTopLeft_S1, internal, instance=Blank-1
*Surface, type=ELEMENT, name=BlankTopLeft
_BlankTopLeft_S2, S2
_BlankTopLeft_S3, S3
_BlankTopLeft_S1, S1
*Elset, elset=_BlankTopRight_S3, internal, instance=Blank-1
*Elset, elset=_BlankTopRight_S4, internal, instance=Blank-1
*Elset, elset=_BlankTopRight_S2, internal, instance=Blank-1
*Elset, elset=_BlankTopRight_S1, internal, instance=Blank-1
 *Surface, type=ELEMENT, name=BlankTopRight
_BlankTopRight_S3, S3
_BlankTopRight_S4, S4
_BlankTopRight_S2, S2
_BlankTopRight_S1, S1
*Surface, type=NODE, name=SetTotalNode_CNS_, internal
SetTotalNode, 1.
*End Assembly
*Amplitude, name=Amp-1
           0.,              0.,           1e-05,              1.
**
```

**** MATERIALS**

```
**
*Material, name=ZEK100
*Density
 1.78e-09,
*Depvar, delete=3
     7,
*User Material, constants=10
45000.,      0.33,    4520.,     0.61,   0.0078,     3.49,     185., 0.188346
 0.266267,     293.
**
```

**** INTERACTION PROPERTIES**

```
**
*Surface Interaction, name=Fric
*Friction
 0.1,
*Surface Interaction, name=NonFric
```

*Friction
0.,
** --
**
** STEP: Step-1
**
*Step, name=Step-1
*Dynamic, Explicit
, 5e-06
*Bulk Viscosity
0.06, 1.2
**
**** BOUNDARY CONDITIONS**
**
** Name: Blankright Type: Symmetry/Antisymmetry/Encastre
*Boundary
_PickedSet110, ENCASTRE
** Name: Die Type: Symmetry/Antisymmetry/Encastre
*Boundary
_PickedSet50, ENCASTRE
** Name: Holder Type: Displacement/Rotation
*Boundary
_PickedSet47, 1, 1
_PickedSet47, 2, 2
_PickedSet47, 6, 6
** Name: Punch Type: Velocity/Angular velocity
*Boundary, type=VELOCITY
_PickedSet45, 1, 1
_PickedSet45, 2, 2
_PickedSet45, 6, 6
**
*** LOADS*
**
** Name: Holder-Die Force   Type: Concentrated force
*Cload
_PickedSet33, 2, -440.
**
**** INTERACTIONS**
**
** Interaction: Die-Nodes
*Contact Pair, interaction=Fric, mechanical constraint=KINEMATIC, cpset=Die-Nodes
Die-1.DieSurf, SetTotalNode_CNS_
** Interaction: Holder-Nodes

*Contact Pair, interaction=Fric, mechanical constraint=KINEMATIC, cpset=Holder-Nodes
Holder-1.HolderSurf, SetTotalNode_CNS_
** Interaction: Punch-Nodes
*Contact Pair, interaction=Fric, mechanical constraint=KINEMATIC, cpset=Punch-Nodes
Punch-1.PunchSurf, SetTotalNode_CNS_
**
**** OUTPUT REQUESTS**
**
*Restart, write, number interval=1, time marks=NO
**
** FIELD OUTPUT: F-Output-1
**
*Output, field, number interval=200
*Node Output
RF, RT, U, UT
*Element Output, directions=YES
PE, PEEQ, S, SDV, STATUS
*Contact Output
CSTRESS,
**
**** HISTORY OUTPUT**: H-Output-1
**
*Output, history
*Node Output, nset=Refpunch
RF2, RT, U2, UT
**
** HISTORY OUTPUT: H-Output-2 Energy
**
*Output, history, variable=PRESELECT
*End Step
** --
**
** STEP: Step-2
**
*Step, name=Step-2
*Dynamic, Explicit
, 0.5
*Bulk Viscosity
0.06, 1.2
**
**** BOUNDARY CONDITIONS**
**

```
** Name: Punch Type: Velocity/Angular velocity
*Boundary, amplitude=Amp-1, type=VELOCITY
_PickedSet45, 1, 1
_PickedSet45, 2, 2, -5.
_PickedSet45, 6, 6
**
** OUTPUT REQUESTS
**
*Restart, write, number interval=1, time marks=NO
**
** FIELD OUTPUT: F-Output-1
**
*Output, field, number interval=200
*Node Output
RF, RT, U, UT
*Element Output, directions=YES
PE, PEEQ, S, SDV, STATUS
*Contact Output
CSTRESS,
**
** HISTORY OUTPUT: H-Output-1
**
*Output, history
*Node Output, nset=Refpunch
RF2, RT, U2, UT
**
** HISTORY OUTPUT: H-Output-2 Energy
**
*Output, history, variable=PRESELECT
*End Step
```